


ผลของการสะสมชั้นฝุ่นที่มีต่อสมรรถนะการจับฝุ่นของระบบตัวกรองเซรามิกแบบแห้ง



นางสาวจิรพรรณ ลักขมิมิรุ โณทัย

วิทยานิพนธ์นี้เป็นส่วนหนึ่งของการศึกษาตามหลักสูตรปริญญาวิศวกรรมศาสตรมหาบัณฑิต

สาขาวิชาวิศวกรรมเคมี ภาควิชาวิศวกรรมเคมี

คณะวิศวกรรมศาสตร์ จุฬาลงกรณ์มหาวิทยาลัย

ปีการศึกษา 2548

ISBN: 974-53-2380-2

ลิขสิทธิ์ของจุฬาลงกรณ์มหาวิทยาลัย

EFFECT OF DUST DEPOSITION ON COLLECTION PERFORMANCE OF CERAMIC
CANDLE FILTER SYSTEM

Miss. Jerapan Laksameearunotai



สถาบันวิทยบริการ

A Thesis Submitted in Partial Fulfillment of the Requirements
for the Degree of Master of Engineering Program in Chemical Engineering

Department of Chemical Engineering

Faculty of Engineering


Chulalongkorn University

Academic Year 2005


ISBN: 974-53-2380-2

Thesis Title	EFFECT OF DUST DEPOSITION ON COLLECTION PERFORMANCE OF CERAMIC CANDLE FILTER SYSTEM
By	Miss Jerapan Laksameearunotai
Field of study	Chemical Engineering
Thesis Advisor	Associate Professor Tawatchai Charinpanitkul, D.Eng.
Thesis Co-advisor	Professor Wiwut Tanthapanichakoon, Ph.D.

Accepted by the Faculty of Engineering, Chulalongkorn University in Partial Fulfillment of the Requirements for the Master's Degree


.....Dean of the Faculty of Engineering
(Professor Direk Lavansiri, Ph.D.)

THESIS COMMITTEE


.....Chairman
(Associate Professor Suttichai Assabumrungrat, Ph.D.)


.....Thesis Advisor
(Associate Professor Tawatchai Charinpanitkul, D.Eng.)


.....Thesis Co-advisor
(Professor Wiwut Tanthapanichakoon, Ph.D.)


.....Member
(Assistant Professor Mana Amornkitbamrung, D. Eng)

จิรพรรณ ลักษณ์อรุโณทัย : ผลของการสะสมชั้นฝุ่นที่มีต่อสมรรถนะการจับฝุ่นของระบบตัวกรองเซรามิกแบบแห้ง (EFFECT OF DUST DEPOSITION ON COLLECTION PERFORMANCE OF CERAMIC CANDLE FILTER SYSTEM) อ. ที่ปรึกษา: รศ.ดร. รัชชัช ชรินพานิชกุล, อ.ที่ปรึกษาร่วม: ศ.ดร. วิวัฒน์ ตัณฑะพานิชกุล, จำนวนหน้า 148 หน้า. ISBN 974-53-2380-2

ตัวกรองเซรามิกแบบแห้งถูกพัฒนาเพื่อใช้ในการกรองฝุ่นที่มีประสิทธิภาพสูงที่อุณหภูมิสูง เนื่องจากตัวกรองเซรามิกแบบแห้งนี้มีความต้านทานความร้อนที่ดีรวมทั้งมีการกักกรองของสารเคมีอีกด้วย การเข้าใจถึงปัจจัยต่าง ๆ ในการทดลองที่มีผลต่อสมรรถนะในการกรองฝุ่น เช่น ความเข้มข้นฝุ่นขาเข้า และระบบการทำความสะอาดตัวกรองนั้นจำเป็นต้องการออกแบบในทางวิศวกรรมและเศรษฐศาสตร์ งานวิจัยนี้ได้ทำการศึกษาการจำลองทางคณิตศาสตร์ของชุดกรองฝุ่นแบบตัวกรองเซรามิกแบบแห้งเพื่อศึกษาค่าความดันตกของตัวกรองเซรามิกในกรณีสะอาดและในกรณีที่มีฝุ่นสะสมในกรณีต่าง ๆ การเข้าใจพื้นฐานต่อการกระจายตัวของความเร็วภายในระบบ จะนำไปสู่การลงทุนต่ำ ลดความเสี่ยงต่ออันตรายที่จะเกิด และง่ายต่อการใช้งานอีกด้วย งานวิจัยนี้ได้เลือกใช้โปรแกรมสำเร็จรูปซึ่งเป็นที่รู้จักในชื่อ FLUENT โดยผลที่ได้นั้นจะสามารถเข้าใจถึงปรากฏการณ์ในการกรองและการสะสมฝุ่นภายในระบบได้ดียิ่งขึ้น

เครื่องวัดค่าผลต่างความดันถูกใช้ในการวัดค่าความดันตกคร่อมตัวกรองเซรามิกซึ่งสามารถเก็บข้อมูลโดยเครื่องเก็บข้อมูล (data logger) จากข้อมูลที่ได้สามารถแสดงความสัมพันธ์ระหว่างค่าผลต่างความดันที่ตกคร่อมตัวกรองเซรามิกเทียบกับเวลา โดยใช้ PLC เป็นตัวควบคุมระบบทำความสะอาดตัวกรอง ซึ่งพิจารณาจากความดันที่เพิ่มขึ้นจากความดันเริ่มต้น โดยทำการเปลี่ยนแปลงค่าตั้งแต่ 15 ถึง 35 มิลลิเมตรน้ำ ซึ่งหัวฉีดถูกเปิดเพื่อทำความสะอาดนาน 100 มิลลิวินาที โดยทั่วไปตัวกรองเซรามิกนี้จะถูกทำความสะอาดแบบไม่สมบูรณ์เพราะเนื่องมาจากมีการตกค้างของฝุ่นแบบถาวรอยู่บางส่วน ถึงแม้ว่าจะเพิ่มระยะเวลาในการเปิดหรือเพิ่มความถี่ในการทำความสะอาดแล้วก็ตามการสะสมของฝุ่นที่เกิดขึ้นบนผิวตัวกรองเซรามิกมีผลต่อประสิทธิภาพในการเก็บฝุ่นและปรากฏการณ์ดังกล่าวก็มีผลต่อค่าความดันแรกเริ่มและความดันตกค้างที่เกิดขึ้นในระบบอีกด้วย โดยสองอิทธิพลนี้ควรนำมาพิจารณาและทำการศึกษาต่อไป

ภาควิชา.....วิศวกรรมเคมี.....ลายมือชื่อนิสิต.....จิรพรรณ ลักษณ์อรุโณทัย
สาขาวิชา.....วิศวกรรมเคมี.....ลายมือชื่ออาจารย์ที่ปรึกษา.....
ปีการศึกษา.....2548.....ลายมือชื่ออาจารย์ที่ปรึกษาร่วม.....

4670267421 : MAJOR CHEMICAL ENGINEERING

KEY WORD: CERAMIC CANDLE FILTER / DUST COLLECTION / SIMULATION

JERAPAN LAKSAMEEARUNOTAI: EFFECT OF DUST DEPOSITION ON
COLLECTION PERFORMANCE OF CERAMIC CANDLE FILTER SYSTEM.

THESIS ADVISOR: ASSOC. PROF. TAWATCHAI CHARINPANITKUL,
D.Eng., THESIS COADVISOR : PROF. WIWUT TANTHAPANICHAKOON,
Ph.D., 148 pp. ISBN 974-53-2380-2

Ceramic candle filters have been developed as a high temperature particulate collecting system with very high collection efficiency because of their good thermal resistance and chemical corrosion resistance. Understanding of dependence of the filter performance on the operating parameters such as inlet dust concentration and regenerating pulse system will be essential for their engineering and economical design. In the present work we have made use of a small scale dust collector with a single ceramic candle filter to investigate the dependence of pressure drop of clean virgin candle filters and filters with dust load on various operating parameters. A fundamental understanding of the particle transport and deposition processes in the filter chamber would lead to lower investment, reduced risk and ease of operation of the filtration systems. One technique frequently used to simulate velocity distribution applies computational fluid dynamics (CFD). Determination of the parameters involved in the calculation of velocity distribution, was supported by a computer package known as "FLUENT". These results have led to a better understanding of the phenomenon of filtration of gas and dust loading distribution.

A differential pressure transmitter is used for monitoring the pressure drop (ΔP) across the ceramic filter which is recorded by a data logger. The plot shows the relationship between the pressure drops across the candle and the cycle time. In this case, the activating pressure drop setting on the programmable logic controller (PLC) will be varied from 15 to 35 mmH₂O, with a pulse duration time of 100 ms.

Generally, the ceramic candle filter was not perfectly cleaned at the start of an experiment, even though it was exposed to a large number of jet pulses. The deposition of dust on the surface of the filter provided a strong effect on the collection of incoming dust and this phenomenon also affected the initial and residual pressure drop of the system. Trade-off of these two effects should be taken into account and investigated further.

Department.....Chemical Engineering.....Student's signature.....*Jerapan Laksameearunotai*
Field of study.....Chemical Engineering.....Advisor's signature.....*J. Charinpanitkul*
Academic year2005.....CO-advisor's signature.....*M. Tanthapanichakoon*

ACKNOWLEDGEMENTS

Firstly, I am very grateful to my advisor, Assoc. Prof. Tawatchai Charinpanitkul, Department of Chemical Engineering, Chulalongkorn University, for his indispensable advice, and his encouragement to continue the course of this work. I would like to express my sincere thanks to Prof. Wiwut Tanthapanitchakoon, Director, National Nanotechnology Center (NANOTEC), Thailand, for his useful guidance, comments, kindness and encouragement for undertaking these studies. It has been a great experience learning a lot of things from him.

The author is grateful to thank you for financial supported by New Energy Development Organization (NEDO) 2004-2005 Grant.

I am also grateful to Assoc. Prof. Sutthichai Assabumrungrut, Asst. Prof. Dr. Mana Amornkitbamrung and Miss. Nattaporn Tonanon for their stimulative comments and participation as the thesis committee.

I would like to express Prof. Takeshi Fukui and Mr. MasahiroYoshikawa, Hosokawa Powder Technology Research Institute, Osaka, Japan, for their useful the experimental data for simulation. I am thankful to acknowledge Prof. Makio Naito, Joining and Welding Research Institute, Osaka University, Japan

I would like to thank my partner, Mr Witsarut and my senior colleagues, Mr. Damrongsak and Kumpanart, for their useful suggestions from them. I would like to thank the officers from KMITL and Kasetsart University, for their suggestion and information on the equipment. I would like to thank the Department of Chemical Engineering, King Mongkut's Institute of Technology Ladkrabang (KMITL) for allowing me to setup the experimental apparatus and using the accessories.

Thank you very much to all members of the Particle Technology and Material Processing Laboratory for their warm collaborations and kindness during my thesis work.

Finally it is my great wish to express my cordial and deep thanks to my parents for their love and encouragement.

CONTENTS

	Page
ABSTRACT IN THAI.....	iv
ABSTRACT IN ENGLISH.....	v
ACKNOWLEDGEMENTS.....	vi
CONTENTS.....	vii
LIST OF TABLES.....	xi
LIST OF FIGURES.....	xii
NOMENCLATURE.....	xv
CHAPTER I INTRODUCTION.....	1
1.1 Introduction.....	1
1.2 Objectives.....	2
1.3 Scope of research	2
1.4 Procedure of research.....	3
CHAPTER II LITERATURE REVIEW.....	4
2.1 Experimental Method.....	4
2.2 CFD modeling.....	8
CHAPTER III THEORY.....	11
3.1 Filtration Phenomena.....	11
3.1.1 Face velocity	11
3.1.2 Pressure drop	13
3.1.3 Pulse jet cleaning.....	15
3.1.4 Collection efficiency.....	16
3.2 Computational Fluid Dynamic (CFD).....	17
3.2.1 Differential equations.....	18
3.2.2 Boundary conditions.....	18
3.2.3 Geometries.....	18
3.2.4 Modeling description.....	19
3.2.5 Numerical method.....	20

	Page
CHAPTER IV EXPERIMENT.....	22
4.1. Materials.....	22
4.1.1. Test dust.....	22
4.1.2. Ceramic candle filter.....	22
4.1.3. Instrument.....	23
4.1.3.1. The instruments used to determine the physical properties were as follows.....	23 23
4.1.3.1.1. Scanning Electron Microscope (SEM).....	24
4.1.3.1.2. Ultracycnometer.....	25
4.1.3.1.3. Laser particle size distribution analyzer	25
4.1.3.1.4. Powder tester.....	25
4.1.3.2. The devices used to carry out experiments	27
4.1.3.2.1. Air compressor.....	27
4.1.3.2.2. Screw feeder.....	27
4.1.3.2.3. Filter and pressure regulator set.....	28
4.1.3.2.4. Pulse air tank.....	29
4.1.3.2.5. Solenoid valve.....	29
4.1.3.2.6. Diaphragm valve.....	30
4.1.3.2.7. Rotameter.....	30
4.1.3.2.8. Differential pressure transmitter.....	32
4.1.3.2.9. Signal conditioner.....	33
4.1.3.2.10. Programmable logic controller (PLC).....	33
4.1.3.2.11. Data logger.....	34
4.1.3.2.12. Anemometer.....	36
4.1.3.2.13. Airborne particle counter.....	36
4.2 Experimental Set-up	37
4.2 Effect investigated.....	39
4.1. The effects were described below.....	39
4.3.1.1. Effect of the pulse duration	39

	Page
4.3.1.2. Effect of pressure differential activated cleaning.....	39
4.3.1.3. Effect of nominal face velocity	39
4.3.1.4. Effect of inlet dust concentration.....	39
4.3.1.5. Effect of inlet port position	40
4.3.2. The experimental procedure.....	40
CHAPTER V RESULTS AND DISCUSSION.....	42
5.1 Results and discussion the results on the properties of dust.....	42
5.1.1 Determination particle size distribution (PSD)	42
5.1.2 Determination of particle shape.....	42
5.1.3 Determination of true density	42
5.1.4 Determination of flowability and floodability.....	42
5.2 Simulation of steady clean air flow through virgin filters.....	43
5.2.1 Effect of air inlet position	44
5.3 Experimental results and discussion.....	51
5.3.1. Effect investigated.....	51
5.3.1.1 Initial pressure drop and residual pressure drop.....	52
5.3.1.2 Outlet dust concentration.....	53
5.3.1.2.1 Effect of pulse duration.....	53
5.3.1.2.2 Effect of pressure differential activated cleaning	58
5.3.1.2.3 Effect of nominal face velocity	62
5.3.1.2.4 Effect of inlet dust concentration	67
5.3.1.2.5 Effect of inlet port position	71
5.3.2. Correlation between face velocity and dust penetration.....	76
5.4 Comparison of the flow distribution calculation between a twin ceramic candle filter system and a single ceramic candle filter.....	80

	Page
CHAPTER VI CONCLUSIONS AND RECOMMENDATIONS.....	85
6.1 Conclusions.....	85
6.2 Recommendation for future work.....	88
REFERENCES.....	89
APPENDIX A Dimension dust removal.....	92
APPENDIX B Dust properties.....	102
APPENDIX C Experimental data.....	108
APPENDIX D Profile velocity vector.....	135
VITA.....	148



สถาบันวิทยบริการ
จุฬาลงกรณ์มหาวิทยาลัย

LIST OF TABLES

	Page
Table 4.1 Dimension of a ceramic candle filter.....	23
Table 4.2 The chemical composition of ceramic candle filter.....	23
Table 4.3 The main conditions carried out in this work	38
Table 4.4 The experimental conditions investigated in this work.....	38
Table 4.5 The converted unit from millimeter water to Pascal.....	39
Table 5.1 Pressure drop for the various cases of air inlet position	47
Table 5.2 Zone of velocity distribution along z-position for the case of the top air inlet.....	50
Table 5.3 Zone of velocity distribution along z-position for the case of the tangential air inlet.....	50
Table 5.4 Zone of velocity distribution along z-position for the case of the bottom air inlet.....	50
Table 5.5 Zone of average velocity distribution along z-position for the three cases of the air inlet.....	50
Table 5.6 The measured dust concentration of ambient air.....	53
Table 5.7 Effect of pulse duration on the initial and residual pressure drops..	56
Table 5.8 Effect of the activating pressure differential on the initial and residual pressure drops.....	60
Table 5.9 Effect of nominal face velocity on the initial and residual pressure drops.....	65
Table 5.10 Effect of inlet concentration on the initial and residual pressure drops	69
Table 5.11 Effect of air inlet position on the initial and residual pressure drops.....	74
Table 5.12 Velocity distribution along z-position for the case of twin ceramic candles.	84

LIST OF FIGURES

	Page
Figure 4.1 Ceramic candle filter.....	22
Figure 4.2 Scanning Electron Microscope (SEM).....	24
Figure 4.3 Ultra pycnometer.....	25
Figure 4.4 Powder Tester.....	26
Figure 4.5 Air compressor.....	27
Figure 4.6 Screw feeder.....	28
Figure 4.7 Filter and Pressure Regulator Set.....	28
Figure 4.8 Pulse Air Tank.....	29
Figure 4.9 Solenoid valve.....	29
Figure 4.10 Diaphragm valve.....	30
Figure 4.11 Rotameter.....	31
Figure 4.12 Differential Pressure Transmitter.....	32
Figure 4.13 Signal Conditioner.....	33
Figure 4.14 Programmable Logic Controller(PLC).....	33
Figure 4.15 Data Logger.....	34
Figure 4.16 Diagram of electrical signal.....	35
Figure 4.17 Anemometer.....	36
Figure 4.18 Airborne Particle Counter.....	36
Figure 4.19 Schematic diagram.....	37
Figure 4.20 The position of inlet port.....	40
Figure 5.1 SEM micrographs of test calcium carbonate	42
Figure 5.2 Unstructured meshes from Gambit's operation on the vessel.....	43
Figure 5.3 A candle filter sub-divided into 8 layers and 4 quadrants for each layer.....	45
Figure 5.4 The 8 layers of the candle filter used in calculation	46
Figure 5.5 The local face velocity as a function of the height for each quadrant element in the case of the single candle filter.....	48

	Page
Figure 5.6 The average local normal face velocity as a function of the candle height for the case of the single candle.....	49
Figure 5.7 Experimental set-up	51
Figure 5.8 Chronology of experimental runs and corresponding P_I and P_R	53
Figure 5.9 Case A100 (24).....	54
Figure 5.10 Case A150 (25).....	54
Figure 5.11 Case A200 (26).....	55
Figure 5.12 The effect of pulse duration on outlet dust concentration.....	57
Figure 5.13 The effect of pulse duration on dust collection efficiency.....	57
Figure 5.14 The effect of pulse duration on dust penetration.....	58
Figure 5.15 Case B15 (4).....	59
Figure 5.16 Case B25 (19)	59
Figure 5.17 Case B35 (20).....	60
Figure 5.18 Effect of the activating pressure differential on outlet dust concentration.....	61
Figure 5.19 Effect of differential pressure on dust collection efficiency	61
Figure 5.20 Effect of the activating differential pressure on dust penetration	62
Figure 5.21 Case C1.216 (19).....	63
Figure 5.22 Case C1.724 (6)... ..	63
Figure 5.23 Case C1.989 (7).....	64
Figure 5.24 Effect of nominal face velocity on outlet dust concentration	66
Figure 5.25 Effect of nominal face velocity on dust collection efficiency....	66
Figure 5.26 Effect of nominal face velocity on dust penetration	67
Figure 5.27 Case D21.82 (19)	68
Figure 5.28 Case D43.64 (18).....	68
Figure 5.29 Case D65.45 (17)	69
Figure 5.30 Effect of inlet concentration on outlet dust concentration.....	70
Figure 5.31 Effect of inlet concentration on dust collection efficiency.....	70
Figure 5.32 Effect of inlet concentration on dust penetration.....	71
Figure 5.33 Case EBOTTOM (19).....	72

	Page
Figure 5.34 Case ETAN (15)	73
Figure 5.35 Case ETOP (14)	73
Figure 5.36 Effect of inlet position on outlet dust concentration.....	74
Figure 5.37 Effect of inlet position on dust collection efficiency.....	75
Figure 5.38 Effect of inlet position on dust penetration.....	75
Figure 5.39 Effect of nominal face velocity on dust penetration in size range of < 0.3 micron.....	77
Figure 5.40 Effect of nominal face velocity on dust penetration in size range of 0.3-0.5 micron.....	77
Figure 5.41 Effect of nominal face velocity on dust penetration in range of 0.5-0.7 micron.....	78
Figure 5.42 Effect of nominal face velocity on dust penetration in size range of 0.7-1.0 micron.....	78
Figure 5.43 Effect of nominal face velocity on dust penetration in range of 1.0-2.0 micron.....	79
Figure 5.44 Effect of nominal face velocity on dust penetration in range of 2.0-5.0 micron.....	79
Figure 5.45 Geometry of the system in front and side view.....	80
Figure 5.46 Local face velocity through each quadrant element as a function of height for the case of twin virgin candles.....	82
Figure 5.47 The average face velocity through each quadrant element as a function of height for the case of twin virgin candles.....	83

NOMENCLATURE

ε	=	void fraction
k_D	=	the permeability constant (m^2)
μ	=	the gas viscosity (Pa/s)
Q	=	the total volumetric flow rate (m^3/s)
A	=	Area of filtration (m^2)
Δx	=	the thickness (m)
ΔP	=	the pressure drop across a filter ($N.m^{-2}$, Pa)
R_D	=	the apparent Darcy flow resistance (m^{-1})
V_f	=	the superficial velocity of filtration (m/s)
k_1	=	the resistance of the filter
W	=	the mass of particles deposited per unit area of the filter
k_2	=	the specific resistance of the cake
N	=	the number concentration
C	=	the mass concentration
α	=	the volume fraction of fibers
η	=	Efficiency of particle collection
π	=	Penetration
C_{in}	=	Inlet gas concentration (kg/m^3)
C_{out}	=	Outlet gas concentration (kg/m^3)
ρ_g	=	Density of gas (kg/m^3)
d_p	=	Diameter of particles (m)
L	=	thickness of the ceramic candle filter (m)
G_k	=	the generation of turbulence kinetic energy due to the mean velocity gradients
G_b	=	the generation of turbulence kinetic energy due to buoyancy
Y_M	=	the contribution of the fluctuating dilatation in compressible turbulence to the overall dissipation rate
α_k and α_ε	=	the inverse effective Prandtl numbers for k and ε respectively
S_k and S_ε	=	user-defined source terms

μ	=	the laminar fluid viscosity
Δm	=	the thickness of the medium coefficient
v	=	the velocity normal to the porous face
B_f	=	dimensionless permeability ($B_f = \alpha/a^2$)
α	=	the permeability of the medium coefficient
C_2	=	the initial resistance factor
γ	=	porosity of medium



สถาบันวิทยบริการ
จุฬาลงกรณ์มหาวิทยาลัย

CHAPTER I

INTRODUCTION

1.1 Introduction

In industrial operations, air pollution has gained concern as a major problem in the last few decades, which seriously affects the environment. The particles issued from thermal power plants are on the order of micrometers in diameter. Emission of different kinds of corrosive or toxic solid or liquid into the atmosphere poses health issue. PM is produced as unwanted byproduct in various industrial processes such as thermal power plants, including those which use diesel oil as main fuel of diesel generators. Fine particles with diameters smaller than 2.5 micrometers are known to have the highest impact on human health because they can penetrate deeply into the human respiratory system. Therefore it is necessary to remove the particulate matter before it is emitted to the atmosphere and threatens the health of the power plant employees and residents in the surrounding communities. It is crucial to develop a high temperature particulate matter collecting system with very high collection efficiency.

Several techniques for reducing soot emission from diesel engines were investigated. Special attention has been given recent years to ceramic candle filters because they have good thermal resistance, chemical corrosion resistance and very high cleaning efficiency of the order of 99.9%. However, they are brittle, lack toughness, and can not be operated under large temperature swings. These ceramic filters offer a reasonable resistance to the flow of the gas, having to work with low filtration velocities and large filtration area. The regeneration mechanism of filter elements in gas filtration plays a very important role in the operation of the process. Development of advanced technologies in the design and operation of the pulse cleaning is one of the important tasks in order to increase the system reliability, to improve the filter service life and to increase the filtering performance. The candle filter is periodically cleaned during the build-up of the cake, which sees the pressure drops of the system increase and the filter is dedusted by a rapid reverse-flow (pulse back procedure) to remove the dust cake.

A fundamental understanding of the particle transport and deposition processes in a filter vessel is needed to improve the effectiveness and reliability of the filtration system. The residual pressure drop also increases with decreasing regeneration efficiency. In case the filter element is always regenerated with constant regeneration efficiency in the same positions the residual dust cake grows continuously. The present work will test an aerosol filtration unit using calcium carbonate known as “Turbo1” in the range of 0.8-1.0 micrometer in diameter.

In fact many interesting effects found in all practical investigations are not yet understood fully or in details. One of the most promising and a practical method is the employment of ceramic filters. Computational fluid dynamics (CFD) is frequently used to predict the flow behavior and simulate cake formation behavior since it offers low cost, low risk and ease of use. To achieve stable operation, it is necessary to identify the time-dependent relation between the pressure drop across the filter candles and deposited dust load, which was strongly influenced by the residual cake pattern during each filtration cycle. In the other words, determination of the process parameters involved in the calculation of pressure drop as a function of time, was supported by a commercially available software package that is well known “FLUENT”. These results have led to the need for a better understanding of the phenomenon of filtration of gas, effects of partial regeneration and dust loading distribution.

1.2 Objectives

This research work sets its objectives to investigate effect of operating conditions and location of inlet port on performance of filtration using a single ceramic candle filter.

1.3 Scope of research work

The scope of this research is as follows:

1. Carry out experiments of face velocity for filtration and the pressure differential for cleaning the candle filter (pulse duration) which influence to the system.

2. Simulate the flow distribution in a single ceramic system and indicate its effect on the dust deposition.
3. Compare calculated flow distributions between a twin ceramic candle filter system and a single ceramic candle system in the same condition.
4. Obtain a relation between the face velocity and dust collection efficiency with the initial (residual) pressure drop of the filter as parameter.

1.4 Procedure of the research

Experimental part

1. Explore and review the related researches
2. Design and construct the experimental setup
3. Carry out the experiments
4. Analyze and discuss experimental results

Simulation part

1. Construct mesh model of the system using GAMBIT operations.
2. Select a suitable CFD model for use with FLUENT.
3. Choose the experimental conditions to simulate the flow phenomenon inside the system.
4. Analyze and discuss the simulation results with respect to the experimental results.

Common part

1. Draw conclusion
2. Write the thesis

CHAPTER II

LITERATURE REVIEW

This chapter will review representative reports on the removal of the particulate matter emitted from the diesel engine using the ceramic candle filter. In particular, the experimental ones will be emphasized here. They are summarized as follows.

2.1 Experimental work

E. Schmidt [1] investigated the compression of dust cakes deposited on filter media by considering the various factors such as particle size distribution, particle charge, adhesive and cohesive properties, and pressure drop across filter element. The filter flow resistance and pressure drop nonlinearly increased with filtration time. There were jumps in pressure drop at a higher cleaning frequency, which is disadvantageous for filtration performance. They predicted the deviation in the time-dependent pressure loss functions from the linear trend. Compression results of different filter cakes were verified by local cake structure analyses, thereby indicating inadequate cake stability.

C.R.N. Silva, V.S. Negrini, M.L. Aguiar and J.R. Coury [2] studied the behavior of the filter during filtration at several superficial velocities with respect to the formation and removal of the deposited layer. The cake porosity decreased and the cake specific resistance increased with increase in the face velocity due to particle settling before reaching the filter. They suggested that the effect of porosity is greater than that of the average diameter of the particles. The estimated cake/fabric adhesion force was estimated as well as the effective distance between the particle surfaces.

K. Smolders and J. Baeyens [3] determined the baseline pressure drop and the effect of the cleaning cycles from the experimental results for various face velocities. The baseline pressure drop increased dramatically and the removal of dust cake was vital for a return to the virgin state. The jet-cleaning velocity was important. Too low velocities were insufficient to adequately clean the filter. In

practice, the total pressure consists of the baseline pressure drop and the pressure drop of the dust layer which is directly affected by the dust load. The equation through porous media can be used to calculate the proportionality factor for predicting the time between two cleaning cycles.

D. Achim and H.F. Umhauer [4] reported that, in order to use the rigid ceramic filter for removal of particles from gas streams at high temperature, a special type of optical particle counter was used to measure both the particle size and the particle concentration simultaneously. The key parameter of the regeneration process, in essence only the tank pressure, possessed the influence on the separation behaviour. In comparing two different rigid filter media, they showed that the membrane-coated ceramic filter media exhibited a better separation and regeneration behaviour than the fibre ceramic, open-pored filter media at identical operating conditions.

K. Chikao and A. Mana [5] captured dust by a ceramic filter using five elements made of different materials and structures. Injecting a high-pressure pulse clean air, the behavior of dust detachment was monitored by high speed video images. At the beginning, the pressure drop across the filter surface increased immediately because of the formation of a dense dust layer on the ceramic filter surface and was followed by a slowdown in the increase in rate due to the formation of a coarse layer. In the cleaning process, the pressure traces had different behaviors after the injection of cleaning air, depending on the filter permeability and the filter material.

D. Thomas et. al [6] studied the increase of pressure drop and filter efficiency (characterized by HEPA filters) during the filter clogging that was linked to both penetration profile inside the filter bed and the deposited structure. Within the range of their study, no influence of either the face filtration velocity or the aerosol concentration on deposit structure was detected. They found that larger particles induced a smaller pressure drop, which is linked to the specific surface area. They carried out not only experimental but also modeling study. Their model described the transition zone between depth filtration and cake filtration, and also penetration profile.

J.C. Ruiz et. al [7] studied the potentiality of symmetric ceramic filters for efficient air filtration, and pointed out the parameters to take into account for defining their properties. The evolution of particle penetration and pressure drop was investigated as a function of pore size, membrane thickness and air flow velocity. The test was carried out with three types of ceramic compositions to capture sodium chloride particles in the range of 0.01-0.7 micron in diameter. Besides, a linear variation of the pressure drop versus the face velocity and a logarithmic variation as a function of CAF thickness were observed, along with the influence of pore diameter on the penetration and pressure drop. Interesting result is a specific correlation between the characteristics of the filter media and the filtration velocity with an acceptable pressure drop.

D. Achim, M.V. Ferer , M. Pulkit , P. Djuranovic , K. Gerhard, and D.H. Smith [8] reported that rigid ceramic filter media widely used for the removal of particles from gas streams at elevated temperature tended to show patchy cleaning when the filter regeneration is incomplete. They also obtained reasonable comparison of the regeneration behavior between modeling and experimental results during the next filtration cycle. The fair agreement of modeling with experiment indicates that the model has real predictive capability for operational filter cleaning. Both filter conditioning and dust cake compression significantly influenced the operational performance of partially regenerated filter media.

J.H. Choi, S.J. Ha and H.J. Jang [9] studied the dust cake formation of fine fly ash from a coal-fired power plant on the ceramic filter by measuring the cake thickness using a laser displacement sensor. They experimentally investigated the different collection efficiencies to obtain dust streams of three different geometric diameters. The effects considered were the face velocity, the overall cake porosity and the pressure drop across the dust cake layers with respect to the variation in the particle size. It was found that cake porosity was strongly dependent on face velocity and mass loading but less dependent on the particle size. However, the correlation for many cases of experimental results in the form of the modified Endo equation expressed well the experimental results for fine particles.

Three filter media with very different physical properties are used in the work by S. Calle et. al. [10] A model describing the behavior of filter media

during clogging and cleaning cycles was developed. The model determined the cleaned fraction at each cycle with the assumption of patchy cleaning. In this study, they determined the pattern of a parameter representative of cleaning, namely the cleaned fraction, from experimental values of the residual pressure drop of a filter medium. However, it had limitation in case of certain treatment undergone by the medium to increase its regeneration capabilities. Moreover, it was based on the assumption of ideal patchy cleaning presenting either totally cleaned or non-cleaned areas, which is far from reality.

L. Andre, B. Marielle, M. Sonia and P. Eric [11] employed ceramic air filters (CAF) with different characteristics to investigate the influence of face velocity and CAF characteristics (porous volume, average pore diameter and thickness) on the values of aerosol penetration and pressure drop. The investigations were carried out by varying all the parameters influencing the filter performance. It was found that face velocity and CAF thickness had a strong influence on the collection efficiency. As expected, if the velocity increased or the thickness decreased, the filter efficiency decreased.

In 2003 C.B. Antonio et. al [12] carried out experiments under coal gasification conditions assuming that the gas velocity was constant and that the layers were formed in equal time interval. They used Darcy's law, the Happel cell model and the Carman-Kozeny equation in calculating the pressure drop during the build-up of dust filter cakes. The adjustment of the cake properties took into account through a constitutive equation the compressive stress which arose from the cumulative drag forces due to gas flow acting on the cake particles. The introduction of an empirical setting factor in the method brought the results closer to the experimental values in all three cases.

T.G. Chuah, C.J. Withers and J.P.K. Seville predicted and measured the pressure and velocity distributions in cylindrical and tapered rigid ceramic filters [13]. They used a cylindrical filter and a tapered filter to investigate both the filtration and the reverse flow process at normal conditions. The positions which were used to measure the pressure difference across the filter at various points along the filter length were the tapping tubes and micromanometer. For the numerical integration, a computer code is employed using FORTRAN 90. Their

work predicted the gas flow along the ceramic candle filter by assuming one-dimensional steady state flow. For the tapered filter, the model's prediction was shown to have good agreement with their experimental data. Moreover, the friction factor term which affects the momentum term in the model had a strong influence on the reverse flow case.

Y. Awni and Al-Otoom [14] predicted the deposited cake thickness on a ceramic candle filter by considering the number of dust particles deposited and their size distribution which were analyzed statistically. Using a random size distribution of the particles, the model predicted the manners in which the collection efficiency, the porosity, and the pressure drop across the filter change with the filtration time in several filter types. The model was shown to be capable of predicting the cake thickness and pressure drop which agreed with the experimental data.

2.2 CFD modeling

J.H Choi, S.M Kum, J.J Ahn, Y.C Bak, J.H Chung, and J.W Lee [15] carried out experimental work in a hot bench unit as well as simulation of the corresponding flow around the pulse nozzle at steady state. Operated at 400 to 600 °C, the bench scale unit employed oil combustion gas and fly ash. The simulation study was carried out using the FLUENT code and the k- ϵ turbulent model of Renormalization Group (RNG). In order to simulate the flow dynamics of the air pulse cleaning, the axial symmetric equation of Navier - Stokes at steady state was solved numerically. During the pulse cleaning, the performance of pulse cleaning was estimated by the measurement of the overpressure in the filter cavity. The pressure drop through the ceramic filter element was calculated using Darcy's law.

Ch. Stocklmayer and W. Hoflinger [16] applied mathematical modeling and computer simulation to the investigation of the influence of the two key parameters - the filtration velocity and the maximum pressure drop. It was found that the residual pressure drop of the filter mainly depended on the compressibility of the dust cake, which successively built up inside the filter medium with every new filtration cycle. Here the compressibility of the dust cake is defined by the relation between the cake compression pressure and withstandable stress. The

effects of the two operational parameters (the filtration velocity and maximum pressure drop) on these two variables (residual pressure drop and dust-cake compressibility) were investigated.

A. Aroussi, K. Simmons, S.J. Pickering [17] examined, through experimental and computational modeling, the deposition process and the factors that affect the build-up of the filter cake of a single filter element in cross-flow and parallel flow. For both flow regimes the validation of the computational study was adequate and a method was developed for predicting the filter cake growth using CFD data. An experimental and computational investigation was also conducted into the particle trajectories in the vicinity of the single filter element in cross-flow and parallel flow. The filter cake formed on the filter element operating predominantly in cross-flow has the same particle size distribution as that in the approaching gas stream. Deposition is essentially uniform. Whether the flow is predominantly parallel to the filter element, the filter cake will be size-differentiated according to vertical and circumferential positions on the filter face. It is likely that the cleaning process will significantly influence the cake composition.

T. Wiwut et.al in collaboration with Hosokawa Powder Technology Research Institute (HPTRI) carried out the simulation and analysis of high-efficiency twin-ceramic-candle filtration process for high-temperature emission gas [18], the simulation results are classified into two main groups: the case of virgin candle filters with clean air, and the case of cyclic operation with dust-laden air. In the former case, as the gas flow rate or the temperature increases, the characteristic pressure drop will directly increase in a linear manner. In this case the effect of the gas flow rate is more important than the effect of the gas temperature. The effect of the candle height on the local face velocity through the clean candles is more significant than that of the quadrant position. In the latter case, it is experimentally observed that a permanent cake is formed on the surface of the twin candles after the pulse-jet system has worked for a period of time. When the filter was pulse-cleaned, only the temporary cake was removed but the permanent cake still remained. It can be considered that the local cake thickness increases as a linear function of the local face velocity. Interestingly,

approximately 20 % of the temporary cake on the adjacent candle was removed compared with its permanent cake thickness. Similar to the case of the virgin candle filter, the local face velocity was shown in 4 zones along the height of the candle filters. As in the case of the virgin filter, the higher the axial position along the filter, the higher the simulated local face velocity. By the way, the face velocity in each quadrant of the same layer did not show any significant difference.



สถาบันวิทยบริการ
จุฬาลงกรณ์มหาวิทยาลัย

CHAPTER III

THEORY

The capture of aerosol particles by a ceramic candle filter is the most common method for air cleaning at high temperature. The particle will deposit and form a powder layer, commonly known as cake. Therefore we should know the properties of ceramic filters for predicting the mechanisms of collection and how the resistance to airflow changes with filter properties and particle size. The characteristics of the ceramic filter include true density, porosity and pore size.

3.1 Filtration Phenomena

In all types of dust collection equipment, selected forces interact with particles to separate them from the gas stream and to make the particles collide with the collector such as cyclone, ESP, scrubber and air filter. These forces are basically tools that can be used for separating particles from the gas stream and all of these conventional force and corresponding collection mechanisms are strongly dependent on the particle size. In some control devices, none of the collection mechanisms are highly efficient for the particle size of interest. These particles are thus classified as "difficult-to-control" due to the inherent limitations of the collection mechanisms. This inherent weakness, which can be seen in a number of studies of actual sources, reveals that stationary sources generating high concentrations of particles in the 0.1 to 0.5 micrometer range may be an especially challenging control problem.

3.1.1 Face velocity [19]

The average velocity of fluid moving through a pipe is defined as the volumetric flow rate of that fluid divided by the cross-sectional area. In monophasic flow, it is equal to the mean velocity of the fluid. In multiphase flow, it is not a physically real velocity but is a convenient parameter for analysis. A certain fluid-flow regime is characterized by swirling as the fluid moves along the pipe. This characteristic makes turbulent flow an efficient flow regime for the pickup and transport of solids. Turbulent flow is characterized by random, irregular, locally circular currents, or vortices. It occurs in long straight pipes when the Reynolds number is above a critical value, corresponding to a high flow rate. Below this value,

the flow is laminar or in the transition zone. For turbulent flow in straight pipes, the velocity increases from zero at the inner wall of the pipe, passes through a thin adjacent layer of laminar flow to reach a near constant value over most of the pipe cross-section. The term superficial velocity is also commonly used. The superficial gas velocity is defined as

$$U_{fs} = \frac{Q_f}{A} \quad (3.1)$$

Similarly, the superficial particle velocity is defined as

$$U_{ps} = \frac{Q_f C_p}{A} \quad (3.2)$$

The fraction of pipe cross-sectional area available for the flow of gas is usually assumed to be equal to the volume fraction occupied by gas, that is, the voidage or void fraction ε . The fraction of pipe area available for the flow of solids is therefore $(1 - \varepsilon)$. And so, the physical gas and particle velocities become,

$$U_{fs} = \frac{Q_f}{A\varepsilon} \quad (3.3)$$

$$U_{ps} = \frac{Q_f C_p}{A(1 - \varepsilon)} \quad (3.4)$$

If pressure drop across a sample is present, transport of the gas includes convective transport, where the gas flows through the sample, depending on the direction of the convective gas flow. Permeability to convective gas flow is given by Darcy's law.

$$k_D = \left(\frac{\mu Q}{A} \right) \left(\frac{\Delta x}{\Delta P} \right) \quad (3.5)$$

It is preferable to present the pressure drop/flow rate results in terms of an apparent flow resistance defined as

$$R_D = \left(\frac{A\Delta P}{\mu Q} \right) \quad (3.6)$$

Usually, the flow in porous media is calculated using Darcy's law. It shows the volumetric flow rate is a function of the flow area, elevation, fluid pressure and proportionality constant. It may be stated in several different forms depending on the flow conditions. Since its discovery, it has been found valid for any Newtonian fluid. If the flow is isothermal, the relationship between filtration velocity and pressure is given as Equation (3.7)-(3.8) Moreover permeability is not constant throughout the filter wall. It can change suddenly near the collection surface.

Darcy's law

$$\vec{v} = -\frac{\kappa_f}{\eta} \nabla P \quad (3.7)$$

$$v_w = \frac{\kappa_f}{2\eta r_0 \ln\left(\frac{r_1}{r_0}\right)} \frac{P^2 - P_o^2}{P} \quad u_r = \frac{\kappa_f}{2\eta r_1 \ln\left(\frac{r_1}{rr_0}\right)} \frac{P^2 - P_o^2}{P} \quad (3.8)$$

3.1.2 Pressure drop [20]

The flow behavior in a system is quite complex. The pressure drop represents the total drag forces exerted by all fibers. The pressure drop is given as

$$\Delta P = \frac{\mu t U_o f(\alpha)}{d_f^2} \quad (3.9)$$

The total pressure drop in the ceramic candle filter (ΔP_T) can be considered as the sum of the pressure drops through the ceramic (ΔP_F) and through the formed powder cake (ΔP_C). This sum can be written as Equation (3.10)

$$\Delta P_T = \Delta P_F + \Delta P_C = k_1 V_f + k_2 V_f W \quad (3.10)$$

The porosity of filtration cake is a very important structural parameter, as the pressure drop in the filter and the necessary force for the removal of the deposited powder layer, depend on it. The average porosity of a cake obtained from the equations could be used for estimating the medium porosity with reasonable accuracy. Of the equations investigated, the well known Ergun correlation was the one which presented the best results and will be used here for estimating cake porosity. For a particle layer of thickness L , composed of particles with mean diameter d_p , the Ergun correlation for the pressure drop can be written as Equation (3.11)

$$\frac{\Delta P}{L} = \frac{150(1-\varepsilon)^2}{\varepsilon^3} \frac{\mu V_f}{d_p^2} + \frac{1.75(1-\varepsilon)}{\varepsilon^3} \frac{\rho_g V_f^2}{d_p} \quad (3.11)$$

where ε is the mean porosity of the layer and μ and ρ_g the gas viscosity and density, respectively. If one considers a very high collection efficiency, the mass of particles deposited on the filter is:

$$M = Qt = LA\rho_p(1-\varepsilon) \quad (3.12)$$

where Q is the mass flow rate of particles of true density ρ_p , A : filtration area and t the filtration time. Therefore:

$$L = \frac{(Qt)}{(A\rho_p(1-\varepsilon))} \quad (3.13)$$

If the second term in Equation (3.11), namely, the inertial term, is assumed to be negligible, the resulting expression is known as Darcy's law. Substituting this in Eq. (3.12) and admitting incompressible cake, one can obtain an expression for the pressure drop in the cake, ΔP_C . Comparing this with Equation (3.11), it becomes:

$$k_2 = \frac{150(1-\varepsilon)}{\varepsilon^3} \frac{\mu}{\rho_p d_p^2} \quad (3.14)$$

where, k_2 , the specific resistance of the cake, is assumed to be constant. It can be seen that k_2 depends on the porosity (ε) and, as mentioned previously, the parameter were generally unknown. Due to this, the theoretical equations to estimate k_2 were not usually used, experimental values being used instead.

The experimental k_2 can be estimated from the increase in the pressure drop in the filter between time 1 and time 2 ($\Delta P_2 - \Delta P_1$) due to the mass of the powder deposited in this time interval ($M_2 - M_1$). This can be written as: [21]

$$k_{2,\text{exp}} = \frac{A (\Delta P_2 - \Delta P_1)}{V_f (M_2 - M_1)} \quad (3.15)$$

3.1.3 Pulse Jet Cleaning

The reverse cleaning velocity through the filter wall varies somewhat along the filter axis, depending on volumetric flow rate of the cleaning gas, filter size, filter permeability, etc. The total pressure of the pulse-jet needed to be 5 MPa to acquire enough cleaning flow. This investigation evaluated the effect of these factors in the pulse jet system. Dust particles collect on the external surface of the filter, and the dust layer is removed by on-line pulse jet cleaning. The cleaning system is also important. To reduce the thermal shock during filter cleaning, the pulse jet should have the highest entrainment ratio while retaining sufficient cleaning velocity. An axisymmetrical or three dimensional simulation requires some unconfirmed models such as the k - ε turbulence model, distribution of permeability and heat transfer in porous media, all of which may cause in appropriate results. Some researchers investigated a simple model and confirmed the results with some experiments, and estimated the required operating condition in the hot gas filtration. In pulse jet cleaning the pressure can be changed. There is a suggestion that filter performance is controlled by the pressure difference in the dust cake. This was not confirmed in their experiments, in which pressure loss recovery improved with cleaning velocity.

Therefore they assumed filter permeability and set the pulse pressure to obtain a particular cleaning velocity. The exit pressure at the nozzle was then approximately the cleaned gas pressure. In order to measure the pressure inside the filter elements during cleaning, measuring devices were added to a pilot plant. In addition to a sufficiently negative differential pressure the cleaning effectiveness is governed by the duration of the reverse flow. At present, additional tests are to be carried out in order to determine, on the basis of the findings so far, the impact of such parameters as pulse pressure, reverse flow duration and reverse flow pressure drop on the cleaning effectiveness.

3.1.4 Collection efficiency

In dust collector system, particles will be separated from a gas stream by settling or impact and trapped at the medium. The particle collection efficiency of the system can be expressed in the form of dust separated and collected by that instrument. On the other hand, it can be expressed in the form of dust discharged from the system called penetration. When ceramic candle filters are used for filtration, their ability to collect particles is usually characterized by their efficiency of collection. A fraction of entering particles is retained by the ceramic filter. This efficiency can be expressed either in terms of particle count collection efficiency η or a mass collection η_m . Generally, mass efficiency is higher than the count efficiency. [22]

$$\eta = \frac{N_{in} - N_{out}}{N_{in}} \quad (3.16)$$

$$\eta_m = \frac{C_{in} - C_{out}}{C_{in}} \quad (3.17)$$

Air-cleaning equipment, on the other hand, is usually characterized in terms of its penetration π , the fraction of entering particles that exit or penetrate the ceramic candle filter.

$$\pi = \frac{N_{out}}{N_{in}} = 1 - \eta \quad (3.18)$$

$$\pi_m = \frac{C_{out}}{C_{in}} = 1 - \eta_m \quad (3.19)$$

At really high efficiencies, large changes in penetration are associated with small changes in efficiency. For example, penetration changes by a factor of 10 when efficiency change by less than 1%, from 99 to 99.9 %. The velocity of the air at the face of a ceramic candle filter, just before the air enters, is called the face velocity, U_0 .

$$U_0 = \frac{Q}{A} \quad (3.20)$$

A is the cross-sectional area of the ceramic candle filter exposed to the entering airstream. Inside a ceramic candle filter, the air velocity U is significantly greater than U_0 because the volume available for air passage is reduced by the volume of fibers, so that

$$U = \frac{Q}{A(1-\alpha)} \quad (3.21)$$

where α is the volume fraction of fibers, called the packing density or solidity. For fibrous filters, α is typically between 0.01-0.3

$$\alpha = \frac{\text{fiber} \cdot \text{volume}}{\text{total} \cdot \text{volume}} = 1 - \text{porosity} \quad (3.22)$$

3.2 Computational Fluid Dynamics (CFD)

Computational Fluid Dynamics (CFD) is the science of predicting fluid flow, heat transfer, chemical reactions, and related phenomena by solving mathematical equations that represent physical laws, using a numerical process.

FLUENT is a common CFD solver for complex flows. It can accurately predict laminar, transitional and turbulent flows with completely unstructured mesh flexibility and solution-based mesh adaptation. FLUENT solvers are based on the finite volume method. Domain is discretized into a finite set of control volumes or

cells. General conservation (transport) equations for mass, momentum, energy, etc., are integrated numerically.

The basic steps are as follows:

- | | | |
|---|---|--|
| 1. Define the modeling goals. | } | Problem Identification
and Pre-Processing |
| 2. Identify the domain that will model. | | |
| 3. Design and create grid. | } | Solver Execution |
| 4. Set up the numerical model. | | |
| 5. Compute and monitor the solution. | } | Post-Processing |
| 6. Examine the result. | | |
| 7. Consider revision to the model | | |

3.2.1 Differential equations

In mathematics, a differential equation is an equation that describes a prescribed relationship between a set of unknowns or dependent variables which are to be regarded as a known function and its (ordinary or partial) derivatives. In practice the "known function" is usually presumed to exist, although rigorously establishing this may require technique from topology. The order of a differential equation is given by the maximum number of times the supposed dependent variables in it has been differentiated.

3.2.2 Boundary conditions

Boundary conditions are needed by every numerical computational method for solving partial differential equations, in the form of integral equation. It can be applied in many areas of engineering and science.

3.2.3 Geometries

First it is assumed that the flow regime in the ceramic filter system considered is defined by the Reynolds number. It can be concluded that the inertial effects are negligible. The most popular turbulence model in use for engineering applications is the k- ϵ model where the scalar variables k- ϵ represent the kinetic energy of turbulence and its dissipation rate, respectively. The following equations describe the steady-state conservation of mass and momentum. The RNG k- ϵ model was derived using a rigorous statistical technique (called renormalization group theory). It is similar in

form to the standard k- ε model. The RNG model has an additional term in its ε equation that significantly improves the accuracy for rapidly strained flows. The effect of swirl on turbulence is included in the RNG model, thereby enhancing accuracy for swirling flows. Using the porous model, a resistance to flow is added as if there were a porous solid that allows some fluid through. When defining the boundary conditions of a porous model, the viscous resistance and porosity need to be specified.

$$\frac{\partial}{\partial t}(\rho k) + \frac{\partial}{\partial x_i}(\rho k u_i) = \frac{\partial}{\partial x_j} \left(\alpha_k \mu_{eff} \frac{\partial k}{\partial x_j} \right) + G_k + G_b - \rho \varepsilon - Y_M + S_k \quad (3.23)$$

$$\frac{\partial}{\partial t}(\rho \varepsilon) + \frac{\partial}{\partial x_i}(\rho \varepsilon u_i) = \frac{\partial}{\partial x_j} \left(\alpha_\varepsilon \mu_{eff} \frac{\partial \varepsilon}{\partial x_j} \right) + C_{1\varepsilon} \frac{\varepsilon}{k} (G_k + C_{3\varepsilon} G_b) - C_{2\varepsilon} \rho \frac{\varepsilon^2}{k} - R_\varepsilon + S_\varepsilon \quad (3.24)$$

3.2.4 Model description

Methods of calculating the turbulent viscosity and model constants will be presented separately for each model. The features that are essentially common to all models will follow, including turbulent production, generation due to buoyancy, accounting for the effects of compressibility, and modeling heat and mass transfer.

The porous media model incorporates an empirically determined flow resistance in a region of the model defined as "porous". In essence, the porous media model is nothing more than an added momentum sink in the governing momentum equations.

Momentum Equations for Porous Media

Porous media are modeled by the addition of a momentum source term to the standard fluid flow equations. The source term is composed of two parts.

- I. A viscous loss term (Darcy, the first term on the right-hand side of Equation (3.11))
- II. An inertial loss term (the second term on the right-hand side of Equation (3.11))

$$S_i = -\left(\frac{\mu}{\alpha} v_i + C_2 \frac{1}{2} \rho |v| v_i\right) \quad (3.25)$$

Darcy's Law in Porous Media

In laminar flows through porous media, the pressure drop is typically proportional to the velocity and the constant C_2 can be considered to be zero. Ignoring convective acceleration and diffusion, the porous media model then reduces to Darcy's Law:

$$\nabla p = -\frac{\mu}{\alpha} \vec{v} \quad (3.26)$$

Assuming isotropic porosity and single phase flow, the general volume-averaged mass and momentum conservation equations are as follows:

$$\frac{\partial(\gamma \rho \vec{v})}{\partial t} + \nabla \cdot (\gamma \rho \vec{v} \vec{v}) = -\gamma \nabla p + \nabla \cdot (\gamma \vec{\tau}) + \gamma \vec{B}_f - \left(\frac{\mu}{\alpha} + \frac{C_2 \rho}{2} |\vec{v}|\right) \vec{v} \quad (3.27)$$

The last bracket in Equation (3.27) represents the viscous and inertial drag forces imposed by the pore walls on the fluid.

3.2.5 Numerical method [23]

The numerical solution of a differential equation consists of a set of numbers from which a distribution of the dependent variable ϕ can be constructed. The numerical analyst and the laboratory experimenter both must remain content with only a finite number of numerical values as the outcome, although this number can, at least in principle, be made large enough for practical purposes. The physical constants of the fluid phase are set to those of air. The flow of air through the housing is modeled using a CFD FLUENT code. In this code, the domain is discretized into arbitrary unstructured tetrahedral. The discretized form of the governing equation such that the conservation principles are obeyed on each tetrahedral. The resulting discretized equations for the variable are given by Equation (3.28).

$$a_p \phi_p = \sum_{nb} a_{nb} \phi_{nb} + S_p \quad (3.28)$$

The summation in the above equation extends over all the neighboring cells of cell p . The SIMPLE algorithm is used for coupling the continuity and momentum equations. All calculations will be obtained using a second order upwind scheme for spatial discretization.



สถาบันวิทยบริการ
จุฬาลงกรณ์มหาวิทยาลัย

CHAPTER IV

EXPERIMENTAL

Filtration led to formation of a dust cake which was difficult to clean. This resulted in a high rate of increase in pressure drop for the filter and may have contributed to failure of filter components due to excessive forces. The present work was carried out using a ceramic candle filter at room temperature and atmospheric pressure. Coated calcium carbonate particles were used as test powder dispersed in the air. The material was very fine (mean particle diameter of 1.6 μm), with an apparent density of 850 kg/m^3 .

4.1. Materials

4.1.1. Test dust

The coated calcium carbonate used in this work was known by its commercial name as Turbo1 and was provided by Lime Quality Co., Ltd.

4.1.2. Ceramic candle filter



Figure 4.1 Ceramic candle filter

Table 4.1 Dimension of a ceramic candle filter

	Unit	Size
Inside diameter	mm	90
Outside diameter	mm	120
Length	mm	1000

Table 4.2 The chemical composition of ceramic candle filter

Composition	Unit	Value
Al ₂ O ₃	%	46
SiO ₂	%	54
Porosity	-	0.85
Density	g/cm ³	0.25
Specific heat	J/kg K	1050

Ceramic candle filter elements were provided by Hosokawa Powder Technology Research Institute and the properties and dimensions were as shown in Tables 4.1 and 4.2.

4.1.3. Instruments

The physical properties of dust particles such as particle size distribution, true density, flowability and floodability were measured for use in designing dust removal equipment. The relevant instruments were divided in two groups.

4.1.3.1. The instruments used to determine the physical properties were as follows.

สถาบันวิทยบริการ
จุฬาลงกรณ์มหาวิทยาลัย

4.1.3.1.1. Scanning Electron Microscope (SEM)



Figure 4.2 Scanning Electron Microscope (SEM)

The dimension and shape of particles were observed via SEM. The images were shown photographically. The SEM device used in this work was shown in Figure 4.1. The specimen was elaborately prepared by grinding as-received solid agglomerates in a granite mortar. An appropriate amount of the coated calcium carbonate was deposited on the carbon film to ensure its uniform dispersion. The specimen was brought to coat with gold and then the specimen was loaded into the sample chamber. Waiting for the attainment of vacuum condition and steady state inside the chamber took about 30 minutes.

4.1.3.1.2.Ultrapycnometer



Figure 4.3 Ultra pycnometer

An ultrapycnometer was used to measure the true volume and density of powders and porous materials. The technique employs Archimedes principle of fluid displacement and Boyle's law to determine the true volume. The displaced fluid is helium gas, which can penetrate into the finest pore to assure maximum accuracy. The true density of the sample is determined by measuring the pressure difference when a known quantity of helium under pressure is allowed to flow from a precisely known reference volume into a sample cell containing the solid or powder materials.

4.1.3.1.3.Laser Particle Size Distribution Analyzer

A Laser Particle Size Distribution Analyzer, Mastersizer-S model, was used to find the size distribution of the particles. It can be used to find the size distribution of particles in the range of 0.05-88 micron, 0.50-880 micron and 4.2-3480 micron.

4.1.3.1.4.Powder Tester

The Powder Tester (type PT-N) was produced by Hosokawa Micron Corp. (Figure 4.4). It was used to estimate the flowability and floodability of the powder. The measured characteristic properties were divided in two groups as follows:



Figure 4.4 Powder Tester

- Mechanical properties
 - Angle of Repose
 - Angle of Spatula
 - Angle of Fall
 - Angle of Difference
 - Compressibility
 - Dispersibility
 - Cohesiveness
- Derived properties
 - Aerated Bulk Density
 - Packed Bulk Density
 - Uniformity

4.1.3.2. The devices used to carry out experiments were as follows

4.1.3.2.1. Air Compressor

The compressor takes in air at atmospheric pressure and delivers it at a higher pressure. It was produced by PUMA (model UB150-500), with 15 horsepowers. The maximum pressure is 135 PSI, and it can generate compressed air at 2617 L/min.



Figure 4.5 Air compressor

The air compressor was connected to two lines: one for feeding compressed air to disperse agglomerated dust discharged from the twin screw feeder and the other for regeneration of the ceramic candle filter.

4.1.3.2.2. Screw feeder

The twin concave screw feeder was produced by K-Tron Feeder (type K-CV-KT20). The feed range is 0.1-9 dm³/hr for the short pitch screw. It was used for feeding test powder at a constant volumetric flow rate.



Figure 4.6 Screw feeder

To facilitate the flow of very fine (cohesive) powders such as used in the experiments, several measures were taken: the shaft of the screw conveyor was equipped with mixer-blades (to break agglomerates), the dust container was vibrated gently and a small amount of compressed air (2 bar) was added to the system.

4.1.3.2.3. Filter and Pressure Regulator Set



Figure 4.7 Filter and Pressure Regulator Set

4.1.3.2.4.Pulse Air Tank



Figure 4.8 Pulse Air Tank

The volume of the pulse air tank was 30 liters. It was used for storing the compressed air for the regeneration system.

4.1.3.2.5.Solenoid valve



Figure 4.9 Solenoid valve

It was made by Goyen, Australia (model RCA302). Solenoid valves are devices that use a solenoid to control valve activation. The solenoid valve control system has a

switching output stage for controlling the solenoid valve, a timer arrangement for preselecting a valve opening time, and an arrangement for preselecting an opening pressure over the valve.

4.1.3.2.6. Diaphragm valve

It was made by Goyen, Australia (model RCA25DD001). The valve was used for fluid control or for shutting off pipeline fluids or gasses from coming in contact with the operating parts of the valve. (Figure 4.10).



Figure 4.10 Diaphragm valve

4.1.3.2.7. Rotameter

A rotameter is a device that measures the flow rate of liquid or gas in a closed tube. The most common type of variable-area meter is the rotameter (Figure 4.11), consisting of a float free to move up and down in a vertical, tapered tube through which the fluid to be measured passes. The float position is usually calibrated and indicated by masks on the tube in terms of volumetric flow rate at standard atmospheric pressure.



Figure 4.11 Rotameter

For operation with a fluid density or at a gas pressure other than the standard, Q_{STP} , the true flow rate, expressed in terms of air at standard conditions, is given by [21]

$$Q_{STP} = (\text{indicated } Q) \left(\frac{\rho_r}{\rho_{STP}} \right)^{\frac{1}{2}} = (\text{indicated } Q) \left(\frac{P_r}{P_{STP}} \right)^{\frac{1}{2}}$$

The effect of a change in viscosity depends on the design of the float and its position in the tube.

4.1.3.2.8. Differential Pressure Transmitter

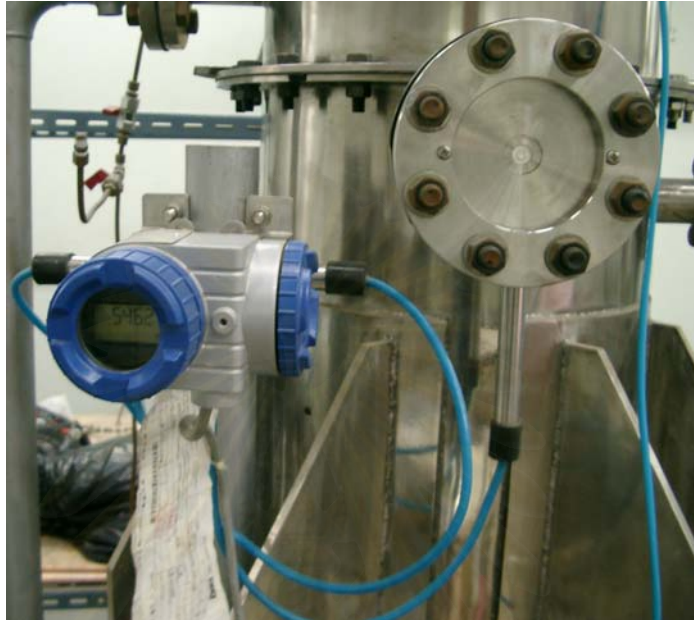


Figure 4.12 Differential Pressure Transmitter

It is one of several transducers designed to measure the pressure difference between two points in a process and transmit a signal proportional to this difference without regard to the absolute pressure at either point. The one used is a remote seal differential pressure transmitter (model FHDB03V4-PDDYY-YO). The process connection is $\frac{1}{4}$ -18NPT in flange size of JIS 10K 80A. The span limit is in the range of 3.2 – 320 mbar. The probe was produced by Fuji Electric Instruments Co, Ltd.

สถาบันวิทยบริการ
จุฬาลงกรณ์มหาวิทยาลัย

4.1.3.2.9. Signal Conditioner



Figure 4.13 Signal Conditioner

Fuji Electric Instruments Co, Ltd. produced the used signal conditioner (type PWBDY-01BY01). The input and output signals are DC 4-20 mA, DC 0-5 V respectively. The power supply was AC 85-264 V.

4.1.3.2.10. Programmable Logic Controller (PLC)



Figure 4.14 Programmable Logic Controller (PLC)

The microprocessor-based industrial control system communicates with other process control components through data links. It is used in process control for simple switching tasks, PID control, complex data manipulation, arithmetic operations, timing and process and machine control.

4.1.3.2.11. Data Logger



Figure 4.15 Data Logger

This data logger was made by WISCO (model ML21/256k). Most modern data loggers are miniature digital computers that sample the data inputs and digitize the results at regular intervals, apply preset calibrations to convert from raw voltages or currents into measured variables, compute statistics such as mean values and variances, and record the results either internally in memory, locally on attached storage media, or transmit the results to a remote user or computer site via telephone line or radio link. Those data loggers that record the results in memory must be periodically serviced.

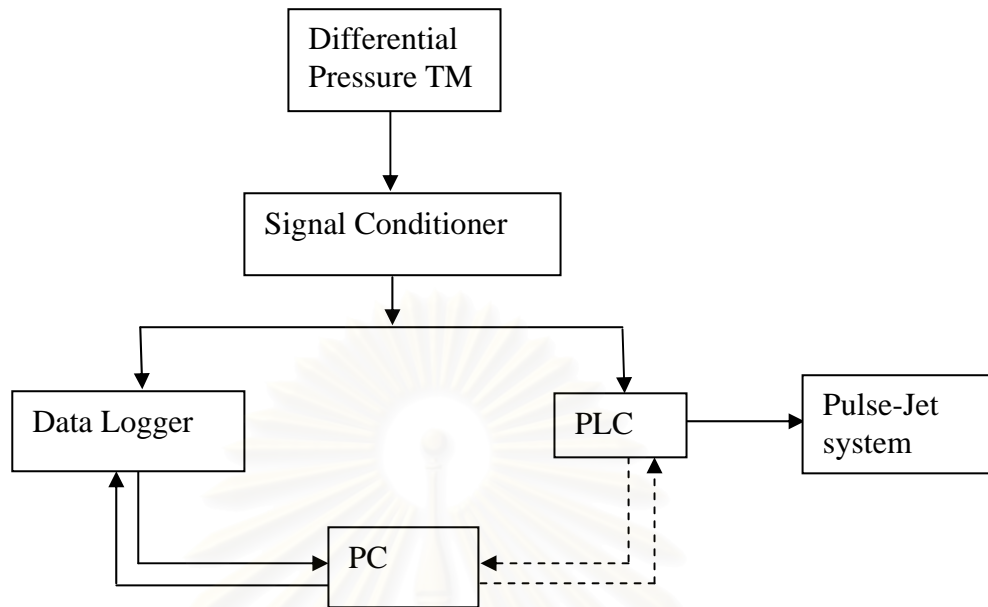


Figure 4.16 Diagram of electrical signal

The present pulse cleaning system consists of a compressed air reservoir (500 liter volume). It can be controlled by using electric signal. It has a storage tank for compressed air (6 bargauge). The air pressure can be regulated between 3-6 bar. It has an other storage tank at the top of chamber to store air at 5 bar for removing dust. Timer and PLC are used to control the pulse duration time, interval time and pressure differential for the cleaning line. In the system, the routes for transferring and recording the differential pressure data are shown in Figure 4.16. In Figure 4.16, the Differential Pressure Transmitter transmits a proportional 4 to 20 mA signal which is converted to a signal of 0-5 Volt by the signal conditioner. Output signal from the signal conditioner is sent to the data logger and to the PLC. The conditions that we want can be imported or exported into the system from the PC to the PLC or Data Logger

4.1.3.2.12. Anemometer



Figure 4.17 Anemometer

It is an instrument for measuring the speed of the wind.

4.1.3.2.13. Airborne Particle Counter



Figure 4.18 Airborne Particle Counter

removed from the ceramic candle filter in this cleaning procedure fell into the hopper. In practice, a residual layer of solid should remain where the cake tear off. These aspects lead to the presence of a residual pressure drop on the newly cleaned filter.

Table 4.3 The main conditions carried out in this work

	Unit	Value
Pulse duration	ms	100
Pressure differential	Pa	245
Face velocity	m/min	1.216
Concentration	g/m ³	21.82
Position		Bottom

The main experimental conditions investigated are shown in Table 4.3. The effects of interest in this work could be divided into 5 cases. The code for showing the results in each run was summarized in Table 4.4. Some conditions were changed while investigating the effects shown in Table 4.3.

Table 4.4 The experimental conditions investigated in this work

Pulse duration(ms)			Pressure differential(mmAq)			Face velocity(m/min)		
100	150	200	15	25	35	1.216	1.724	1.989
A100	A150	A200	B15	B25	B35	C1.216	C1.724	C1.989
Concentration(g/m ³)			Port position					
21.82	43.64	65.45	Bottom	Tangential	Top			
D21.82	D43.64	D65.45	EBOTTOM	ETAN	ETOP			

Note the unit of pressure drop was converted from millimeter of water column to Pascal as shown in Table 4.5

Table 4.5 The converted unit from millimeter water to Pascal

Pressure differential	
mmAq	Pa
15	147
25	245
35	343

4.3. Effect investigated

4.3.1. The effects were described below.

4.3.1.1. Effect of the pulse duration

During the build-up of the filter cake, the pressure drop across the filter element gradually increased, making a regeneration of the filter medium indispensable. The observed pressure drop immediately after each regeneration is called the residual pressure drop. The cleaning procedure consisted of 3 different values of pulse duration, 100, 150 and 200 ms respectively. The duration time is the opening of diaphragm valve for cleaning a ceramic candle filter.

4.3.1.2. Effect of pressure differential activated cleaning

The filtration pressure differential was the increased pressure from the initial pressure drop which was varied as three different values in the unit of millimeter water as shown in Table 4.4 and Pascal as shown in Table 4.5. This effect was implemented and controlled by the PLC.

4.3.1.3. Effect of nominal face velocity

Three different filtration velocities (m/min) as shown in Table 4.4 were investigated. Moreover, the filtration process continues until the pressure drop reaches a maximum (when the pressure drop rise exceeded 15, 25 and 35 mmA) as measured by the differential pressure transmitter.

4.3.1.4. Effect of inlet dust concentration

In Table 4.4, the inlet concentration was varied in three cases. This concentration was adjusted using the screw feeder. All data was recorded by the data logger.

4.3.1.5. Effect of inlet port position

The effect of inlet port position as shown in Figure 4.20 was investigated: bottom axial, bottom tangential and top radial inlets.



Figure 4.20 The 3 positions of the inlet port

4.3.2. The experimental procedure

4.3.2.1. Prepare enough dust to carry out a run and set the value of pulse duration wanted.

4.3.2.2. Adjust the pressure regulator to yield the wanted gas flow rate and then turn off the regulator.

4.3.2.3. Collect data for calculating the differential pressure to input into the PLC.

4.3.2.4. Calculate the set value of the pressure differential pressure necessary to initiate candle filter cleaning.

4.3.2.5. Turn on the regulator.

4.3.2.6. Feed dust via the twin screw feeder.

4.3.2.7. Collect the data on the data logger.

4.3.2.8. Wait until 1000 cycles have been reached, then stop the twin screw feeder.

4.3.2.9. Shut off the regulator.

4.3.2.10. Take out and clean the candle filter thoroughly.



สถาบันวิทยบริการ
จุฬาลงกรณ์มหาวิทยาลัย

CHAPTER V

RESULTS AND DISCUSSION

5.1. Results and discussion of the results on the properties of dust

5.1.1. Determination of particle size distribution (PSD)

The PSD of test dust which was dispersed by water was determined with a Laser Particle size distribution analyzer as shown in Appendix B. The data was plotted as cumulative volume versus particle diameter. The mean diameter of the particle was in the range of 0.8-1.02 micrometer.

5.1.2. Determination of particle shape

For the test calcium carbonate, the shape of the dust was obtained using SEM micrographs, as shown in Figure 5.1. The shape of agglomerated dust is irregular.

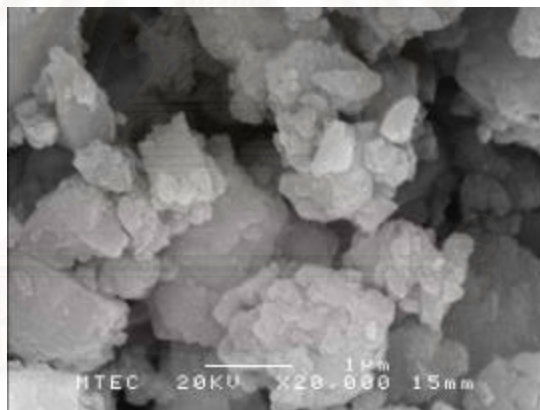


Figure 5.1 SEM micrographs of test calcium carbonate

5.1.3. Determination of true density

The average true density of calcium carbonate measured from Ultracycrometer 1000 is 2.6995 g/cm^3 as shown in Appendix B.

5.1.4. Determination of flowability and floodability

The powder tester could calculate the flowability of the dust by automatic calculation of the instrument. The test result on the degree of flowability is normal. Another result of the powder tester was the floodability index. The latter index was

fairly high and it means that the dust tended to flush, thereby indicating a good capability to spread. The results are shown in Table B.2 and B.3 [Appendix B]

5.2. Simulation of steady clean air flow through virgin filters

Computational fluid dynamics (CFD) has a great potential to predict the flow field characteristics inside a chamber as well as the corresponding pressure drop. The pressure drop across the chamber is an important parameter in the evaluation of chamber performance. This computer simulation model enables the simulation of the 3-dimensional isothermal fluid flow. The filter medium is defined by flow resistance. The numerical calculation was made with a fine numerical grid as shown in Figure 5.2

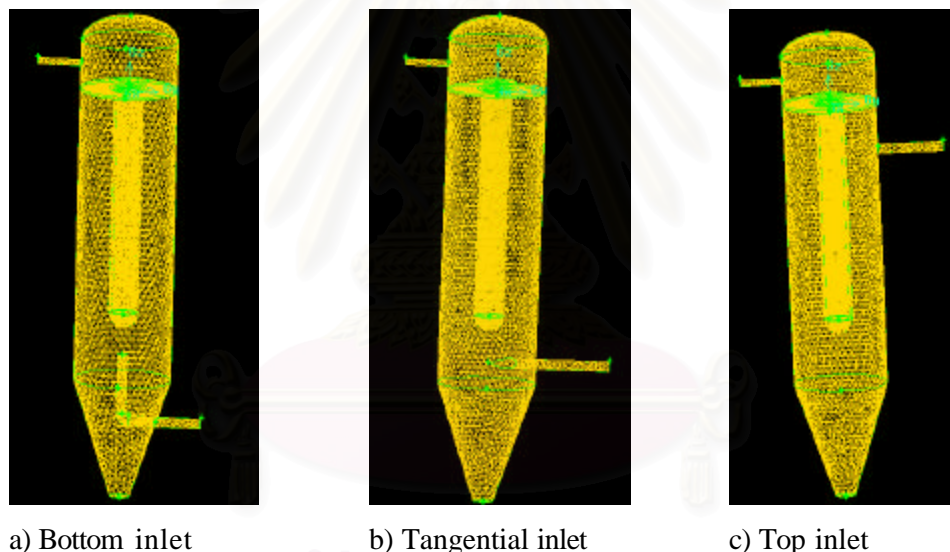


Figure 5.2 Unstructured meshes from Gambit's operation on the vessel

A computational grid as shown in Figure 5.2 which has three different positions for feeding is used for simulating the gas flow condition in the vessel. The aim of this work was to investigate the influence of two important operational parameters of the filtration (distribution of filtration velocity and pressure drop of the filter) assuming the uniformity of flow resistance of the filter. (Additional details of the flow simulation features and the computational schemes may be found in the FLUENT User's Guide [24]) This arrangement allows simulation of the filtration process by using a flow rate of $27.5 \text{ m}^3/\text{hr}$. It is expected that the variation of gas density and

temperature likewise will be small. Therefore, it is assumed here that the flow is isothermal and the gas behaves as an incompressible fluid. The complicated swirling turbulent flow demands that suitable numerical technique and turbulence model be employed in the CFD code when modeling the chamber pressure drop. It should be emphasized that the model assumes an extremely dilute concentration of particles. Here, the RNG k- ϵ model was used due to its simplicity and robustness. The segregated solution algorithm was selected. The present work makes use of settings that control the discretization of the convection terms in the solution equations. Discretization schemes available for the pressure, momentum, and (if relevant) energy equations in the present FLUENT program package use the second-order upwind method. Pressure-velocity coupling was selected from the list of the available schemes in SIMPLE and the second order upwind scheme was used to interpolate the variables on the surface of the control volume.

In the CFD calculations, small face velocity deviations were observed, which are less than 20 % of the deviations on the surface of the ceramic candle filter and similar in magnitude to the experimental errors. While there was a slight pressure drop in the inlet region, the main pressure drop of about 110 Pa occurred as the gas passed through the permeable walls of the ceramic filters, which also depends on the gas inlet position. The gas velocity magnitude was relatively low, of the order of 6.7 m/s in the upper part of the vessel. The velocity magnitude inside the porous filter was much lower, of only a few cm/s. On the filter surfaces and inside the ceramic filter walls, the velocity became radially inward with a value of about 2.77 cm/s. It should be noted that in all of the present experiments and corresponding simulations the flow rate of the influent gas stream was always kept constant by automatically adjusting the inlet pressure (or the total pressure drop of the unit). Simulation cases are classified into two main groups as follows: virgin candle filters with a single candle filter, and with twin candle filters.

5.2.1. Effect of air inlet position

This work investigated the velocity distribution belonging to each inlet port position. Originally it was thought that the local face velocity (normal velocity) of the gas flowing through each small part of the candle wall should essentially be identical if the filter candles are clean and only clean air is used. Our CFD simulation results,

however, indicate that significant deviations in the local face velocity could happen even in our case of symmetrical single candle filter unit. For the twin-candle filter system of interest, we looked at the spatial distribution of flow around each candle. First, each ceramic candle was divided along the height into 8 layers, which were further subdivided to 4 equal elements (quadrants) per layer as shown in Figs. 5.3 and 5.4. In order to obtain the spatial distribution of the gas flow through each portion of a single candle filter, and thus the deviation for the case of single candle filter, we obtain the “local” normal flow rate and “local” normal mass or volume flux through each of the 32 elements by carrying out simulation.

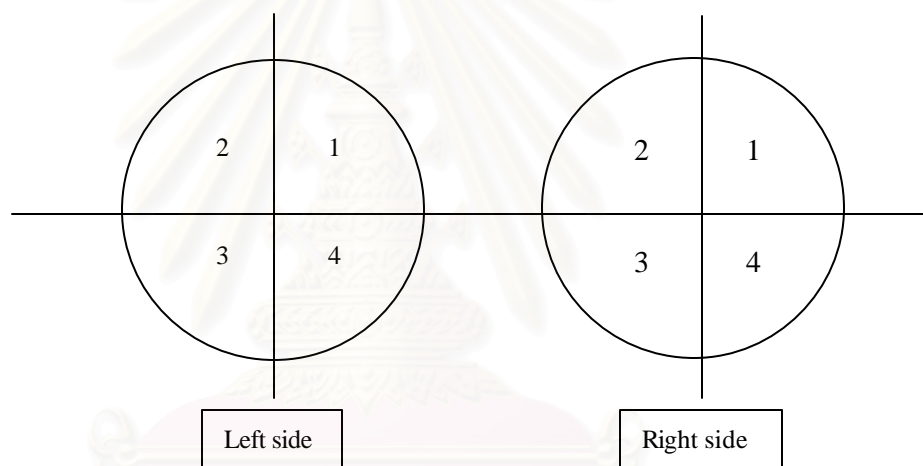


Fig. 5.3 A candle filter sub-divided into 8 layers and 4 quadrants for each layer

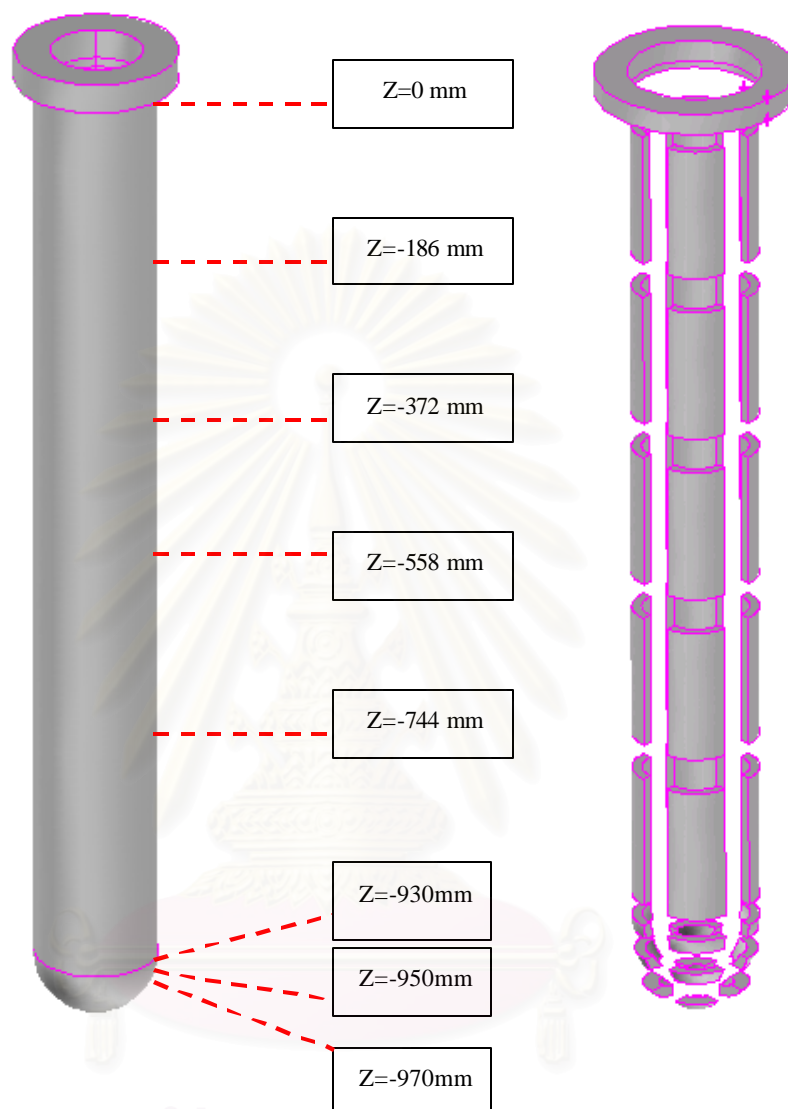


Fig. 5.4 The 8 layers of the candle filter used in calculation

First we characterize the wall property of the virgin filter candles by estimating the value of the total pressure drop that would yield the same viscous or flow resistance as the experimental value in the case of clean air flow through the filter. For simplicity we assumed that the two candles have identical characteristics. It is found that the tested viscous resistance of the virgin candle wall should be $1.39 \times 10^8 \text{ m}^{-2}$ when the total gas flow rate is $7.74 \times 10^{-3} \text{ kg/s}$.

Influent velocity	4.89	m/s
Influent gas temperature	300	K
Turbulent kinetic energy (k)	0.09	m^2/s^2
Energy dissipation rate (ϵ)	2.13	m^2/s^3

For this calculation, the ceramic candle filter has a steady viscous resistance. Table 5.1 shows the measured values of the total pressure drop and static pressure drop for each air inlet position. It is clearly seen that both the total pressure drop and static pressure drop of the top air inlet position are the lowest. The measured pressure drop across the ceramic candle filter for the top inlet position and the tangential inlet position are slightly different. For the bottom air inlet position, the pressure drops are the highest because the position required 2 90-degree turns of the air going through the ceramic candle filter.

Table 5.1 Pressure drop for the various cases of air inlet position

Position	Top	Tangential	Bottom
Total pressure drop(Pa)	96.67	103.66	141.08
Static pressure drop(Pa)	96.54	102.85	139.63

Figure 5.5 compares the local normal face velocities of clean air through a single virgin candle filter for three different air inlet positions. We can conclude that the height (Z) of the candle filter affects the local face velocity more than the location of the quadrant element. At the base of the cylindrical candle, the normal face velocity is highest and it decreases as the height increases. Especially, the normal face velocity through the hemispherical cap decreases remarkably. The case of bottom air inlet position has the highest face velocity at $z=-970$ mm because this case feeds air directly towards the bottom of the ceramic candle filter. However at $z= -950$ and -930 mm, the normal face velocity of the bottom inlet case is lower than the other two inlet cases.

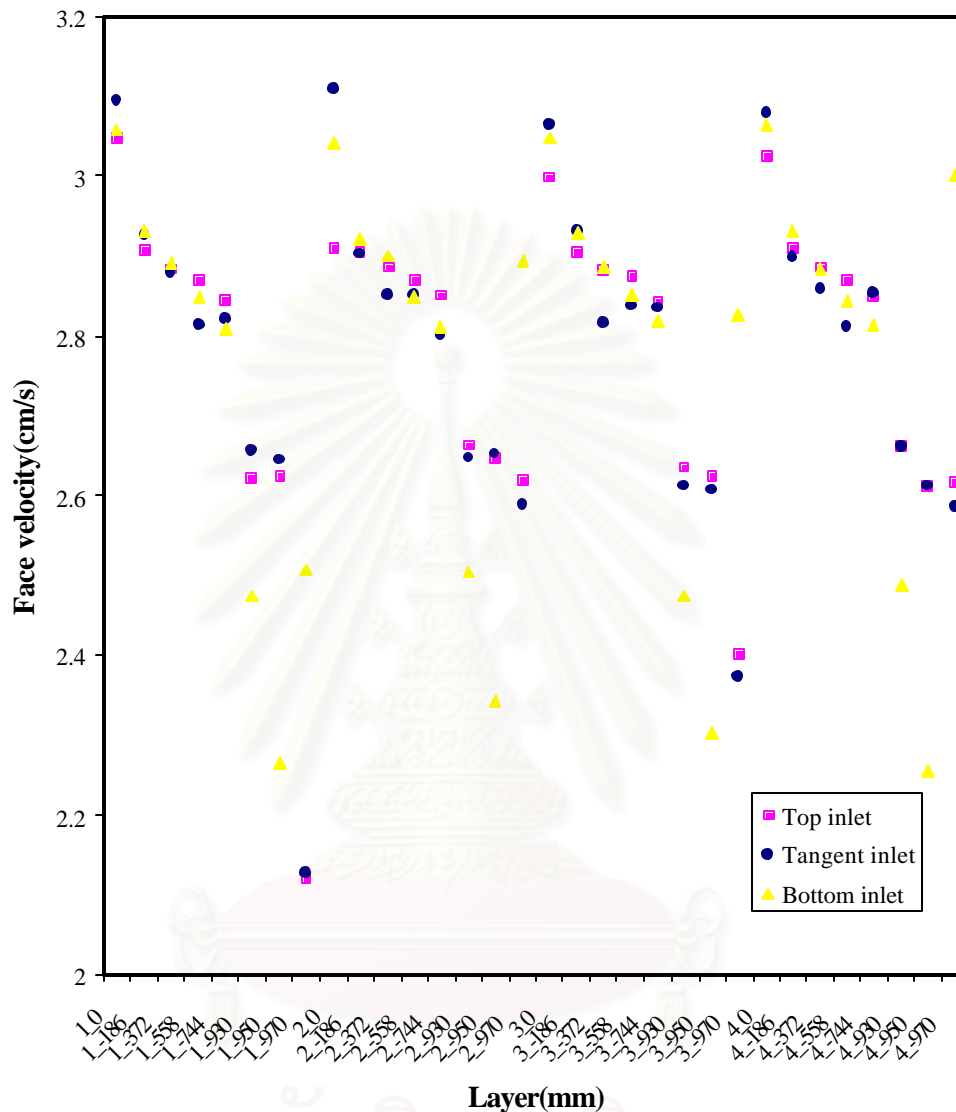


Figure 5.5 The local face velocity as a function of the height for each quadrant element in the case of the single candle filter.

According to Figure 5.5, we can conclude that the local normal face velocity distribution is insignificantly affected by the location of the quadrant of the candle filter. Fig. 5.6 shows the average local normal face velocity as a function of the candle height. In Figure 5.6, the layer at -930 mm. represents the edge between the lower end of the cylindrical portion of the candle and the hemi-spherical cap. The layer at -970 or the top of the hemi-spherical cap shows an exceptionally high normal face velocity for the case of bottom inlet. For the case of tangential and top inlets, the local normal

faces velocity decreases monotonically along the downward z -direction. It should be pointed out that this interesting observation has not been obtained via previous simulation or reported in any experiment before. It can clearly be seen that the local normal face velocities can differ by as much as 20% between the base and the cap. Similarly, Table 5.2 shows the average local normal face velocity distribution as a function of the candle height. In Zone 2, there is not much difference in the normal face velocity among the 4 layers. In Zone 3, the normal face velocity drops further from Zone 2 because they form the lateral portions of the hemi-spherical cap.

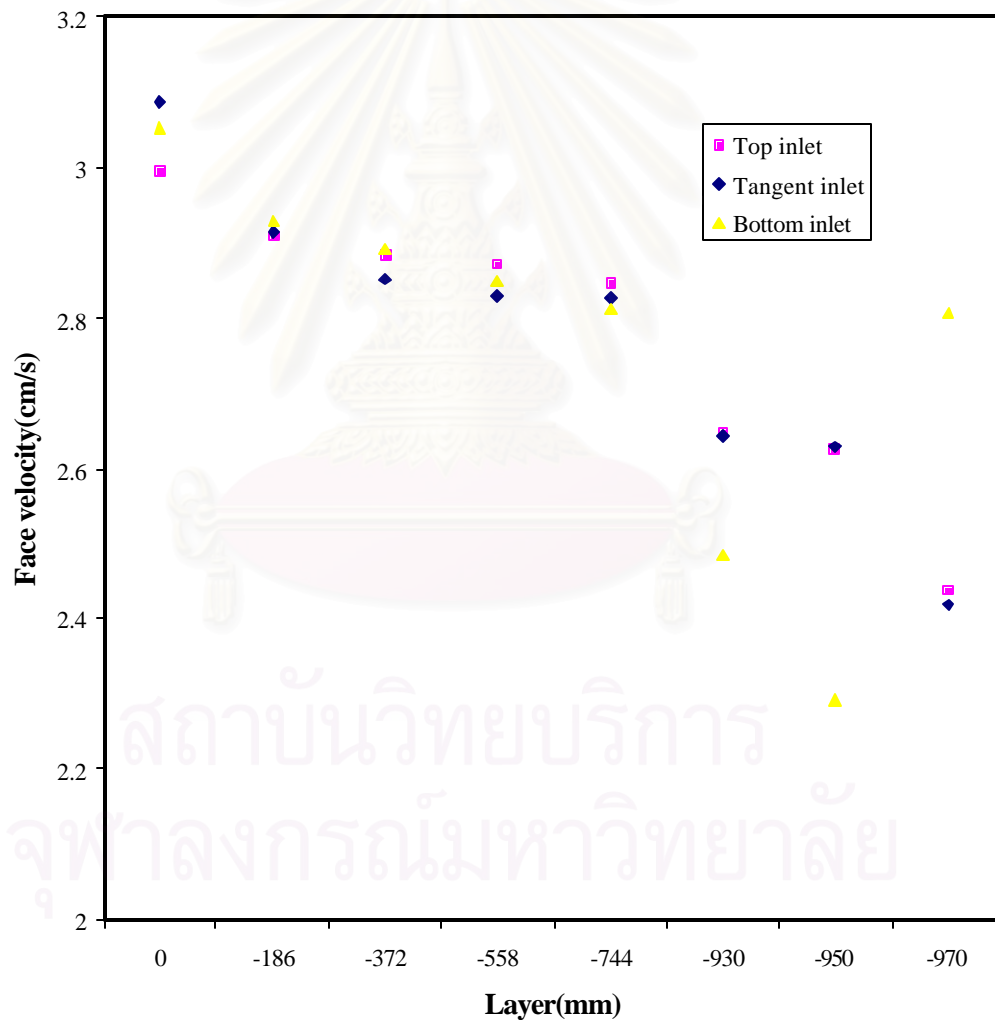


Figure 5.6 The average local normal face velocity as a function of the candle height for the case of the single candle

Table 5.2 Zone of velocity distribution along z-position for the case of the top air inlet

Zone	Layer(mm)	Average velocity(cm/s)
1	0	2.99
2	-186, -372, -558, -744	2.88
3	-930, -950	2.64
4	-970	2.44

Table 5.3 Zone of velocity distribution along z-position for the case of the tangential air inlet

Zone	Layer(mm)	Average velocity(cm/s)
1	0	3.09
2	-186, -372, -558, -744	2.85
3	-930, -950	2.64
4	-970	2.42

Table 5.4 Zone of velocity distribution along z-position for the case of the bottom air inlet

Zone	Layer(mm)	Average velocity(cm/s)
1	0	3.05
2	-186, -372, -558, -744	2.87
3	-930, -950	2.39
4	-970	2.81

Table 5.5 Zone of average velocity distribution along z-position for the three cases of the air inlet

Zone	Layer(mm)	Average velocity(cm/s)
1	0	3.04
2	-186, -372, -558, -744	2.87
3	-930, -950	2.55
4	-970	2.55

From Figure 5.6, the average velocity (0 to 744 mm. for the various positions) is not quite different. At the hemi-spherical cap, the average velocity at the bottom is different from the top and tangential inlet position because the feed port points directly towards the bottom of the ceramic candle filters. The profiles of velocity vectors for each inlet position are shown graphically in Appendix D.

5.3. Experimental results and discussion.

5.3.1. Effect investigated

A knowledge of the filtration behavior of the range of dusts likely to be encountered by a given filter will lead to improved design of the filter; for instances, the appropriate face velocity, pressure differential (the allowable pressure drop), pressure to be tolerated by the hold-down device and design of dirty gas flow system. As dirty air is filtered in the system, the residual pressure drop gradually approaches a certain threshold, beyond which the filtration process becomes uneconomic because of excessive pressure losses and short cycle times. As a consequence, the filter medium has to be replaced. A dedusting system must be used to periodically clean the ceramic candle filter shown in Figure 5.7. The pulse air pressure needs to be as high as 5 MPa to give an effective cleaning performance. The irregular pattern of the filter cycles is strongly related to the initial pressure drop of the filter. The observed number of pulses depends on the initial clogging condition of the filter and the filtration conditions. Therefore, a trade-off must be made between higher collection efficiency and higher pressure drop across a ceramic candle filter.



Figure 5.7 Experimental set-up

5.3.1.1. Initial pressure drop and residual pressure drop

Two related characteristic parameters are the initial pressure drop (P_I) and the residual pressure drop (P_R). A ceramic candle filter was not perfectly clean at the start of a consecutive experimental run, even though it was exposed to a large number of jet pulses. The initial pressure drop is the observed pressure drop when a new experimental run starts. It is known that a thin layer of filter cake often remains on the surface of the filter after cleaning. Actually, the residual pressure drop is also a good measure of the dust remaining in the depth of the filter medium. The residual pressure drop is calculated as the difference between the initial pressure drop when the next experiment starts after pulse cleaning and the initial pressure drop of the present run. The recorded experimental data consists of the pressure drop across the filter versus time, average outlet dust concentration and average collection efficiency during a run of the experiment. Most of the initial pressure drops of virgin candle filters ranged between 20 to 25 Pa. Unfortunately, it happens quite often in practice that the residual pressure drop does not reach an asymptotic value, but increases steadily due to particles lodged firmly inside the filter medium which can not be removed by pulse cleaning. In fact, after the candle filter was regenerated, the pressure drop across the ceramic candle filter would be 175-250 Pa because there was some permanent deposition of particles.

Figure 5.8 shows a comparison of the initial pressure drop and the residual pressure drop observed during each run. Generally, the initial pressure drop of the same filter will be increased slightly with each new experimental run. However, P_I could be decreased if the new face velocity decreases, for instances, in cases C1.724 (8). When case C1.724 (8) was finished, the running of B35 (9) was carried out continuously with an average face velocity 1.216 m/min. The initial pressure drop of B35 (9) was clearly seen to decrease as the residual pressure drop remained essentially constant. When the position of the air inlet is changed, it can also change the initial pressure drop. Interestingly, the case of bottom inlet position had a lower residual pressure drop than the other inlet positions even though its initial pressure drop was higher than the others. The local normal face velocity for the cases of the top and tangent inlets has been shown to be distributed better than the case of bottom

inlet. When the filter was regenerated, the case of bottom inlet was most effectively cleaned because it was most severely clogged at the bottom.

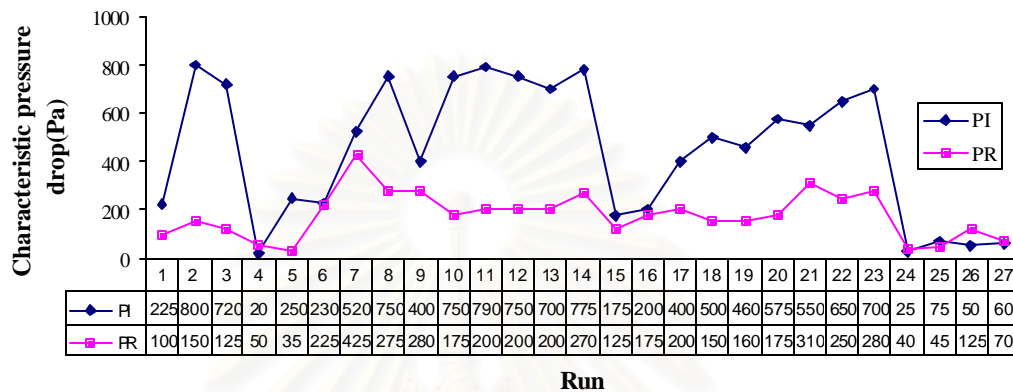


Figure 5.8 Chronology of experimental runs and corresponding P_I and P_R

5.3.1.2. Outlet dust concentration (dust penetration)

The outlet dust concentration was measured by an Airborne Particle Counter. The observed dust collection efficiency was very high and the outlet dust concentration was lower than that of the ambient air shown in Table 5.6.

Table 5.6 The measured dust concentration of ambient air (19/08/48: 10.15 am)

Particle size(micron)	Out door		
	1	2	Av
<0.3	93754	96393	95073.5
0.3-0.5	8047	8841	8444
0.5-0.7	3764	4185	3974.5
0.7-1	2324	2564	2444
1.0-2.0	1016	1146	1081
2.0-5.0	143	150	146.5

5.3.1.2.1. Effect of pulse duration

Figures 5.9-5.11 show the patterns of the pressure drop in relation to time of experimental runs with different pulse durations. Case A100 (100 millisecond duration) was most efficient because it did not suffer excessive pressure drop after each pulse cleaning.

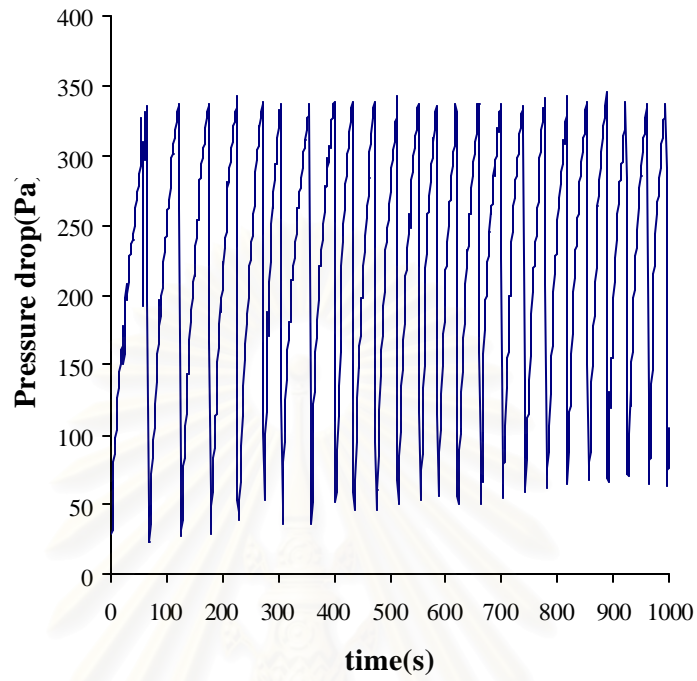


Figure 5.9 Case A100 (24)

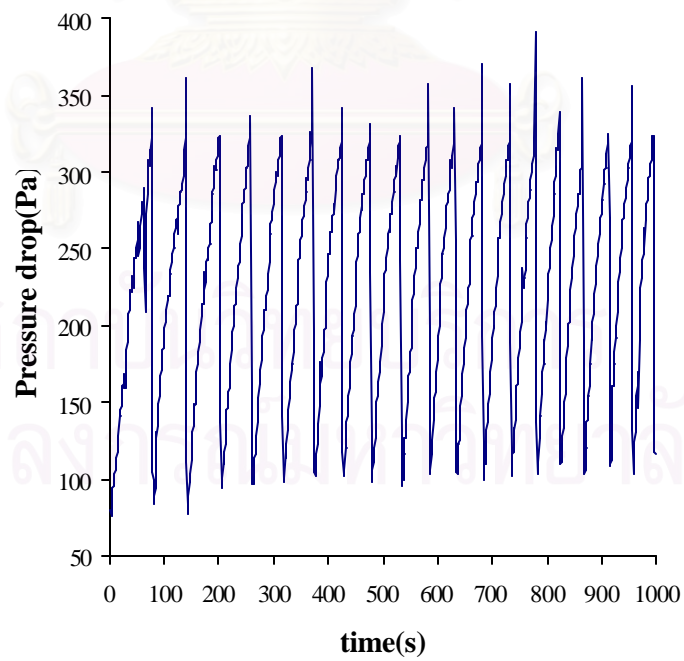


Figure 5.10 Case A150 (25)

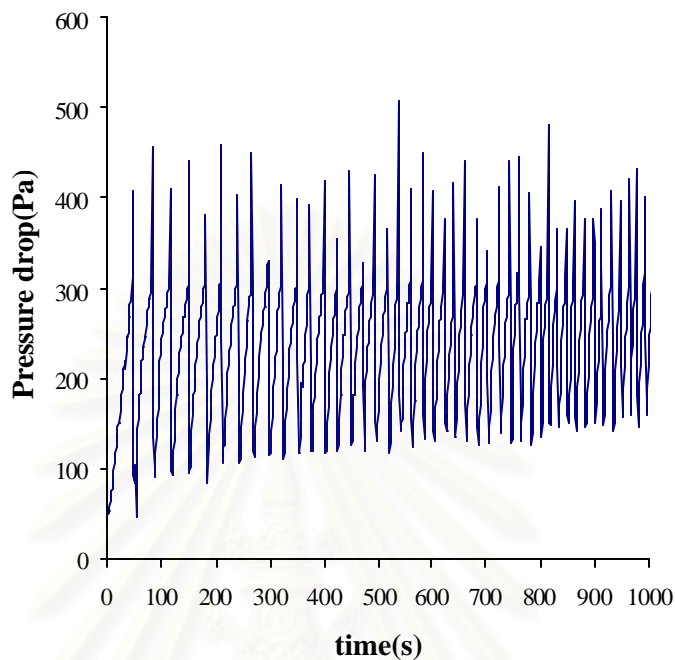


Figure 5. 11 Case A200 (26)

The pulse duration had no clear effect on the residual pressure drop. Even when the duration time is 200 ms, the increase in residual pressure drop was not negligible. In Table 5. 3, case A100 (24) was carried out starting from a virgin filter, which had a residual pressure drop of 40 Pa. When the filter was reused in cases A150 (25) and A200 (26), the residual pressure drop increased slightly. It may be concluded that the pressure drop pattern depended more on the initial pressure drop than the pulse duration. Although case A200ms was cleaned for a longer period than the first two, it could not prevent the formation of permanent cake which penetrated into the candle wall. Moreover, the residual pressure drop value depended on the initial pressure drop, as can be seen when comparing between case A100 (19) and A100 (24). Similarly, cases A150 and A200, respectively, showed the same trend of results as cases A100.

Table 5.7 Effect of pulse duration on the initial and residual pressure drops

	A							
	100			150		200		
	1	19	24	22	25	2	23	26
P_i (Pa)	225	460	25	650	75	800	700	50
P_R (Pa)	100	160	40	250	45	150	280	125
P_R/P_i	0.4	0.3	1.6	0.4	0.6	0.2	0.4	2.5

The above results reveal that the cleaning efficiency depends on the pulse duration. Therefore, the design of the solenoid valve and the injection nozzle should be optimized to improve the cleaning efficiency of a ceramic filter. It is shown in Figure 5.12 that the outlet dust concentration increased rapidly with the lengthened pulse duration. As the duration of pulse gas increased the quantity of injected gas increased, thereby raising the transient interval pressure of the chamber. When pulsing ended, the face velocity through the filter jumped in order to release the extra backup pressure, thereby reducing the filtration efficiency. The resulting outlet dust concentration was shown in Figure 5.13. Excessive pulse cleaning could also damage the surface of a ceramic candle filter. In terms of dust penetration, it was obvious that the case of A200 had the highest dust penetration, as shown in Figure 5.14.

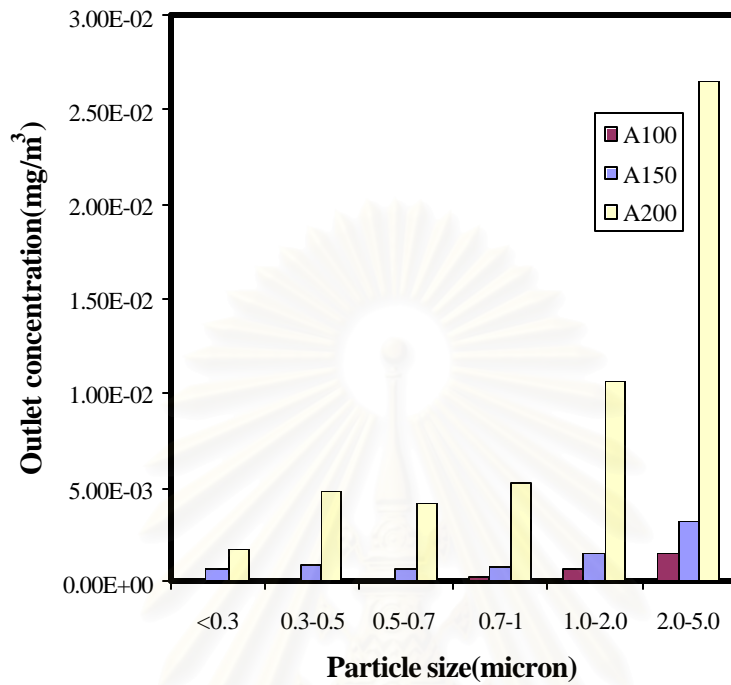


Figure 5.12 The effect of pulse duration on outlet dust concentration

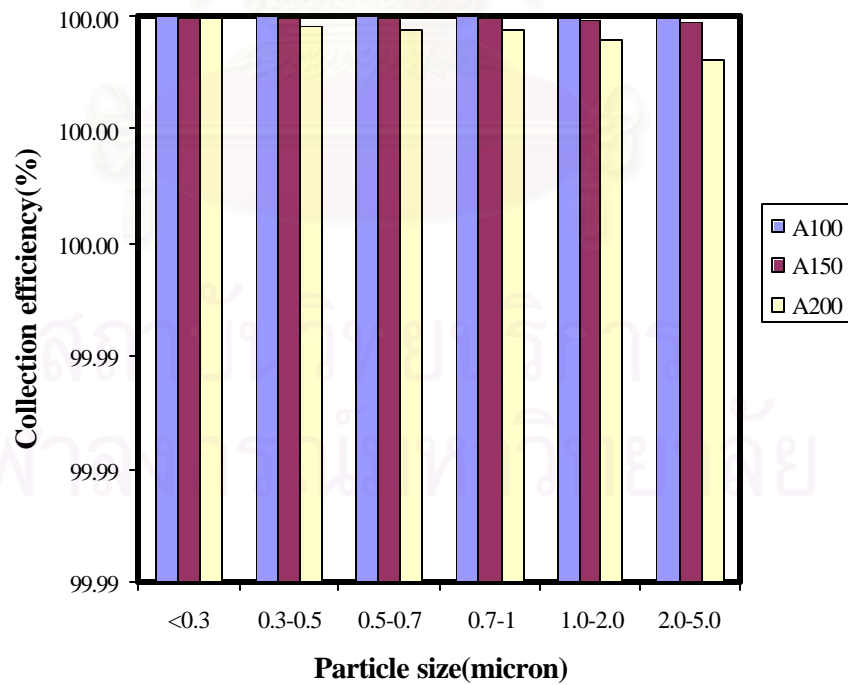


Figure 5.13 The effect of pulse duration on dust collection efficiency

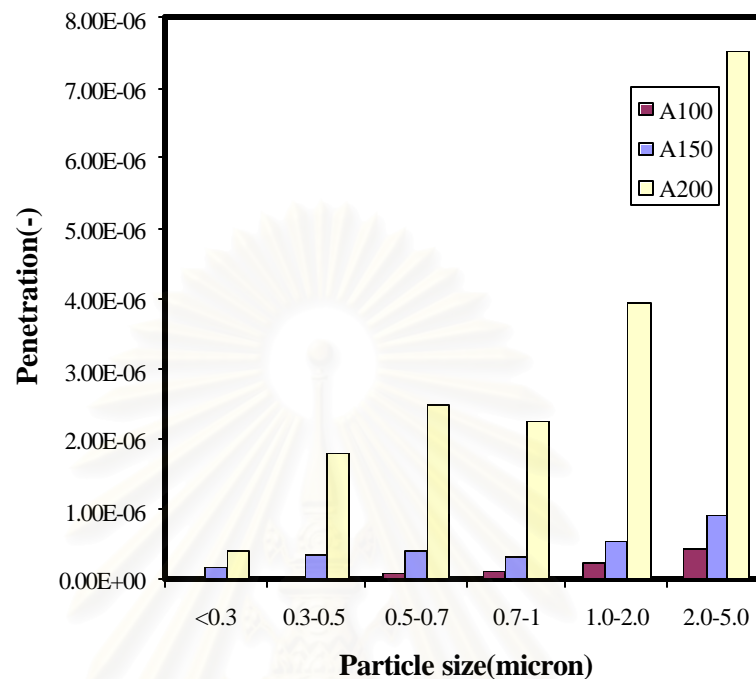


Figure 5.14 The effect of pulse duration on dust penetration

5.3.1.2.2 Effect of pressure differential activated cleaning

In our previous experiments, pulse cleaning was carried out periodically at a fixed time interval. In this section, the cleaning action was activated when the measured pressure drop increased above the current initial pressure drop by 15, 25, or 35 mmAq. The experimental results reveal that, when the initial pressure drop was the same, a lower pressure differential activated cleaning led to a larger residual pressure drop, as shown in cases B15(21) and B35(20) in Table 5.8. However, it can be concluded that, if the activating pressure differential was lower than 25 mmAq, the cleaning action was repeated more frequently. Therefore, both the lowest and the highest activating pressure differential resulted in a higher residual pressure drop. In summary, an intermediate value of 25mmAq is most appropriate in this work.

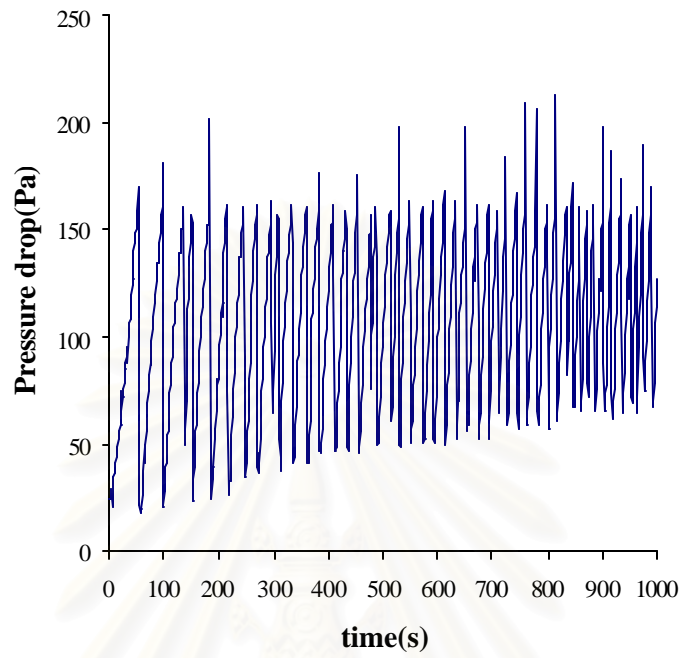


Figure 5.15 Case B15 (4)

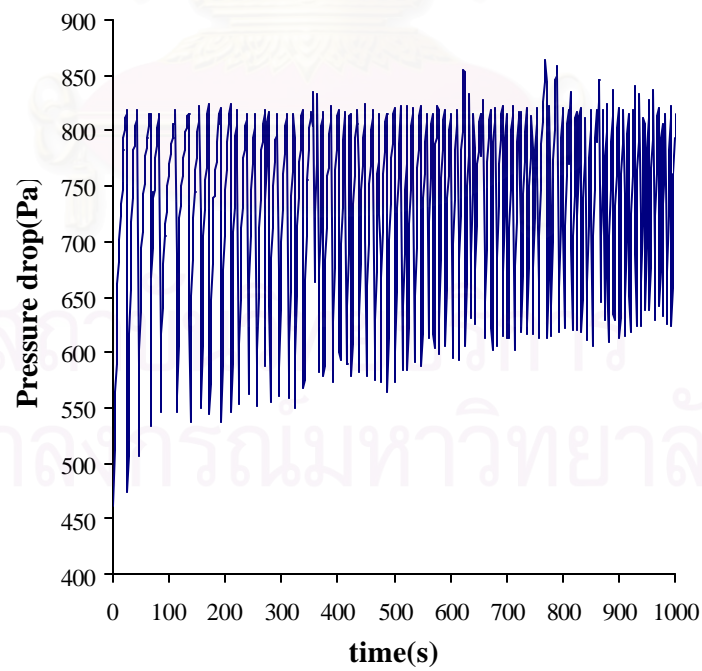


Figure 5.16 Case B25 (19)

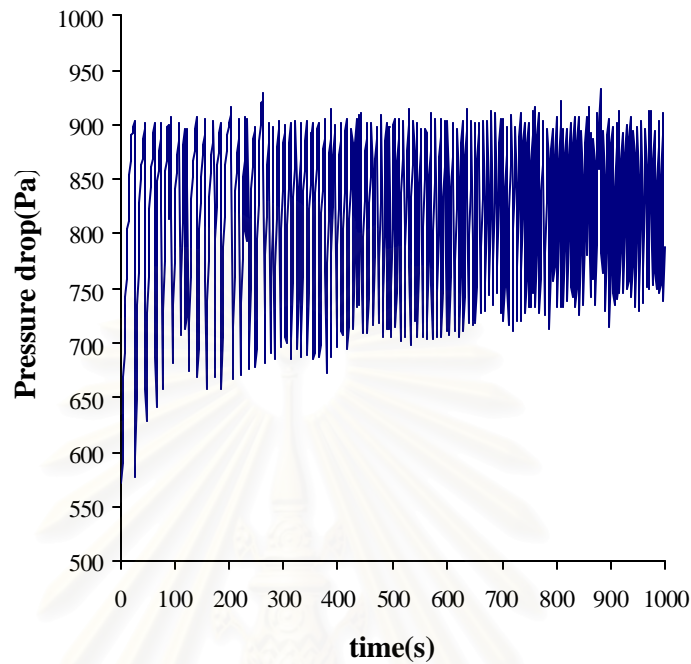


Figure 5.17 Case B35 (20)

Table 5.8 Effect of the activating pressure differential on the initial and residual pressure drops

	B								
	15			25			35		
	3	4	21	1	19	24	5	9	20
P_i (Pa)	720	20	550	225	460	25	250	400	575
P_R (Pa)	125	50	310	100	160	40	35	280	175
P_R/P_i	0.2	2.5	0.6	0.4	0.3	1.6	0.1	0.7	0.3

The above results should help lead to optimization of the capacity and operating costs of the ceramic filter. On the whole, the 25 mmAq value is the appropriate activating pressure differential in this work. It can be inferred that the 15 mmAq case experienced too frequent cleaning, which may damage the permanent cake on the filter surface as shown in Figure 5.15. However, since the initial and residual pressure drops in cases B15 (4) and B25 (19) were significantly different; it is not possible to make a fair comparison here.

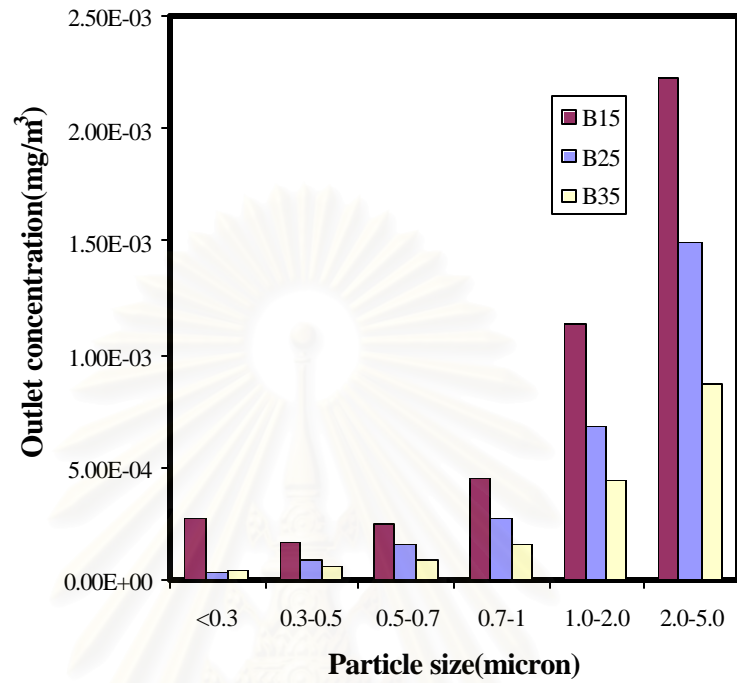


Figure 5.18 Effect of the activating pressure differential on outlet dust concentration

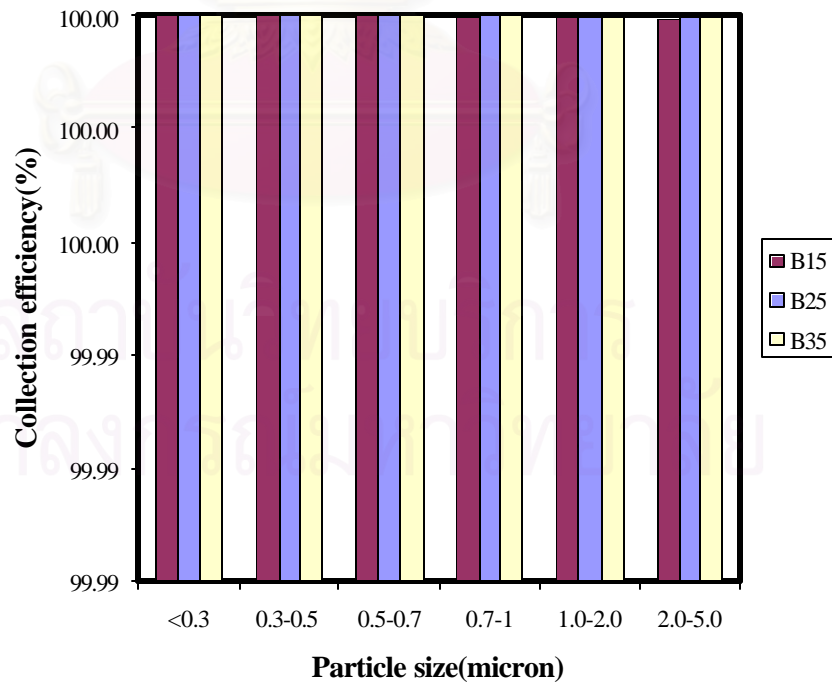


Figure 5.19 Effect of differential pressure on dust collection efficiency

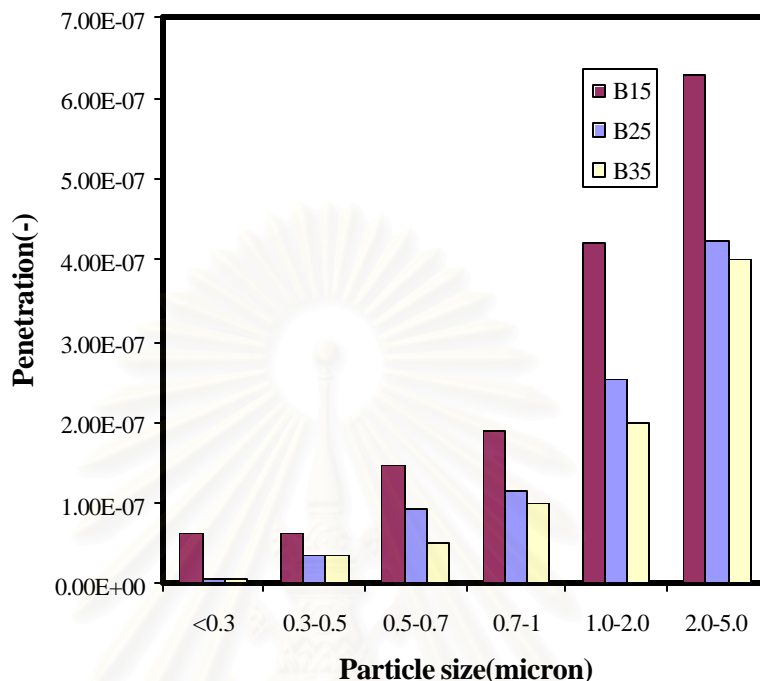


Figure 5.20 Effect of the activating differential pressure on dust penetration

5.3.1.2.3. Effect of nominal face velocity

When the nominal face velocity was gradually reduced, the pressure drop began to be unstable. The operation was found to be stable down to a minimum filtration velocity (1.216m/min), even though the over-pressure during pulse jet regeneration was similar at each nominal face velocity. As the cycle progressed, the residual pressure drop increased quite sharply for C1.724 and C1.989. These phenomena express the low regeneration capacity in these cleaning conditions. It should be noted that C1.216 presents the lowest residual dust inside the filter. The issue is an important one, as it affects the dust concentration emitted from processes. For different filtration velocities (face velocity), the observed pressure drop as a function of cycle's time is illustrated in Figures 5.21-5.23.

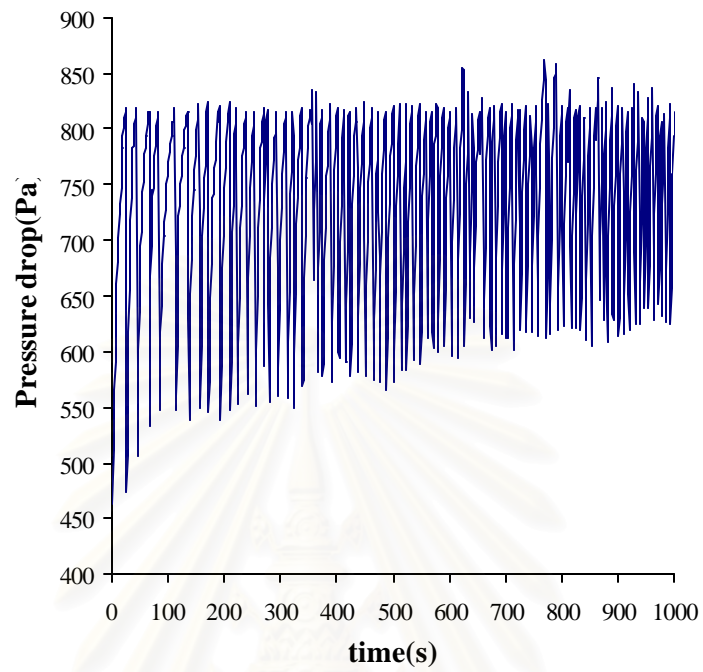


Figure 5.21 Case C1.216 (19)

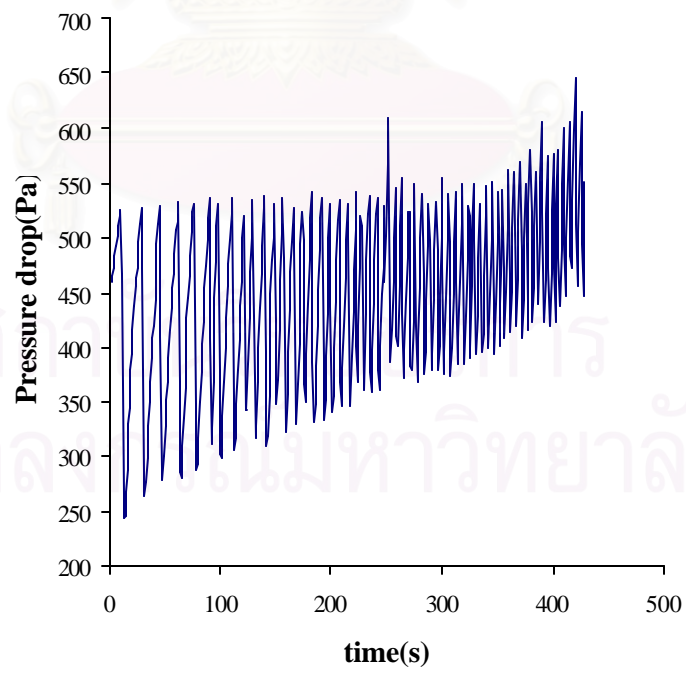


Figure 5.22 Case C1.724 (6)

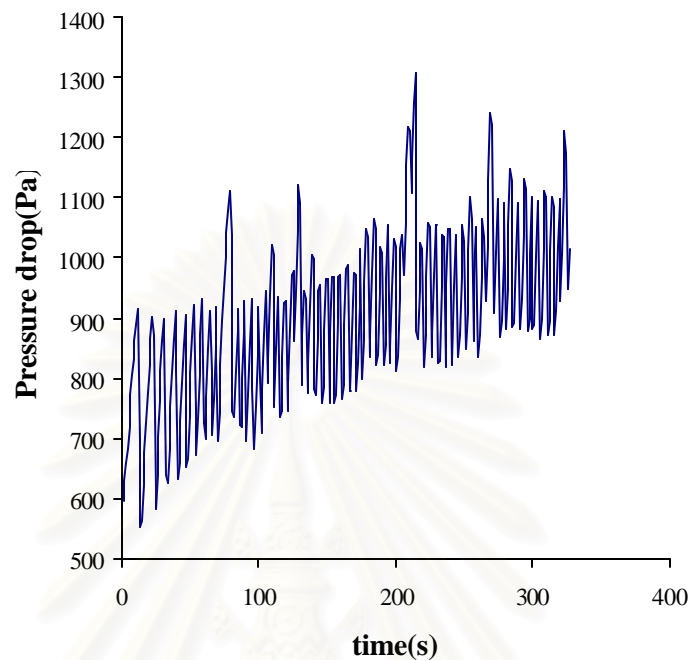


Figure 5.23 Case C1.989 (7)

The trend depends on the average filtration velocity and the pressure drop can be excessive at high filtration velocities. The slope between the pressure drop versus time for case C1.724 was approximately 0.5, while for C1.989 approximately 0.67. It can be concluded that the slope of C1.989 was steeper than C1.724 when the trend of pressure drop increased. A comparison between the results for cases C1.216, C1.724 and C1.989 shows that, the experimentally observed unstable operation can most likely be attributed to problem with cake detachment. When case C1.724 (6) has finished, case C1.989 (7) was carried out next. This made the initial pressure drop to increase rapidly. The residual pressure drop increase was easily seen because it had some permanent cake deposited on the filter.

Table 5.9 Effect of nominal face velocity on the initial and residual pressure drops

	C					
	1.216			1.724		1.989
	1	19	24	6	8	7
P_i (Pa)	225	460	25	230	750	520
P_R (Pa)	100	160	40	225	275	425
P_R/P_i	0.4	0.3	1.6	1	0.4	0.8

From Figure 5.24, the outlet concentration of this effect clearly shows that case C1.216 had the lowest outlet dust concentration because it was the appropriate face velocity to filter the dirty gas. Case C1.989 has a lower efficiency than C1.724 because the residual pressure drop of C1.989 was higher. It can be concluded that the collection efficiency depended on the residual pressure drop and the face velocity. However, the nominal face velocity had more influence on the collection efficiency than the residual pressure drop. It is obvious from the dust penetration that case C1.742 was not appropriate to use for filtration. For case C1.989 the small particles not exceeding 1 micron in size could penetrate through the surface of the ceramic candle filter better than case C1.742.

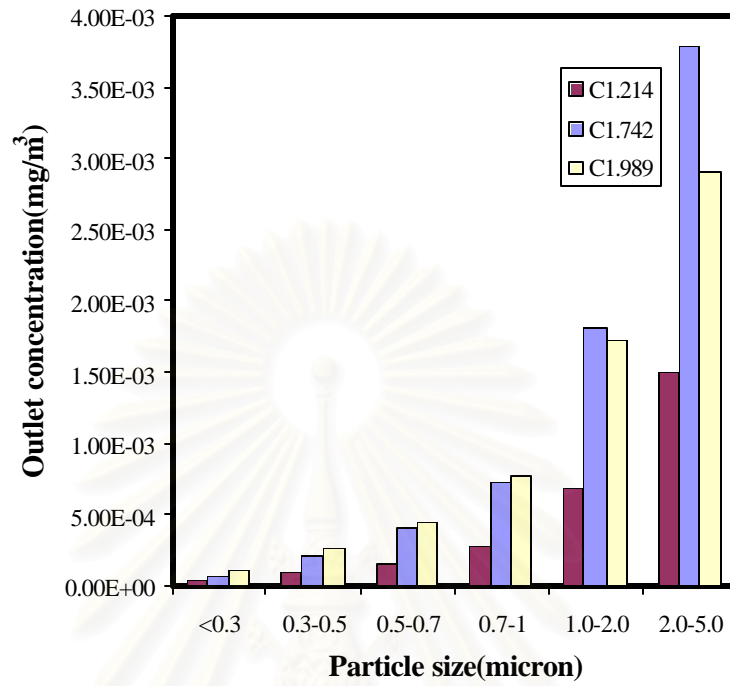


Figure 5.24 Effect of nominal face velocity on outlet dust concentration

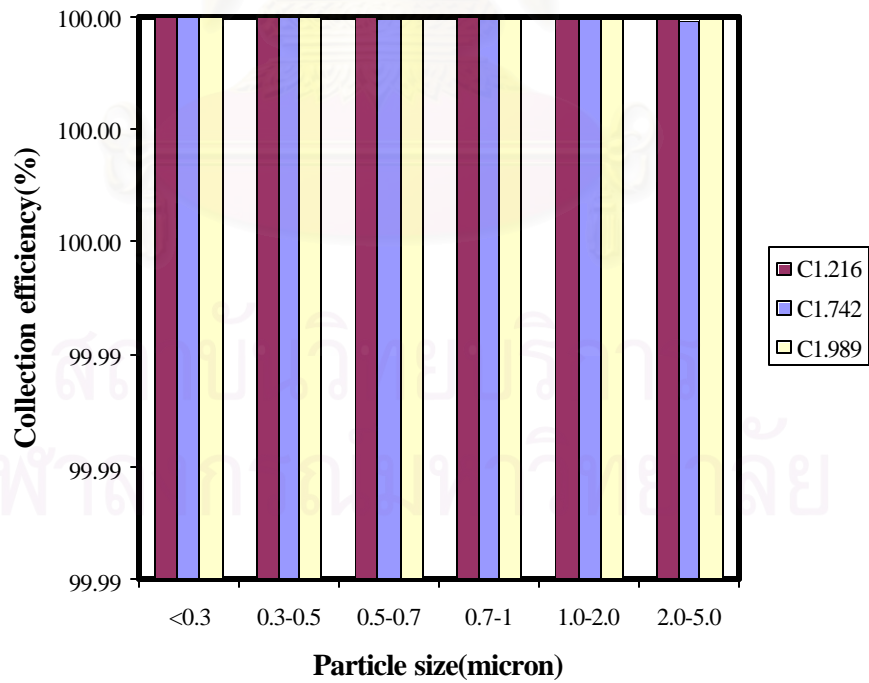


Figure 5.25 Effect of nominal face velocity on dust collection efficiency

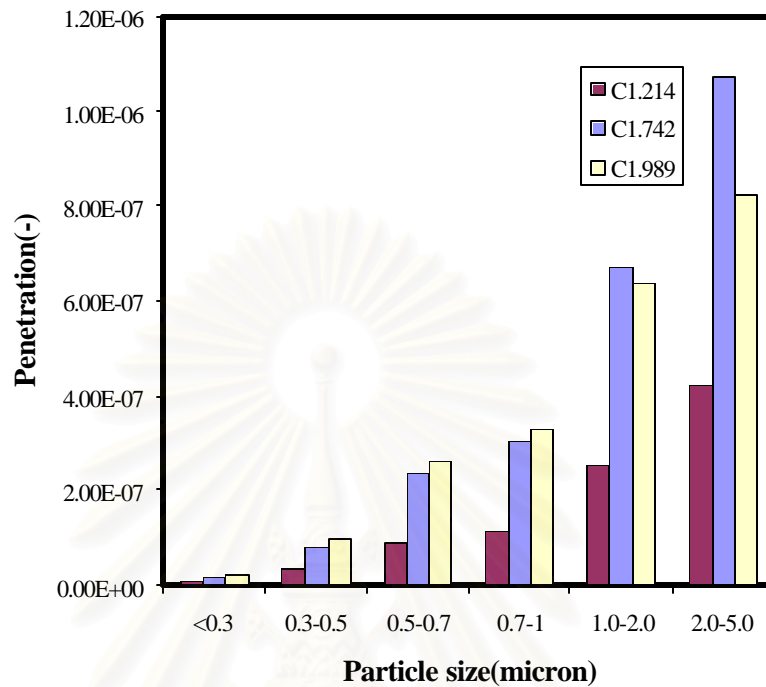


Figure 5.26 Effect of nominal face velocity on dust penetration

5.3.1.2.4. Effect of inlet dust concentration

Inlet dust concentration will directly affect the cake thickness deposited on the filter medium. A higher inlet concentration generally results in a higher residual pressure drop. For this case, the face velocity was fixed at 1.214 cm/s. It can be clearly seen from Figure 5.27-5.29 that the higher the inlet dust concentration, the more frequent the optimal cleaning of the filter.

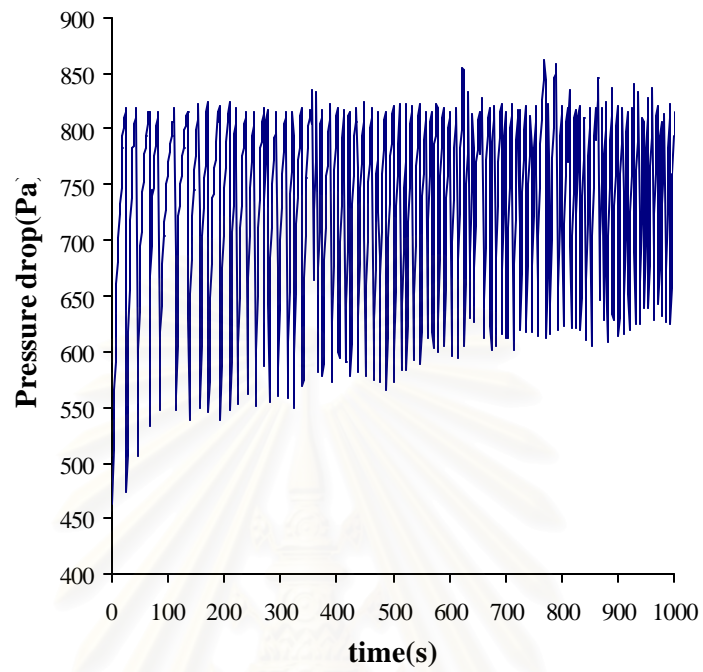


Figure 5.27 Case D21.82 (19)

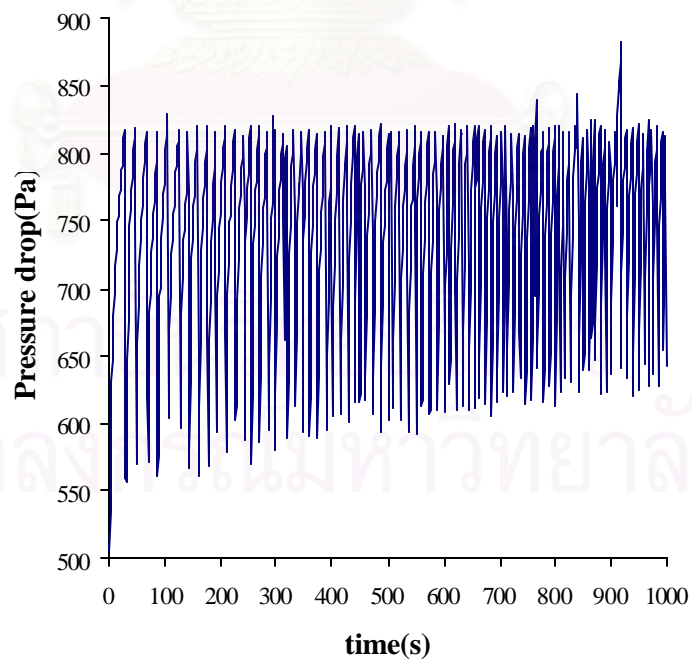


Figure 5.28 Case D43.64 (18)

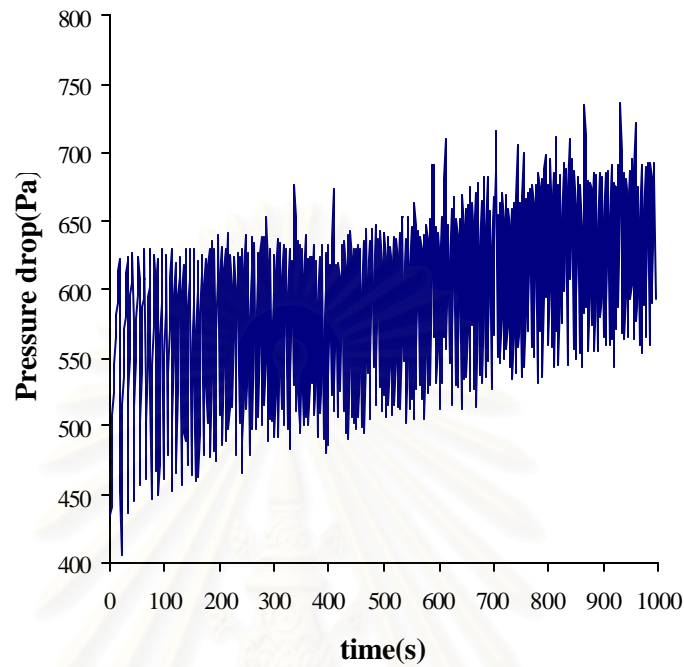


Figure 5.29 Case D65.45 (17)

If the dust collection efficiency is essentially 100%, the rate of cake formation would be proportional to the inlet dust concentration. If we use a high concentration, more dust will be collected on the filter than the case of a low concentration. The cake formation rate can also be estimated from the slope of the pressure drop versus time. In case D43.64 in Figure 5.28, it was approximately 0.1 and in case D65.45 in Figure 5.29 approximately 0.15. It can be concluded that case D65.45 had a higher dust deposition rate than case D43.64. Between case D43.64 (10) and 65.45 (11), the residual pressure drop increased gradually but the effect was obviously less than the face velocity effect.

Table 5.10 Effect of inlet concentration on the initial and residual pressure drops

	D						
	21.82			43.64		65.45	
	1	19	24	10	18	11	17
P_I (Pa)	225	460	25	750	500	790	400
P_R (Pa)	100	160	40	175	150	200	200
P_R/P_I	0.4	0.3	1.6	0.2	0.3	0.3	0.5

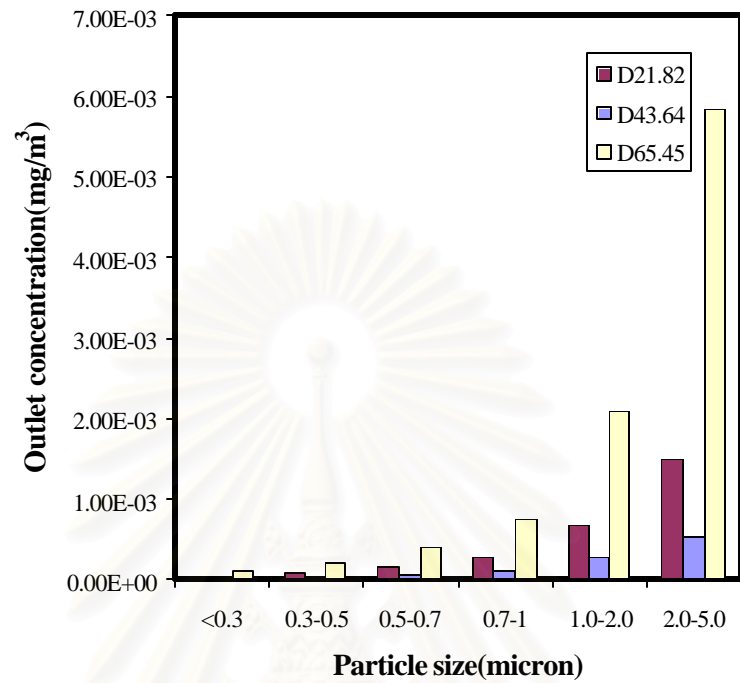


Figure 5.30 Effect of inlet concentration on outlet dust concentration

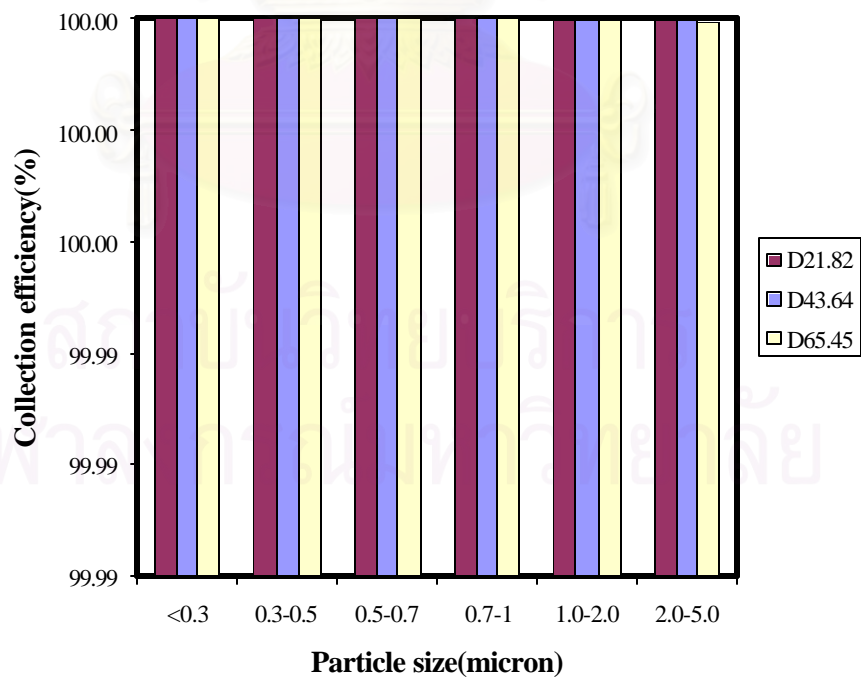


Figure 5.31 Effect of inlet concentration on dust collection efficiency

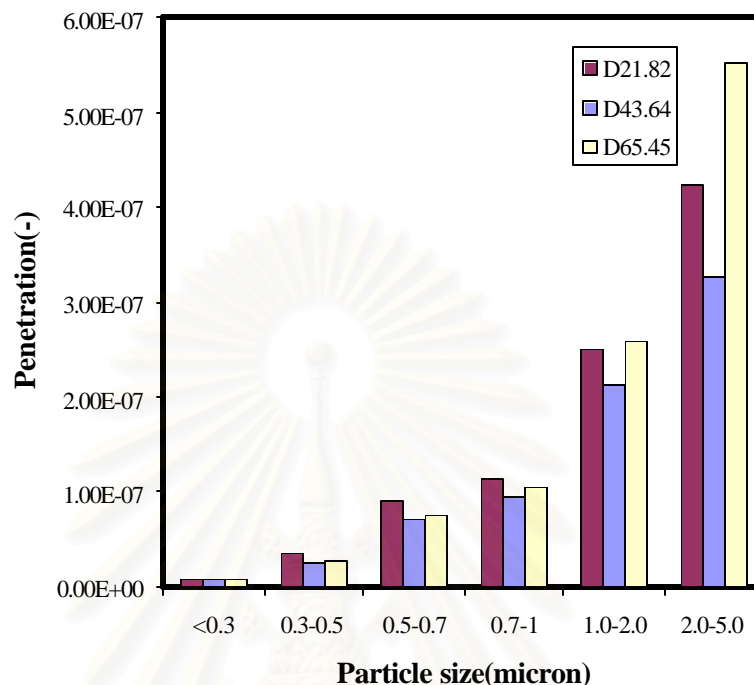


Figure 5.32 Effect of inlet concentration on dust penetration

Generally speaking, the thicker the cake becomes, the higher the collection efficiency. However, case D43.64 was most effective because the collection efficiency was the highest due to an appropriate thickness for capturing dust from upstream. Although the outlet dust concentration of case D21.82 was lower than that of case D65.45, in terms of collection efficiency, the efficiency of case D21.82 is slightly lower than case D65.45 because the inlet dust concentrations of the two cases were not equal. Between cases D21.82 and D65.45, the cake of D65.45 was thicker than that of D21.82, as determined from the residual pressure drop. The collection efficiency of case D43.64 can be investigated more easily by the use of dust penetration.

5.3.1.2.5. Effect of inlet port position

In section 5.3.1.1, the position of gas inlet port was found by simulation using clean air to affect the pressure drop across the filter. The top port position was shown to have the lowest pressure drop, followed by the tangential port position. Therefore, it is interesting to see if the port position has any effect on the pressure drop across the

filter. The general tendency of the experimental pressure drop pattern did not clearly show any difference in the influence of the port position because we did not have enough virgin filters to start anew with each port position.

Table 5.11 can not show clearly that the initial and the residual pressure drop was significantly affected by the different port positions. However, it is clear in all cases that the lower the initial pressure, the lower the residual pressure drop becomes but the higher the ratio of P_I / P_R becomes.

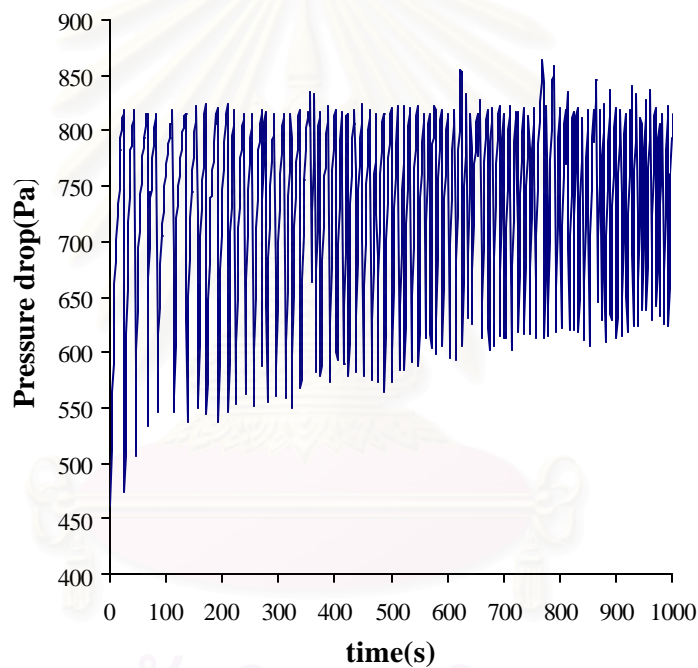


Figure 5.33 Case EBOTTOM (19)

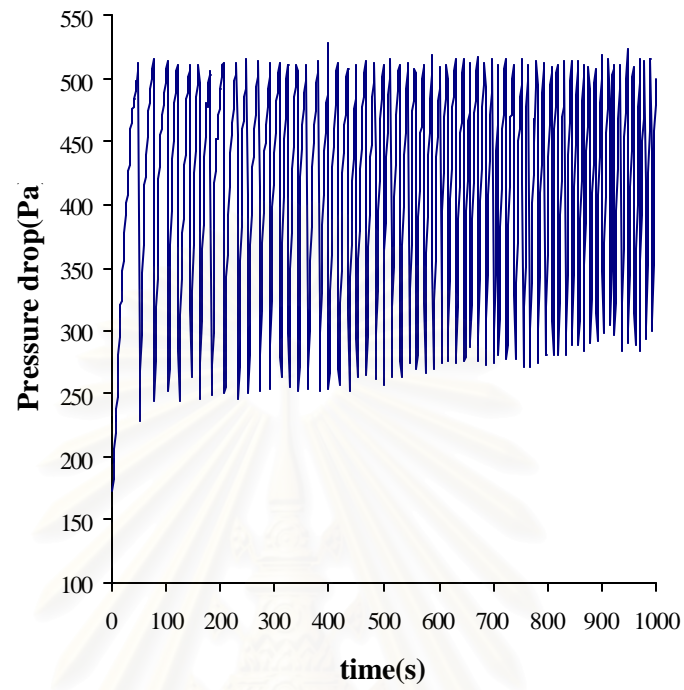


Figure 5.34 Case ETAN (15)

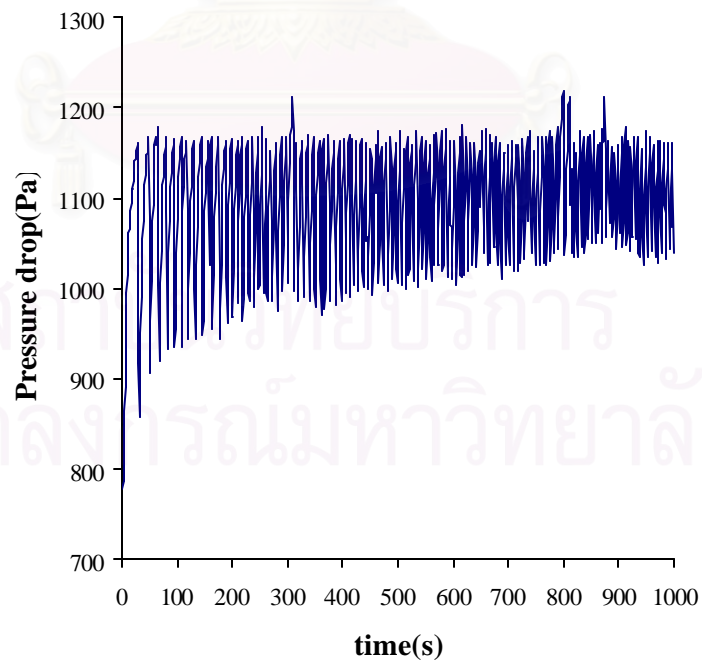


Figure 5.35 Case ETOP (14)

Table 5.11 Effect of air inlet position on the initial and residual pressure drops

	E								
	BOTTOM			TAN				TOP	
	1	19	24	12	13	15	16	14	27
P_I (Pa)	225	460	25	750	700	175	200	775	60
P_R (Pa)	100	160	40	200	200	125	175	270	70
P_R/P_I	0.4	0.3	1.6	0.3	0.3	0.7	0.9	0.3	1.2

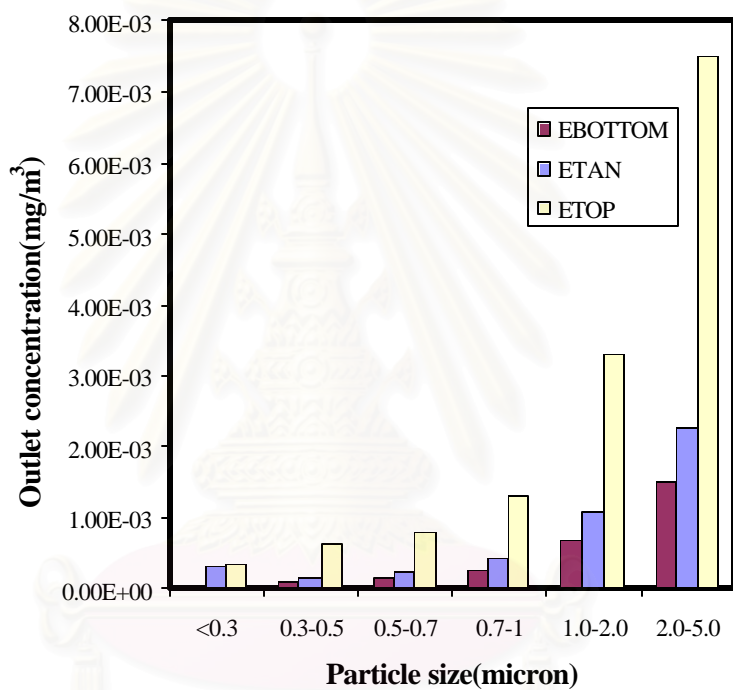


Figure 5.36 Effect of inlet position on outlet dust concentration

สถาบันวิทยบริการ
จุฬาลงกรณ์มหาวิทยาลัย

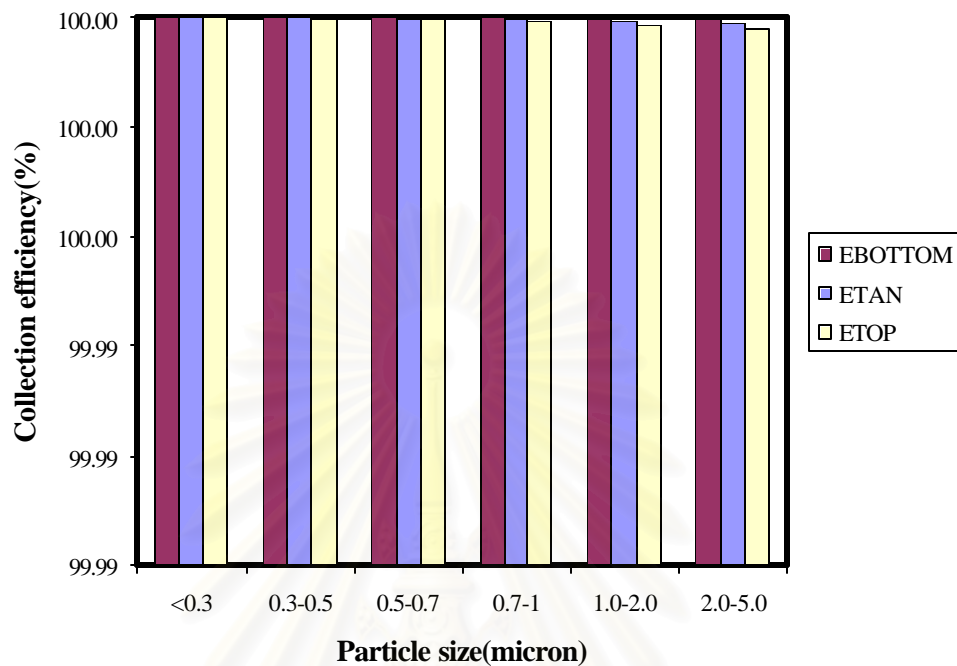


Figure 5.37 Effect of inlet position on dust collection efficiency

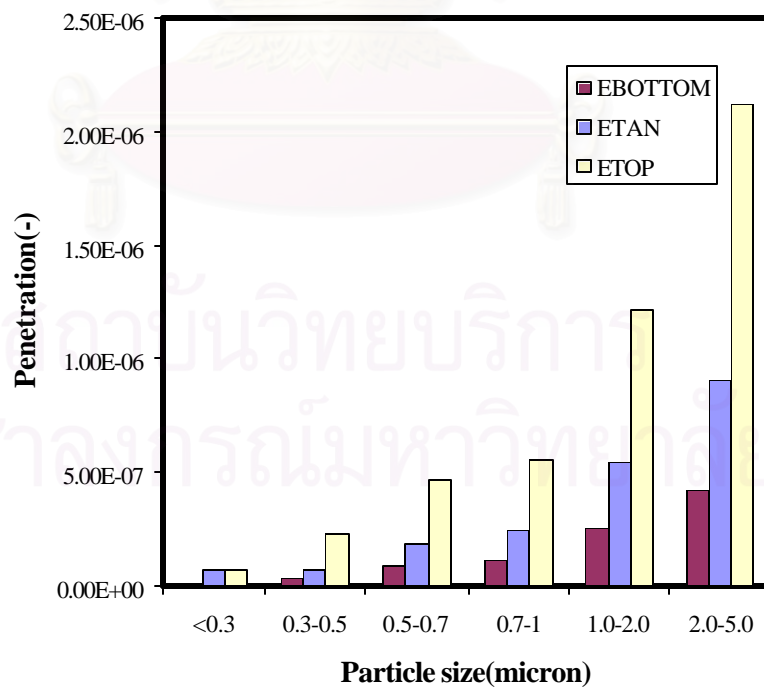


Figure 5.38 Effect of inlet position on dust penetration

With respect to dust collection efficiency, the bottom inlet port was apparently the best position for feeding as shown in Figure 5.37. When the tangential position was compared with the top position, the former shows a slightly better efficiency than the latter at similar initial pressure drops. This may be attributed to the fact that the tangential position distributes the air flow more uniformly than the top position. Figure 5.38 shows the corresponding dust penetration.

Collection efficiencies in excess of 99.9% were attained in all cases, even for extremely fine dusts (<0.3 microns). Therefore, the dust penetration of the particles in various size ranges should make it easier to understand the filtration phenomena. Obviously, the initial pressure drop and residual pressure drop will slightly influence the collection efficiency.

5.3.2. Correlation between face velocity and dust penetration

This section investigates the effect of nominal face velocity at the surface of the ceramic candle filter while the dust concentration was constant. For better understanding of this section, Figures 5.39-5.44 present the correlation between pressure drop and dust penetration versus the different face velocities.

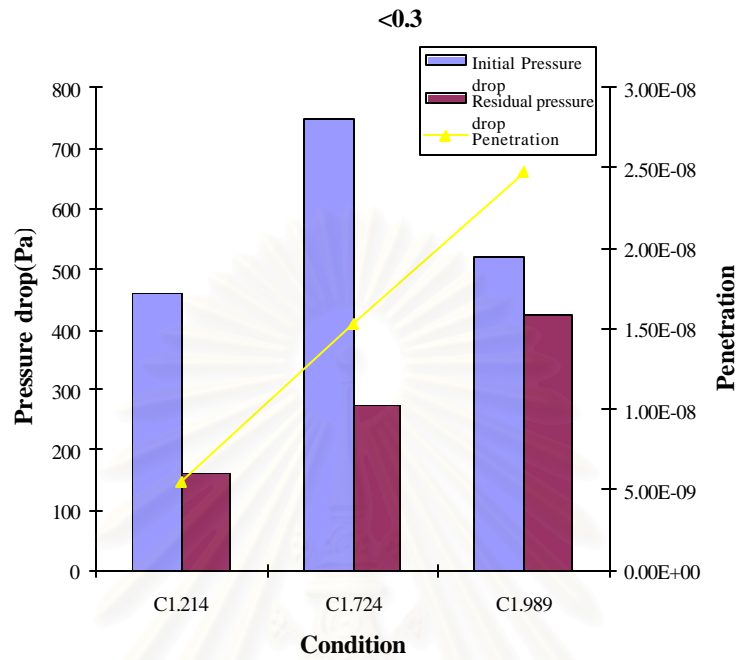


Figure 5.39 Effect of nominal face velocity on dust penetration in size range of < 0.3 micron

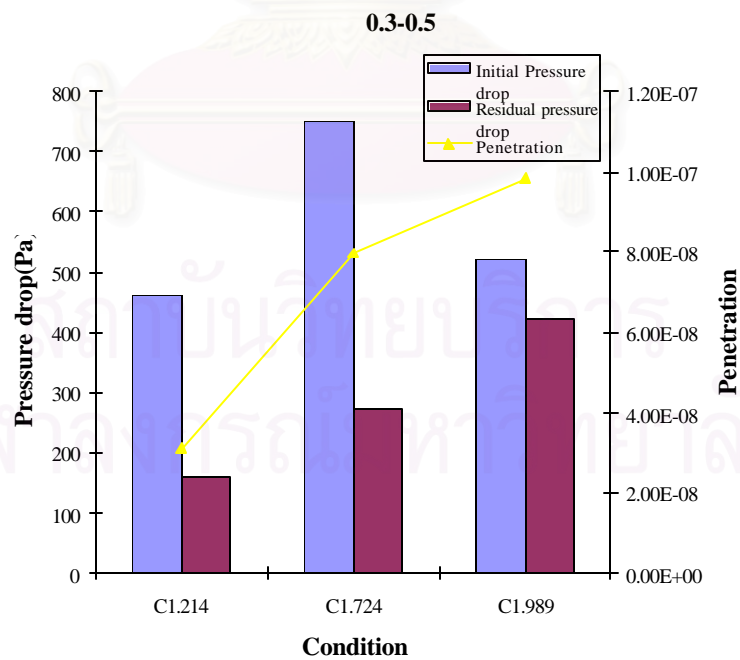


Figure 5.40 Effect of nominal face velocity on dust penetration in size range of 0.3-0.5 micron

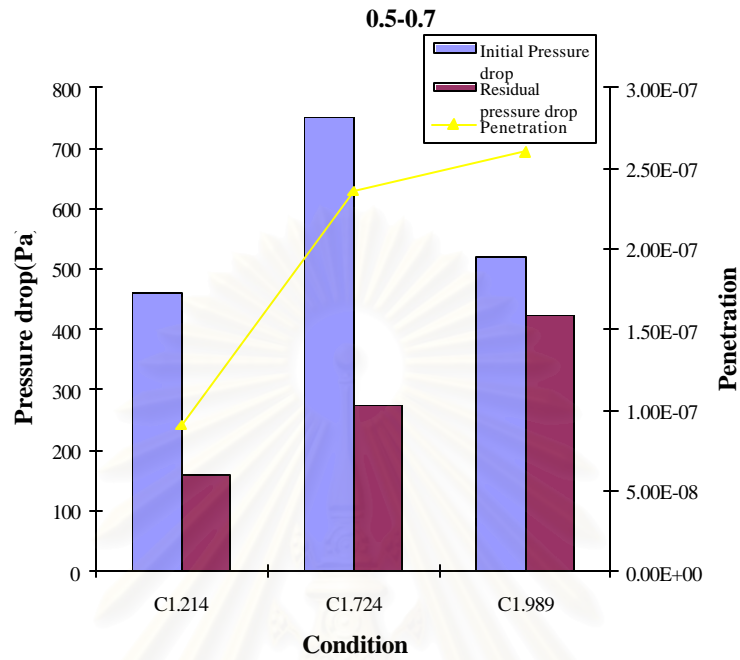


Figure 5. 41 Effect of nominal face velocity on dust penetration in range of 0.5-0.7 micron

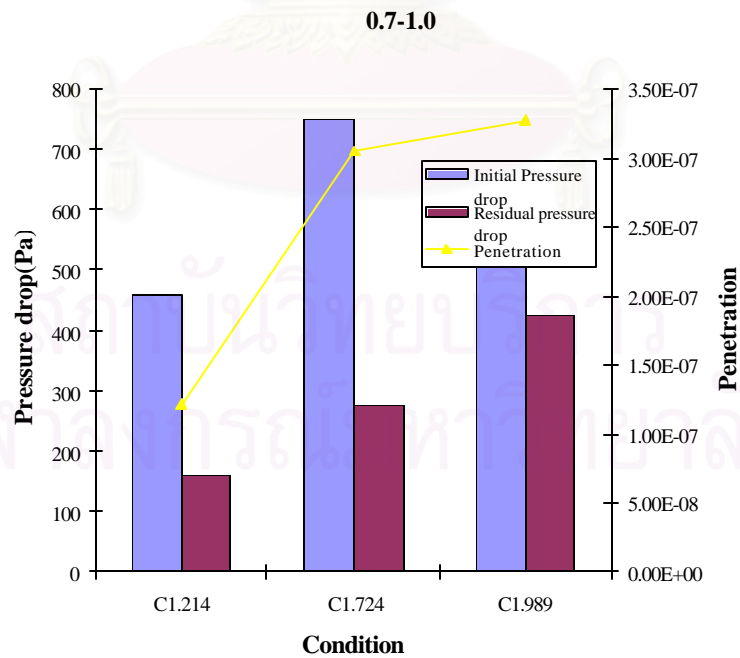


Figure 5. 42 Effect of nominal face velocity on dust penetration in size range of 0.7-1.0 micron

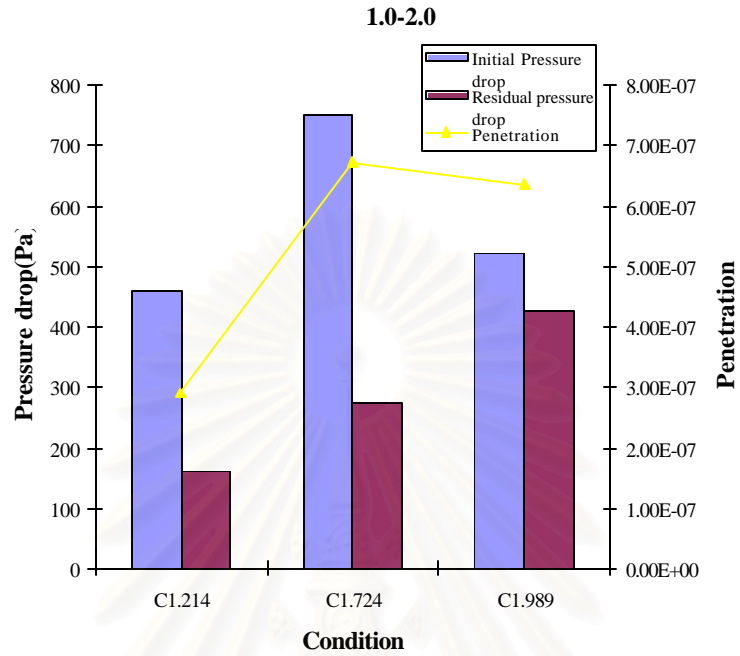


Figure 5. 43 Effect of nominal face velocity on dust penetration in range of 1.0-2.0 micron

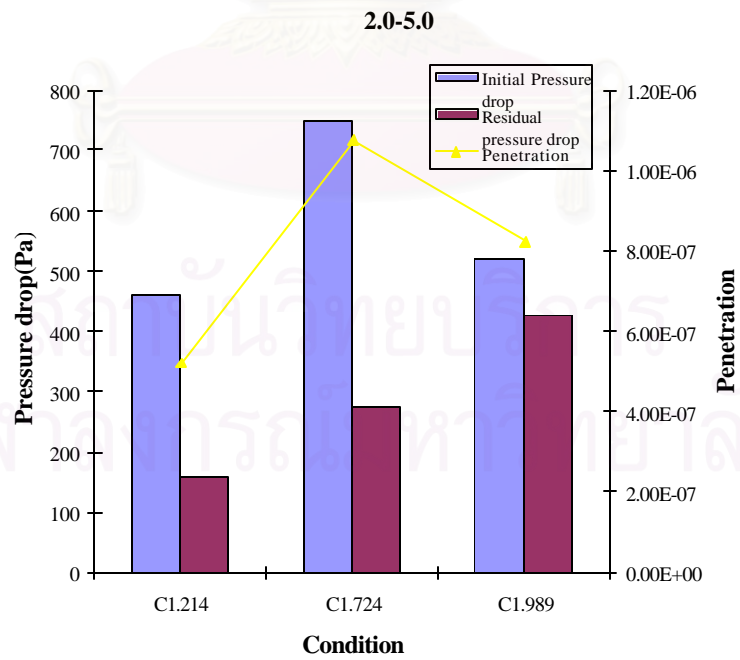
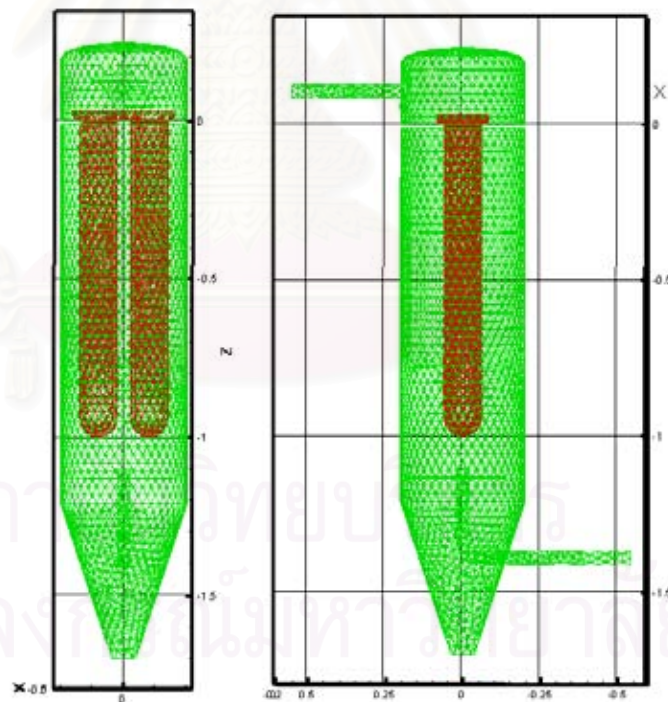


Figure 5. 44 Effect of nominal face velocity on dust penetration in range of 2.0-5.0 micron

For particles smaller than 1.0 micron, the penetration was strongly affected by the face velocity. The higher the face velocity, the higher the penetration becomes. For particles between 1.0 – 5.0 micron, the ability of particles in penetrating through the ceramic candle filter, as shown in case C1.989 (Figures 5.43-5.44), was gradually decreased. Obviously, it is harder for the bigger particles to penetrate through the ceramic candle filter than the smaller ones.

5.4. Comparison of the flow distribution between a twin ceramic candle filter system and a single ceramic candle filter system

CFD predictions are compared between a single and a twin ceramic candle filter system. It is shown that the CFD numerical calculation showed good agreement when compared with experimental data (a single ceramic candle filter), and predictions from a published empirical correlation.



Front view

Side view

Figure 5.45 Geometry of the system in front and side view

Originally it was thought that the local face velocity (normal velocity) of the gas flowing through each part of the candle wall should be identical if the filter

candles are clean and only clean air is used. Our CFD simulation results, however, clearly indicate that significant deviation in the local face velocity happened in both cases of single and twin candle filter units. Since the filters are brand-new and only clean air is used, it is reasonable to assume that the gas flow rate through the candle filter on the left is always equal to that on the right in the case of the twin ceramic candles. We characterize the wall property of the virgin filter candles by estimating the value of the pressure drop that would give the same viscous or flow resistance as the simulation value in the case of a single ceramic candle filter of clean air flow through the filter. For simplicity we assume that the twin-filter candles have identical characteristics. It is found that the tested viscous resistance of the virgin candle wall should be $6.95 \times 10^7 \text{ m}^{-2}$ when the total gas flow rate is $7.74 \times 10^{-3} \text{ kg/s}$ and the feed position is the top position. The pressure drop across the ceramic candle filter from the simulation was predicted as 97.75 Pa which was essentially the same as the case of a single ceramic candle filter with the same top inlet position.

For the twin-candle filter system of interest, we looked at the spatial distribution of flow around each candle. According to Figure 5.46 we can conclude that as in the single candle case, the local normal face velocity distribution is insignificantly affected by the position of the quadrant of the candle filter. In brief, the trend of the local velocity through the left candle is found to be the same as that through the right side at the conical part of the ceramic candle filter. However, the local face velocity through the candle filter changed remarkably on the hemi-spherical cap.

สถาบันวิทยบริการ
จุฬาลงกรณ์มหาวิทยาลัย

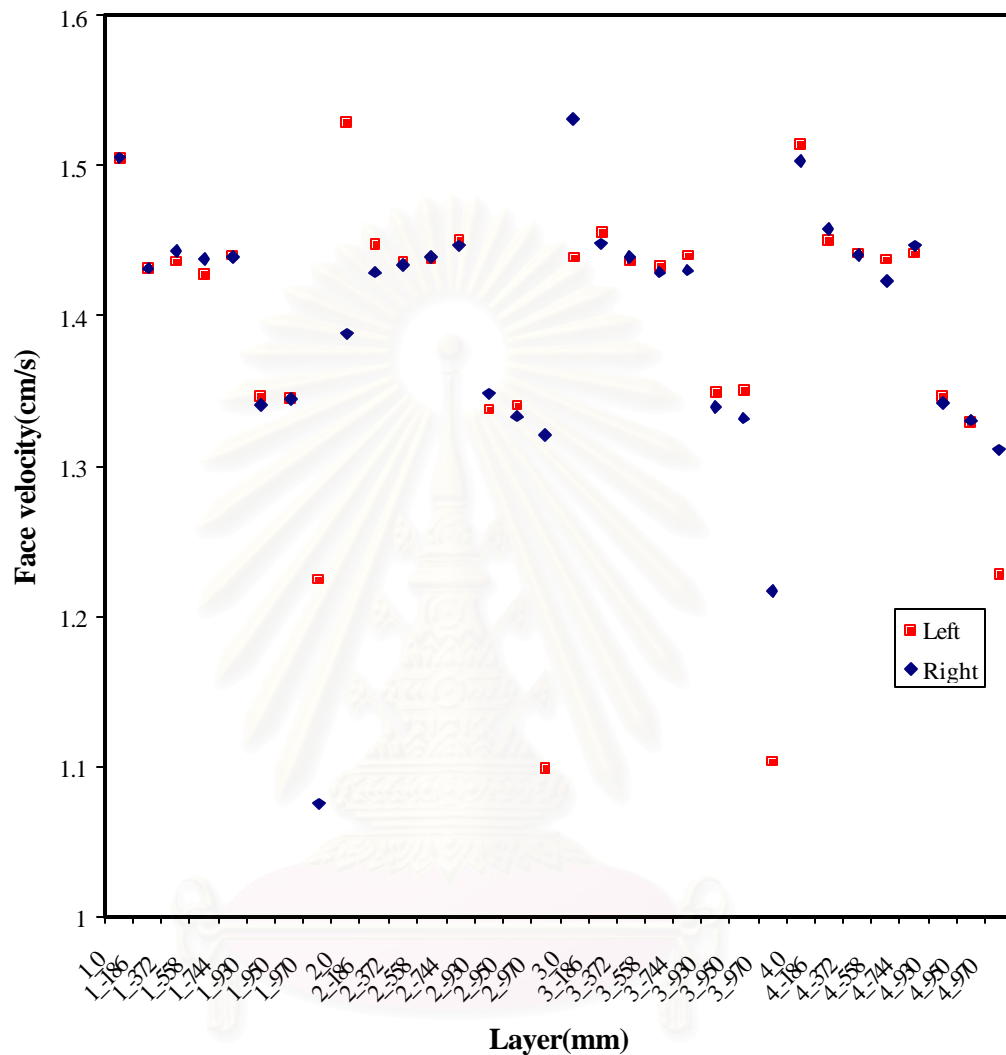


Figure 5.46 Local face velocity through each quadrant element as a function of height for the case of twin virgin candles

Figure 5.46 shows the average local face velocity at each height. It can clearly be seen that the local face velocities can be classified into 4 groups along the candle height. Figure 5.47 and Table 5.12 show the average local face velocity distribution as a function of the candle height. In Zone 1, there is not much difference in face velocity among the 4 layers. In Zone 3, the face velocity obviously drops further from Zone 1. Zones 1-2, do not show significant difference in face velocities in various quadrants. The face velocity, however, decreased sharply in Zone 3 (at $z = -930$). At

$z=-970$, the face velocities obviously differed. The left hand side of the filter has a slightly higher face velocity at the first and the fourth quadrants because the position of inlet port into the system was pointed between the left and the right of the ceramic candles. On the right hand candle, the face velocity at the second and the third quadrants had slightly higher face velocities than the other two.

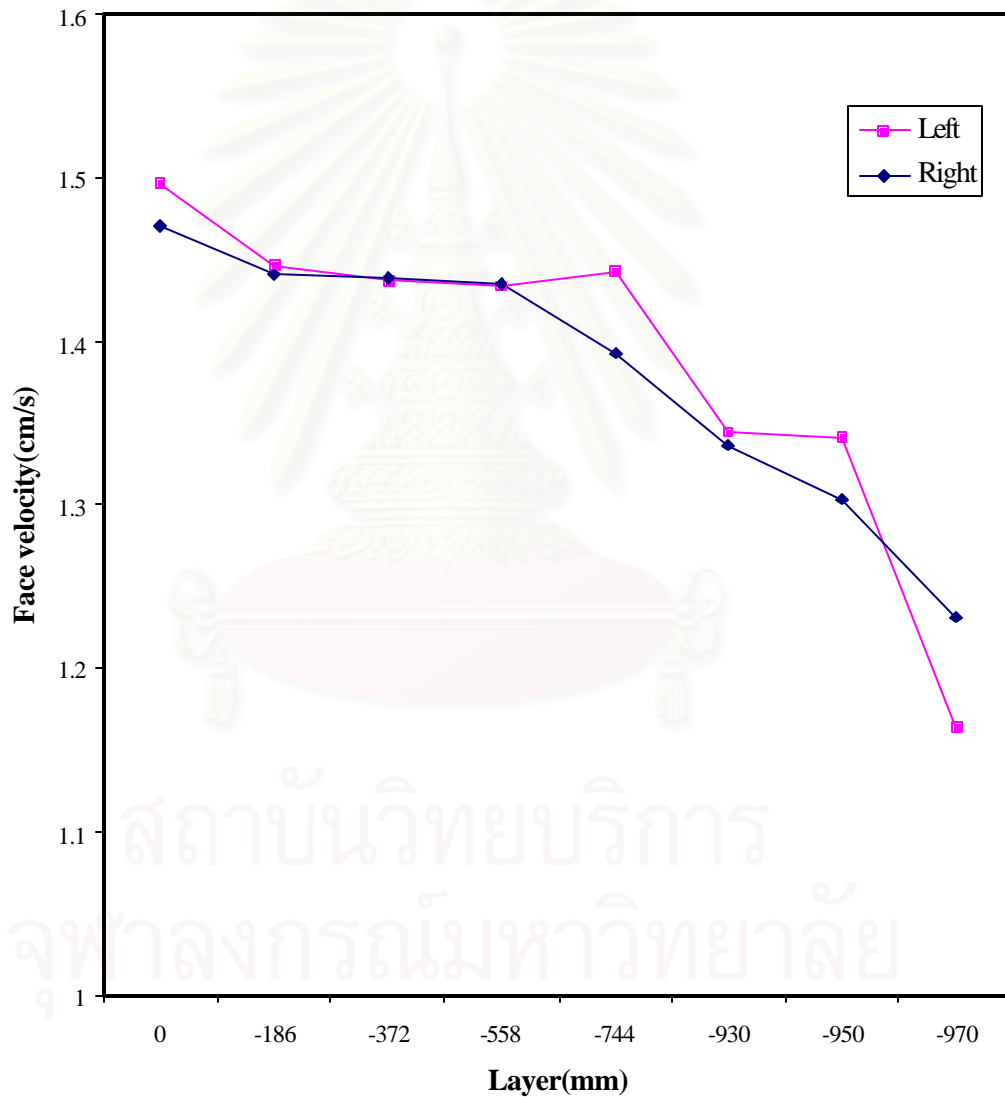


Figure 5.47 The average face velocity through each quadrant element as a function of height for the case of twin virgin candles

Fig. 5.47 shows the average local face velocity along z -direction for each candle. Layer -930 mm represents the boundary between the lower end of the cylindrical portion and the hemispherical cap. Layers -950 and -970 belong to the hemispherical cap. It should be pointed out that this interesting observation has not been obtained via simulation before. The air flow rate through the left hand candle was slightly higher than the other as shown in Table 5.12. The velocity distribution was divided to 4 zones; the face velocity decreased obviously at the hemi-conical cap. As mentioned in section 5.2.1, the spatial distribution of flow at the surface each candle of a single ceramic candle filter was similar to the case the twin ceramic candle filter. Moreover, since the surface area of twin candle filters is as much as twice that of the single candle filter, the average velocity in the case of twin candle filters is half of that of the single candle filter also. The profiles of velocity vectors for each inlet position of the twin ceramic candles filter are shown graphically in Appendix D.

Table 5.12 Velocity distribution along z position for the case of twin ceramic candles.

Layer(mm)	Average velocity(cm/s)	
	Left hand side	Right hand side
0	1.50	1.47
-186, -372, -558, -744	1.44	1.43
-930, -950	1.34	1.32
-970	1.16	1.35

สถาบันวิทยบริการ
จุฬาลงกรณ์มหาวิทยาลัย

CHAPTER VI

CONCLUSION AND RECOMMENDATION

6. Conclusion and recommendation

6.1. Conclusion

Obviously, the ceramic candle filter after utilization has never fully come back to a virgin state because some powder remained deposited permanently on the surface of the filter element. The event happened so often in practice that the residual pressure drop did not reach an asymptotic value, but increased slowly due to accumulation of particles lodged inside the filter medium which were not removed by pulse cleaning. Pulse duration, pressure differential, filtration velocity, influent dust concentration and position of gas inlet port have significant effects on filter performance. The observed rise in pressure drop was in many cases not linear, but showed a sudden sharp increase depending on the clogged state of the filter.

6.1.1. Simulation of steady clean air flow through virgin filters

In order to extensively investigate the performance of a candle filter it is necessary to simulate the results using FLUENT package. The following conclusions are obtained. The height (Z) of the candle filter affected the distribution of the local face velocity more than the location of the quadrant. At the base of the ceramic candle filter, the local normal face velocity was the highest and it decreased along the lower height. Especially, the face velocity through the spherical cap ($z=-930$ - 950 and -970 mm) decreased remarkably. The percentage of velocity deviation varied in the range of 0-20 % along the height of the ceramic candle filter. Especially, the normal face velocity deviation through the hemi-spherical cap increased remarkably.

The measured pressure drops across the ceramic candle filter for the top air inlet port position and the tangential inlet position were only slightly different. For the bottom air inlet position, the pressure drops were the highest compared to the other two positions. At the hemi-spherical cap, the average local air velocity for the bottom inlet position was higher than the top and tangential inlet positions because the feed port pointed directly towards the bottom of the ceramic candle filters.

6.1.2. Experimental results and discussion

Dust collection efficiency in excess of 99.9% was attained, even for the extremely fine dust fraction. However, the initial pressure drop and residual pressure drop of each experimental run influenced the collection efficiency. The increase in initial pressure drop indicated gradual accumulation of permanent cake (clogging) but the process could be retarded by reducing the face velocity.

6.1.2.1. Effect of the cleaning pulse duration

The pulse duration time was an important parameter in this work and a shortest duration time (100 ms) was found to be more appropriate in terms of collection efficiency than a duration time of 150 or 200 ms. Nevertheless, it may be concluded that the cyclic pressure drop pattern depended more on the initial pressure drop than the pulse duration.

6.1.2.2. Effect of pressure differential activated cleaning

Here a rapid increase in the pressure drop resulted in a higher cleaning frequency, which generally is disadvantageous for filter performance. The experimental results also revealed that, when the initial pressure drop was the same, a lower setting of the pressure differential activated cleaning led to a larger residual pressure drop. However, if the setting of the activating pressure differential was lower than 25 mmAq, the cleaning action was repeated too frequently. In short, both the lowest and the highest settings of the activating pressure differential resulted in a higher residual pressure drop. In summary, an intermediate value of 35 mmAq was most appropriate in this work because this case not only got the highest efficiency but also saved the air consumption for cleaning the ceramic candle filter.

6.1.2.3. Effect of nominal face velocity

The system operation was found to be stable down to a minimum filtration velocity of 1.216 m/min, and the over-pressure during pulse jet regeneration was similar at each nominal face velocity. Case C1.216 presents the lowest remaining dust inside the filter. As the nominal filtration velocity increased, the pressure drop became excessive at too high filtration velocities. The nominal face velocity was found to have more influence on the collection efficiency than the residual pressure drop. It is obvious from the dust penetration that case C1.742 and C1.989 were not appropriate to use for filtration. In case C1.989, fine particles not exceeding 1 micrometer in size

could penetrate through the surface of the ceramic candle filter better than in case C1.742. Particles exceeding 1 micrometer in size could not penetrate through the surface of the ceramic candle filter because they were captured on the cake that was deposited on the ceramic candle filter.

6.1.2.4. Effect of inlet dust concentration

Inlet dust concentration directly affects the cake thickness deposited on the filter medium. A higher inlet concentration generally leads to a higher residual pressure drop. The higher the inlet dust concentration, the more frequent the optimal cleaning of the filter. The residual pressure drop increased gradually when the inlet dust concentration increased, but the effect was less than the face velocity effect. As expected, the thicker the cake became, the higher the observed collection efficiency.

6.1.2.5. Effect of air inlet port position

It is interesting to see if the inlet port position has any effect on the pressure drop across the filter. The general tendency of the experimental cyclic pressure drop pattern did not clearly show any significant difference in the influence of the port position because we did not have enough virgin filters to start anew with each different port position. It is clear in all cases that the lower the initial pressure drop, the lower the residual pressure drop became but the higher the ratio of P_1 / P_R became. The bottom inlet port was apparently the most suitable position for feeding. When the tangential inlet position was compared with the top inlet position, the former showed a slightly better efficiency than the latter at similar initial pressure drops. This may be attributed to the fact that the tangential position distributed the spatial air flow more uniformly than the top position.

6.1.3. Correlation between face velocity and dust penetration

This section investigates the effect of nominal face velocity at the surface of the ceramic candle filter while the dust concentration was kept constant. For particles smaller than 1.0 micrometer, the penetration was strongly affected by the face velocity. The higher the face velocity, the higher the penetration became. For particles between 1.0 – 5.0 micrometers, the ability of the particles in penetrating through the ceramic candle filter decreased. Obviously, it is harder for the bigger particles to penetrate through the ceramic candle filter than the smaller ones.

6.1.4. Comparison of the flow distribution between a twin ceramic candle filter system and a single ceramic candle filter system

In the CFD simulation, we considered the case of clean virgin filter with clean air flow to see the local face velocity through each quadrant at the same layer of the virgin filter and found that the velocities were essentially the same. Each zone exhibited the average face velocity shown in Table 5.5 (single ceramic candle) and Table 5.12 (twin ceramic candles). The pattern of the face velocity distribution in the single candle case was the same as the twin candles case. In summary, the effect of the candle height was more significant than that of the quadrant for both cases. The percentage of velocity deviation varied in the range of 0-20 % along the height of the ceramic candle filter. At $z=0$, the percentage of normal face velocity deviation through the filter was highest. By the way, the face velocity deviation for both cases did not show any significant difference in each quadrant of the same layer.

6.2. Recommendation for future work

Dust properties as well as porous structures of ceramic candle filter and potential physical/chemical interactions between dust cake and gas should be themes of future investigations.

REFERENCES

- [1] E.Schmidt. Experimental investigations into the compression of dust cakes deposited on filter media. Filtration & Separation 32 (1995): 789-793
- [2] C.R.N. Silva, V.S. Negrini, M.L. Aguiar and J.R. Coury. Influence of gas velocity on cake formation and detachment. Powder Technology 101 (1999): 165-172
- [3] K. Smolders and J. Baeyens. Cleaning of hot calciner exhaust gas by low-density ceramic filters. Powder Technology 111 (2000): 240-244
- [4] D. Achim and H.F. Umhauer. The influence of conditioning and regeneration on the separation behaviour of rigid surface filters for the separation of particles from gases. Powder Technology 120 (2001): 223-231
- [5] K. Chikao and A. Mana. Effect of filter permeability on the release of captured dust from a rigid ceramic filter surface. Powder Technology 118 (2001): 113-120
- [6] D. Thomas, P. Penicot, P. Contal, D. Leclerc and J. Vendel. Clogging of fibrous filters by solid aerosol particles Experimental and modeling study. Chemical Engineering Science 56 (2001): 3549-3561
- [7] J.C. Ruiz, Ph. Blanc, E. Prouzet, P. Coryn, P. Laffont and A. Larbot. Solid aerosol removal using ceramic filters. Separation Purification Technology 19 (2000): 221-227
- [8] D. Achim, M.V. Ferer , M. Pulkit, P. Djuranovic , K. Gerhard and D.H. Smith. Patchy cleaning of rigid gas filters—transient regeneration phenomena comparison of modelling to experiment. Powder Technology 124 (2002): 55-66
- [9] J.H. Choi, S.J. Ha and H.J. Jang. Compression properties of dust cake of fine fly ashes from a fluidized bed coal combustor on a ceramic filter. Powder Technology 140 (2004): 106-115
- [10] S. Calle, P. Contal, D. Thomas, D. Bemer and D.Leclerc. Description of the clogging and cleaning cycles of the filter media. Powder Technology 123 (2002): 40-52
- [11] L. Andre, B. Marielle, M. Sonia and P. Eric . Separation Purification Technology 32 (2003): 81-85

- [12] C.B. Antonio, G. Leonardo and Jr. A procedure for calculating pressure drop during the build-up of dust filter cakes. Chemical Engineering and Processing 42 (2003): 495-501
- [13] T.G. Chuah, C.J. Withers and J.P.K. Seville. Prediction and measurements of the pressure and velocity distributions in cylindrical and tapered rigid ceramic filters. Separation Purification Technology 40 (2004): 47-60
- [14] Y. Awni and Al-Otoom. Prediction of the collection efficiency, the porosity, and the pressure drop across filter cakes in particulate air filtration. Atmospheric environment 39 (2005): 51-57
- [15] J.H Choi, S.M Kum, J.J Ahn, Y.C Bak, J.H Chung, and J.W Lee. Characteristics of Pulse Cleaning in the Ceramic Filter Unit at High Temperature [Online]: <http://www.netl.doe.gov/publications/proceedings/99/99korea/jhchoi.pdf>
- [16] Ch. Stocklmayer and W. Hoflinger, Simulation Practice and Theory 6 (1998): 281-296
- [17] A. Aroussi, K. Simmons and S.J. Pickering. Particulate deposition on candle filters. Fuel 80 (2001): 335-343
- [18] T. Wiwut, T. Charinpanitkul, W. Jintaworn, L. Jerapan, A. Mana, T. Fukui, M. Yoshikawa and M. Naito. (2004). Simulation and analysis of high-efficiency twin-ceramic-candle filtration process for high-temperature emission gas [CD-ROM]. Report of NEDO project 2004.
- [19] G. Phillip, S.G. Heidi and R. Donald. Transport properties of porous membranes based on electrospun nanofibers. Colloids and surfaces A: Physicochemical and Engineering Aspects 187-188 (August 2001): 469-481
- [20] S. Ergen, Chemical Engineering Progress 48 (1952): 89
- [21] D. Leith and R.W.K. Allen. Dust filtration by fabric filters, in: R.J. Wakeman (Ed.), Progress in Filtration and Separation 4 (1986): 1-57.
- [22] Aerosol Technology: properties, Behavior, and Measurement of Airborne Particles. 2nd edition. USA : John Wiley & Sons, Inc., 1999.: 206-207
- [23] S.V. Patankar. Numerical Heat Transfer and fluid Flow: 25-26
- [24] FLUENT User's Guide Version 6.1 2003: FLUENT India.



APPENDICES

สถาบันวิทยบริการ
จุฬาลงกรณ์มหาวิทยาลัย



APPENDIX A

Dimensions of the dust removal system

สถาบันวิทยบริการ
จุฬาลงกรณ์มหาวิทยาลัย

The dust removal system consists of many parts. Figures A1-A12 shows the dimensions and diagrams of the dust removal system design plan. Design all of the system are shown in Figure A1

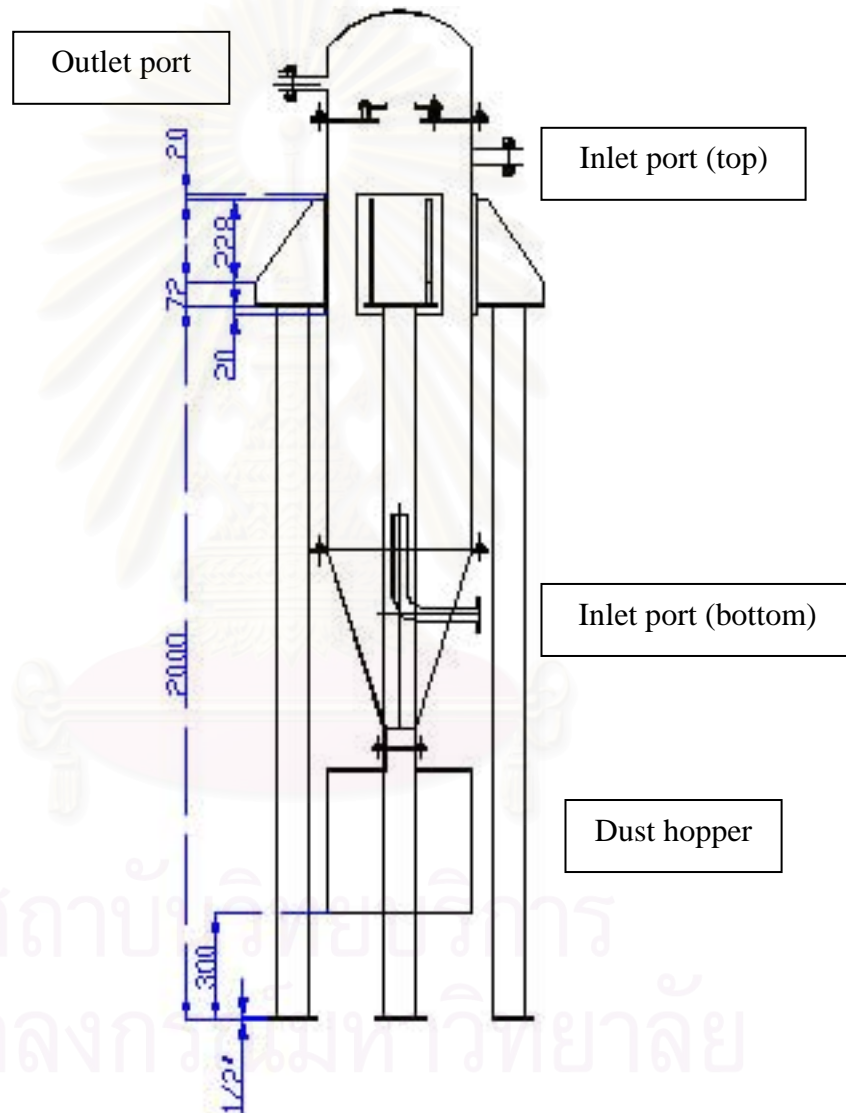


Figure A1 The height of the housing

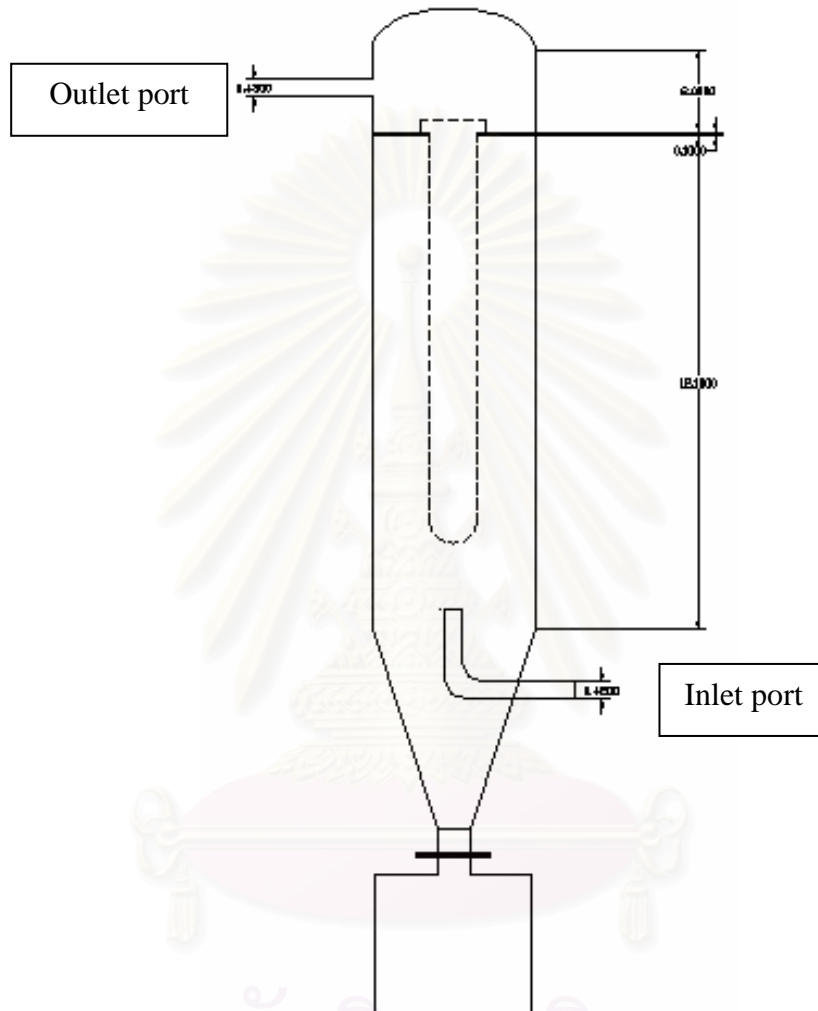


Figure A2 the inside view of the chamber

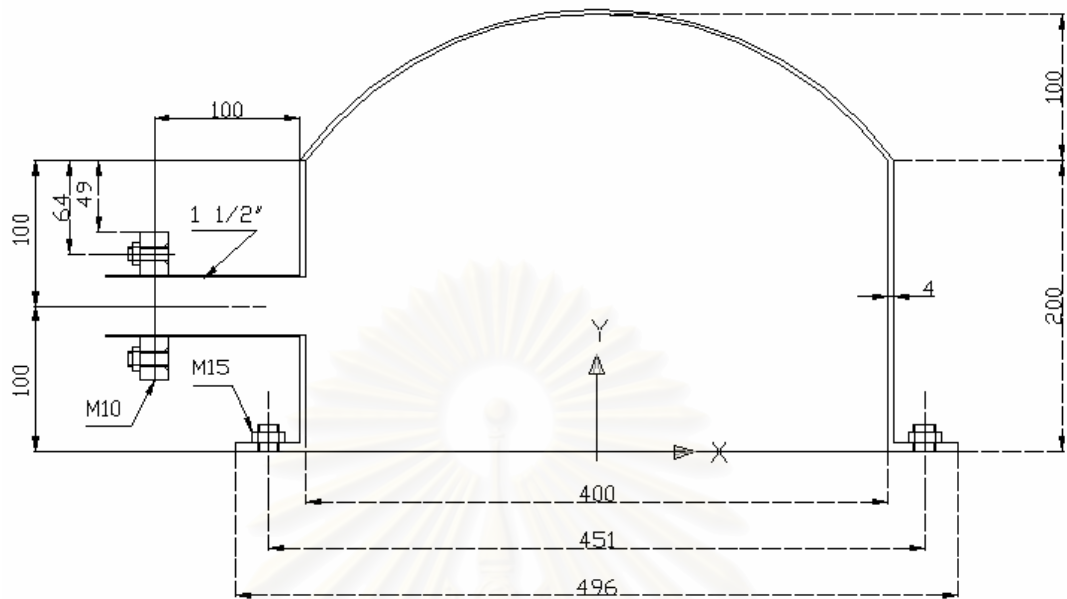


Figure A3. The cap of the chamber

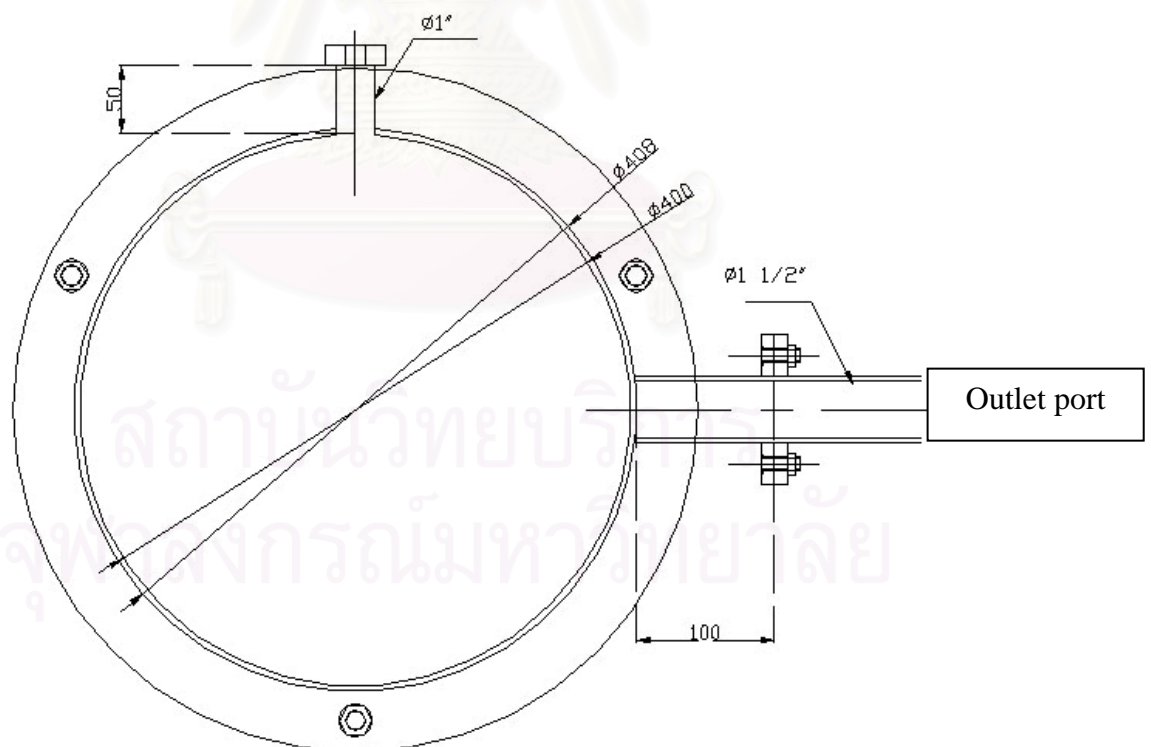


Figure A4. The top view of the flange near the outflow port

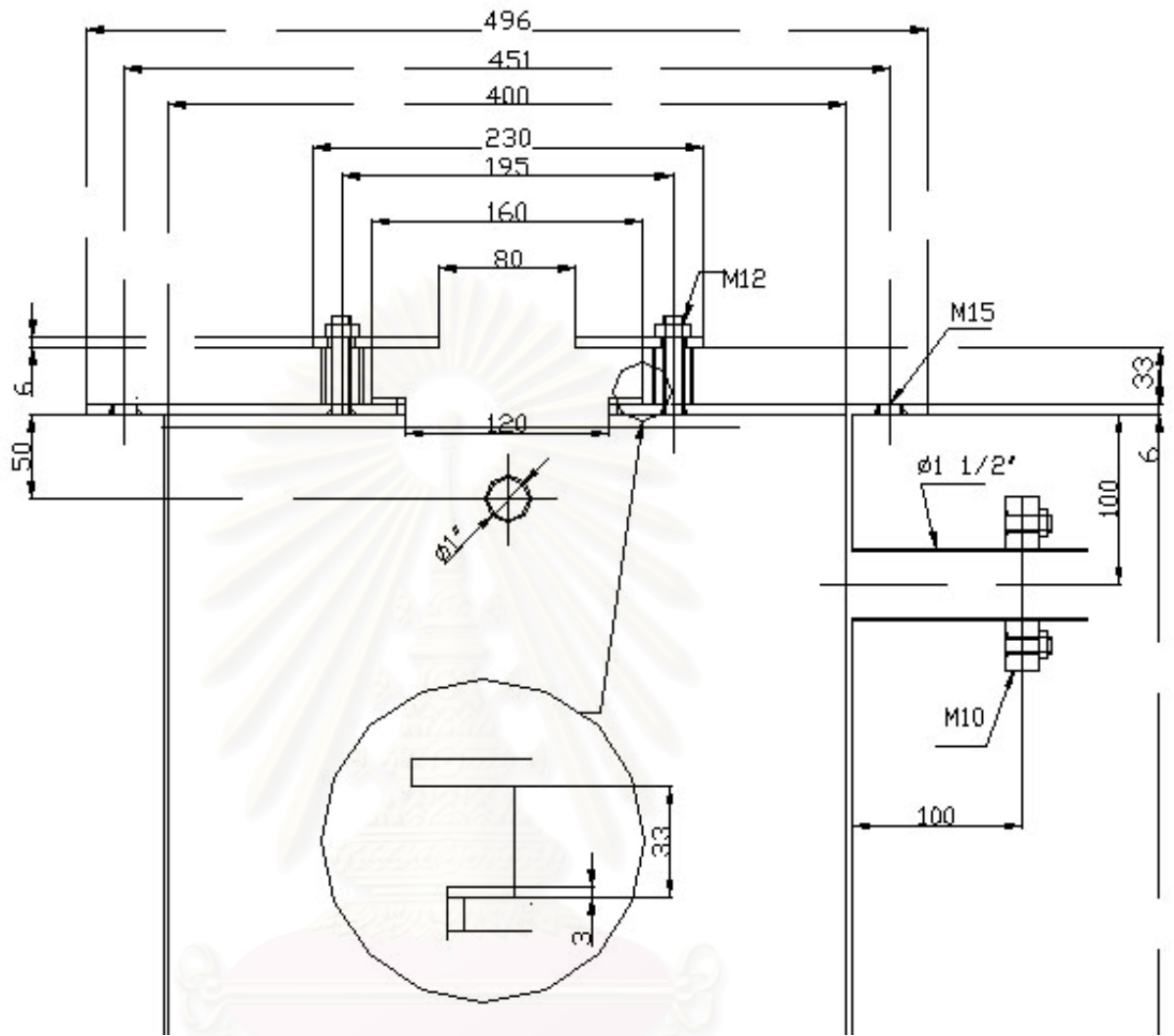


Figure A6 The side view of the flange to hold a candle filter

สถาบันวิทยบริการ
จุฬาลงกรณ์มหาวิทยาลัย

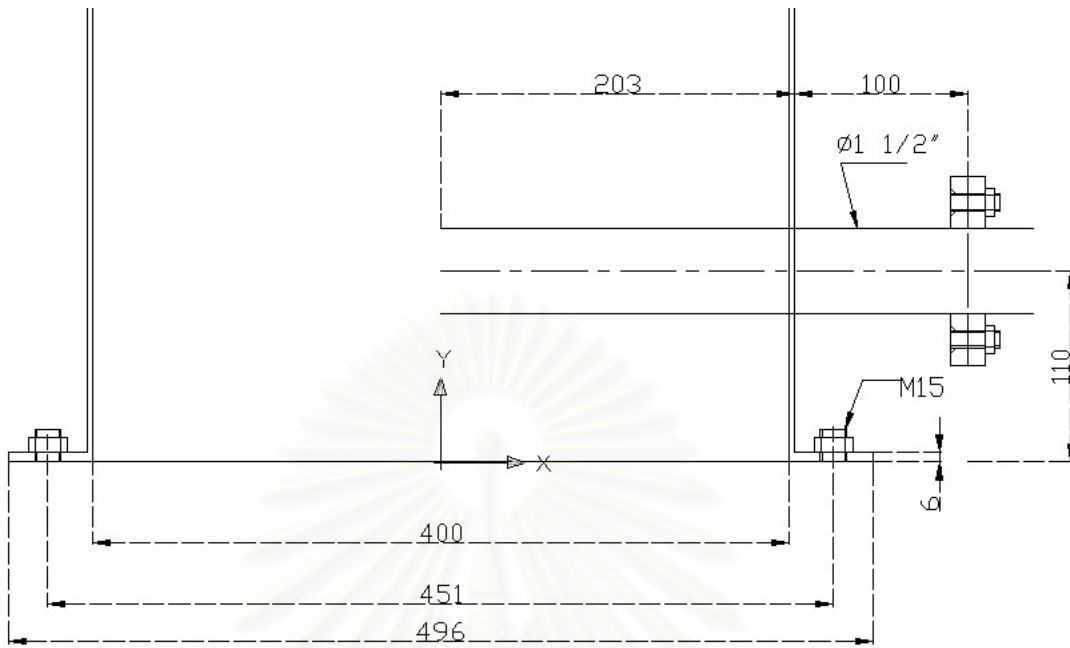


Figure A7 The side view of the position of tangential inlet port

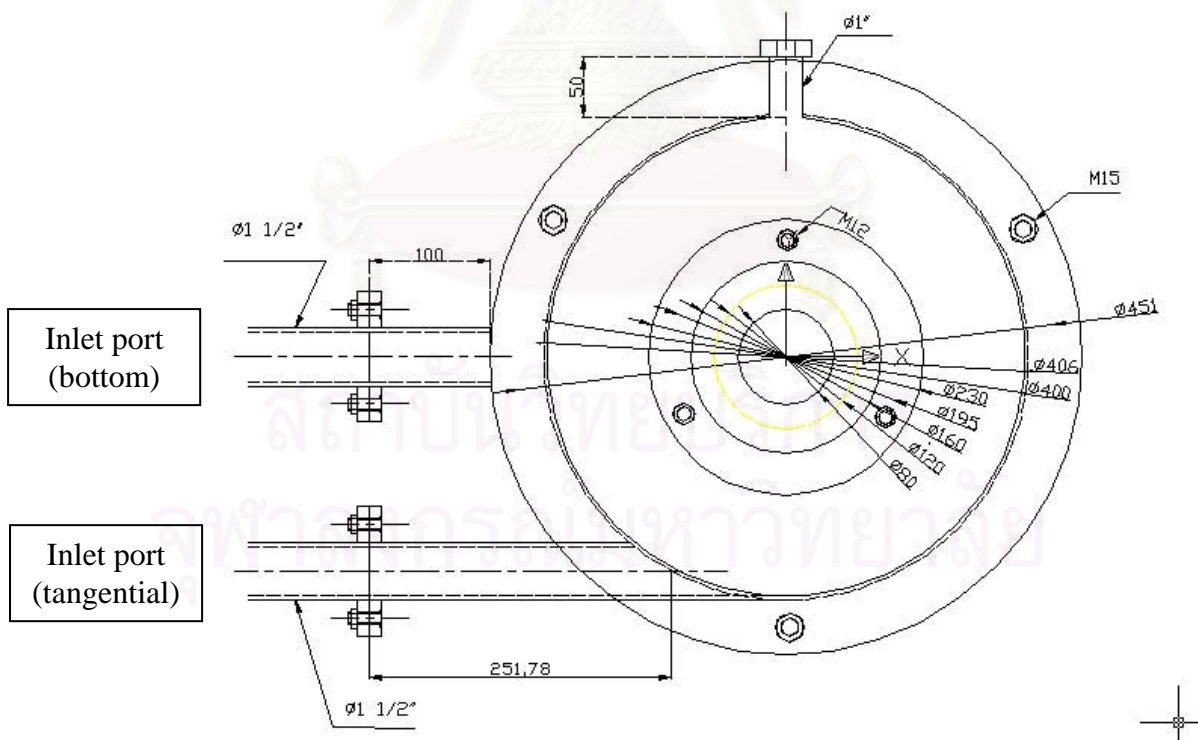


Figure A8. The top view of the bottom flange of the chamber

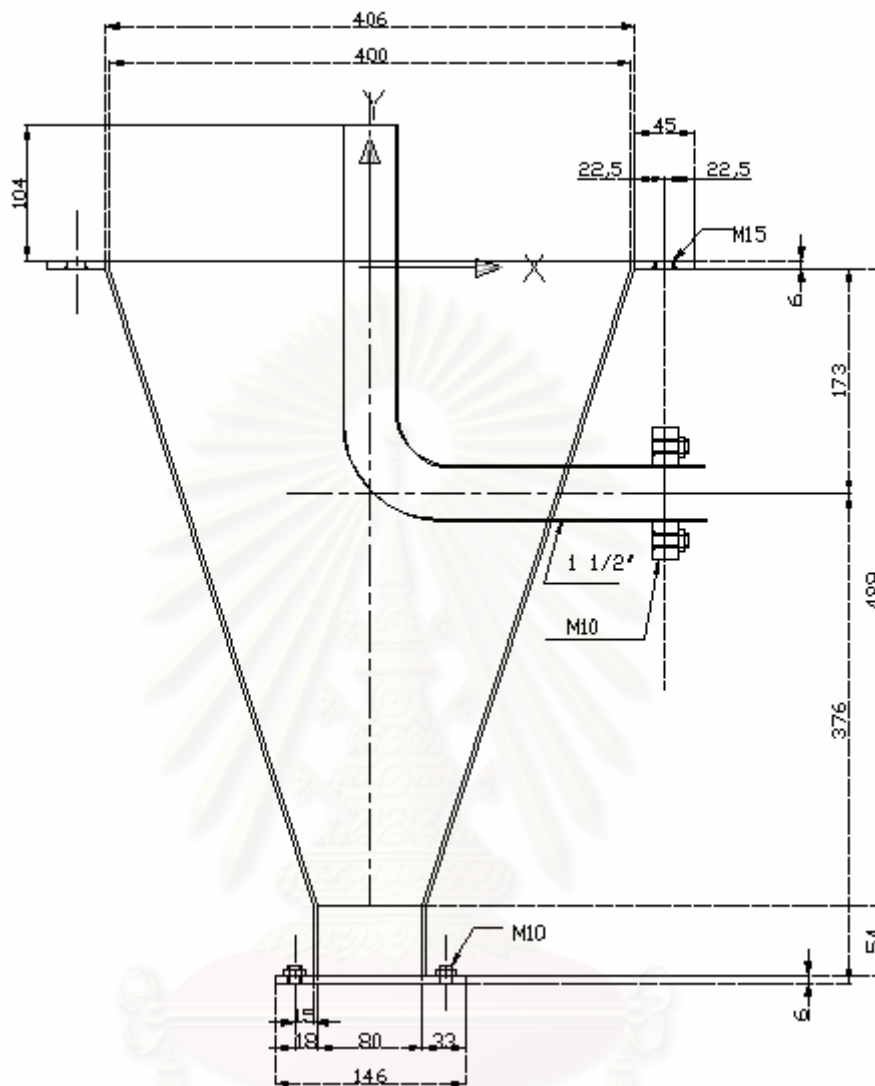


Figure A9. The conical part of the chamber

สถาบันวิทยบริการ
จุฬาลงกรณ์มหาวิทยาลัย

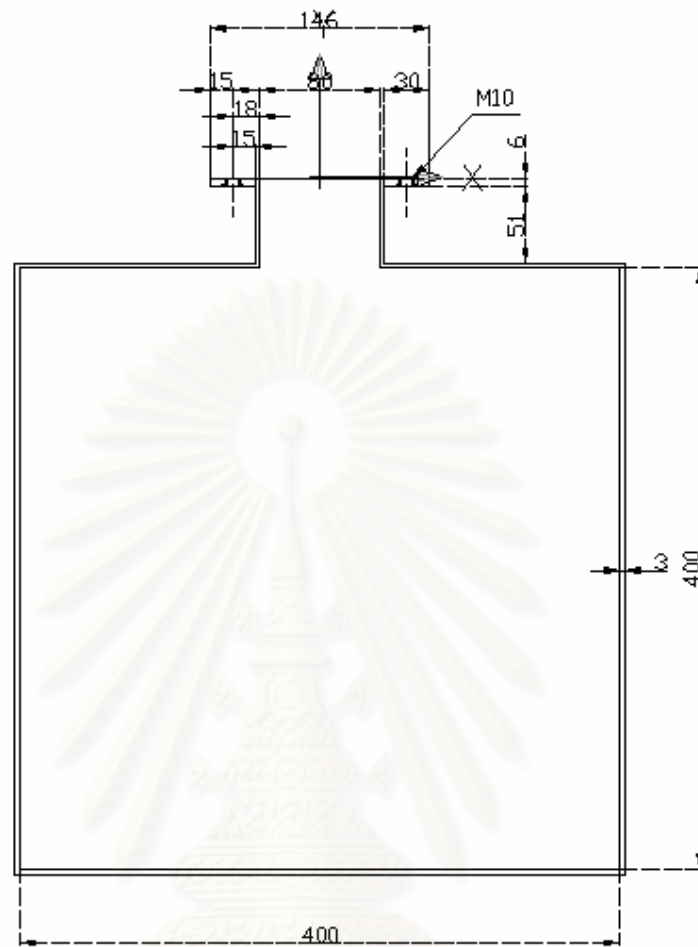


Figure A10. The hopper of the chamber

สถาบันวิทยบริการ
จุฬาลงกรณ์มหาวิทยาลัย

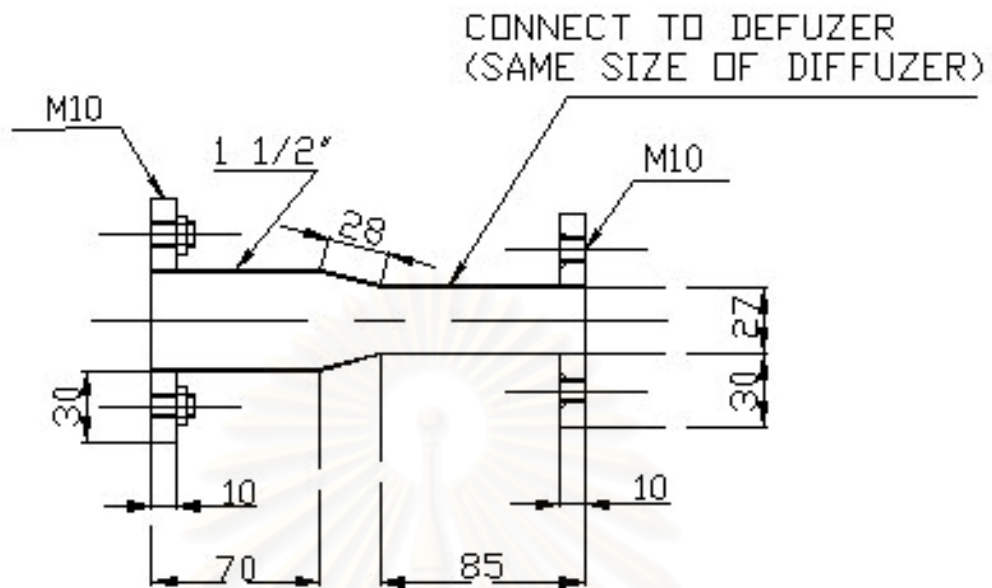


Figure A11. The connector
This part is used to connect to the air diffuser

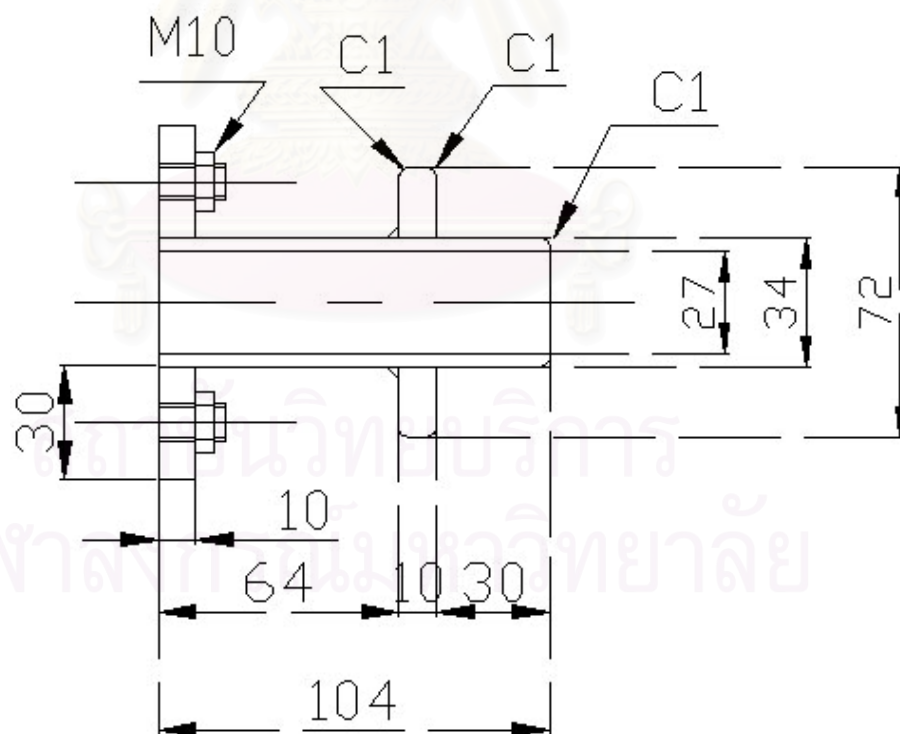
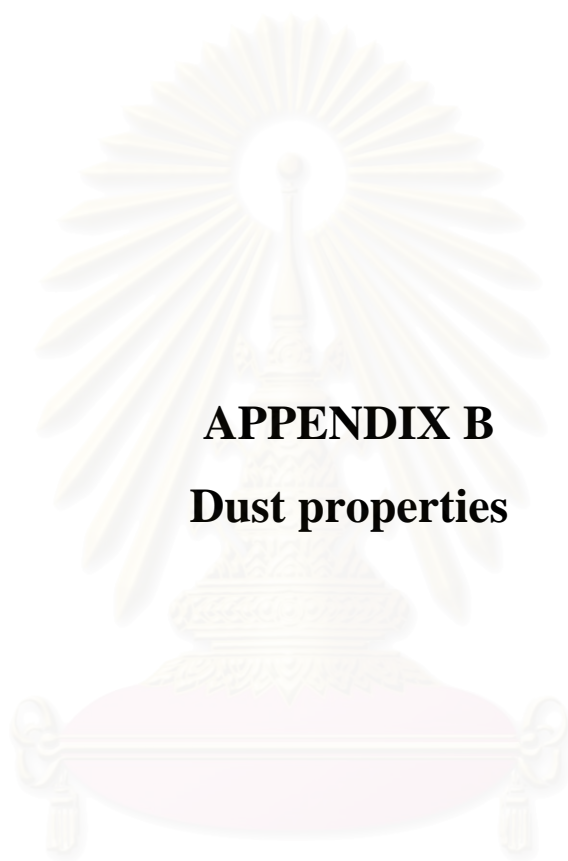


Figure A12. The air diffuser
The diffuser is used to disperse the agglomerated dust coming from screw feeder.



APPENDIX B
Dust properties

สถาบันวิทยบริการ
จุฬาลงกรณ์มหาวิทยาลัย

1. Ultracycnometer (for analyzing the true density of dust)

Used to find the true density of porous and non-porous solid, the “Ultracycnometer” measures the accurate volume of powder using the principle of Archimedes for fluid substitution. The fluid is a known gas of small molecules which gas into the void (volume) of solids. Assuming ideal gas, the simple equation of state $PV=nRT$ is used to calculate the volume from the pressure at a fixed temperature.

The presence of impurities in the (porous) solid sample can affect the results in several ways.

1. The actual weight of the sample is less than the weight indicated when weighed.
2. Contaminants may fill some pores thereby causing a large sample volume to be observed.
3. Volatile impurities will cause erroneous readings due to evaporation loss. The calculation makes use of Equations B.1 and B.2

$$V_p = V_c - V_R \left[\frac{P_1}{P_2} - 1 \right] \quad \text{B.1}$$

V_p = Volume of powder (cm^3)

V_c = Volume sample Cell (cm^3)

V_R = Reference volume (cm^3)

Calculate the true density by the following equation

$$D = \frac{M}{V} \quad \text{B.2}$$

Table B.1 The result of the measured true density

Mass(g)	No. of experiments	Volume(cm^3)	Apparent Density(g/cm^3)	SD
1.073	1	0.3954	2.7140	0.0138
	2	0.3965	2.7059	
	3	0.3966	2.7056	
	4	0.3984	2.6931	
	5	0.4006	2.6787	
	Average	0.3975	2.6995	

2. Laser Particle Size Distribution Analyzer

The data are plotted as volume (mass) versus particle diameter of Turbo1.

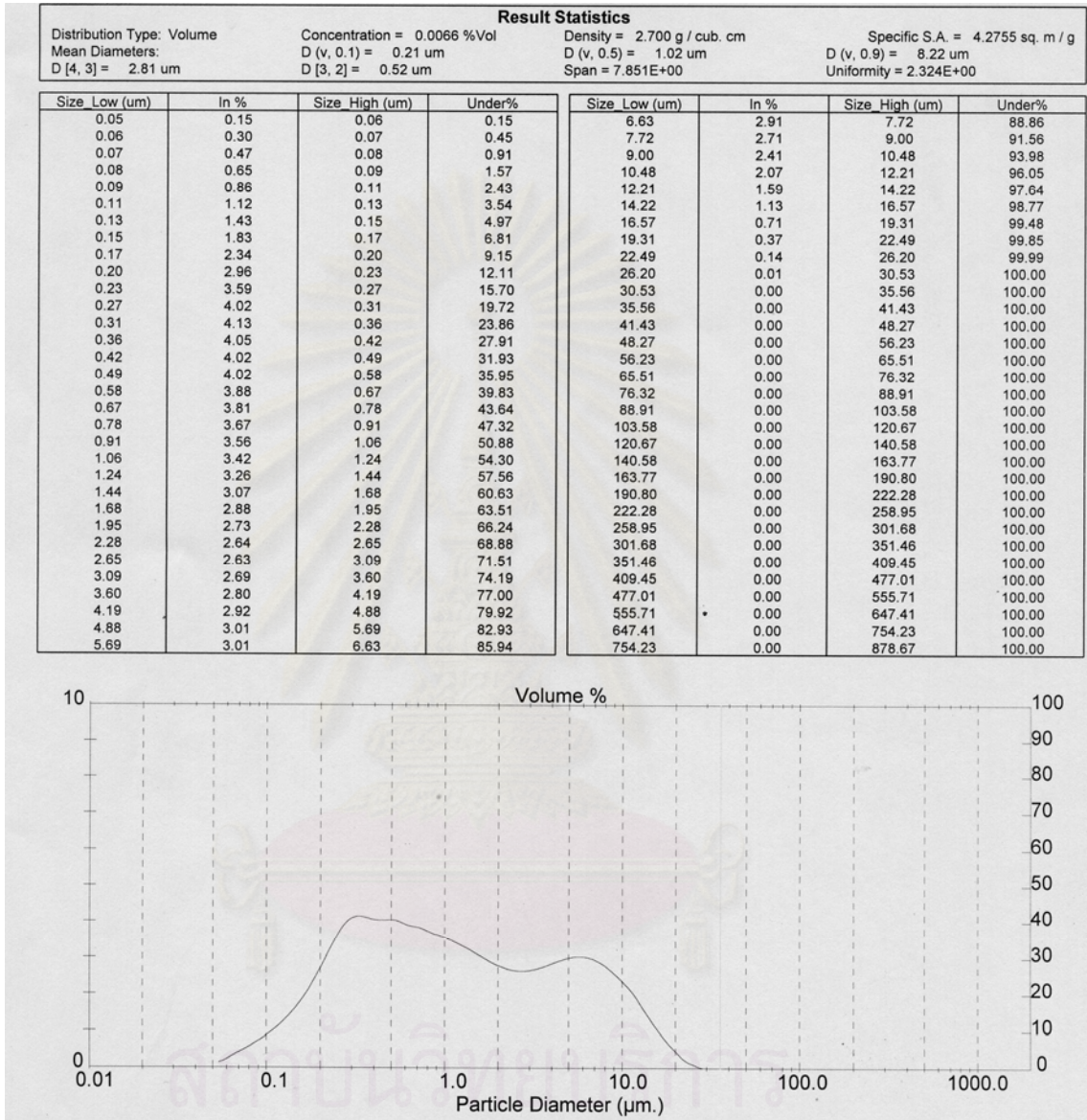


Figure B.2 The dust size distribution as determined by Laser Particle Size Distribution Analyzer

3. Powder Tester

The Powder Characteristics Tester is a single instrument which provides seven mechanical measurements and three supporting measurements of dry bulk powder samples.

1. Angle of Repose

The angle of repose is measured from a heap carefully built up by dropping the material through a vibrating screen and glass funnel onto a horizontal plate.

2. Angle of Fall

The angle of fall is measured from a heap to which a certain shock has been given.

3. Angle of Difference

The angle of difference is the difference between the angle of repose and the angle of fall.

4. Aerated Bulk Density

Aerated bulk density is obtained by dropping the sample through a vibrating chute to a fixed volume cup.

5. Packed Bulk Density

Packed bulk density is obtained by tapping the sample a specific number of times from a constant height and measuring the compressibility caused by the shock of dropping.

6. Compressibility

Compressibility is determined from the measurement of the aerated and packed bulk densities.

7. Cohesiveness

Cohesiveness is defined by the residue of the powder remaining on a mesh. This results from applying a constant amplitude of vibrations for a certain period of time to the sample powder on a screen.

8. Angle of Spatula

Measurement is made for the angle of the powder formed on a spatula.

9. Dispersibility

Through dropping a certain volume of the powder from a constant height, this characteristic is obtained from the residue staying on a watch glass.

10. Uniformity

Uniformity is obtained by measuring the dispersibility or by sieving. Uniformity of a given sample is defined as the ratio of the values d_{60}/d_{10} .

Table B.2 The powder characteristics and flowability measured by the Powder Tester

Angle of Repose	53.2	degree	Index	12
Aerated Bulk Density	0.714	g/cc		
Packed Bulk Density	1.264	g/cc		
Compressibility	43.5	%	Index	2
Spatula(Before impact)	62.1	degree		
Spatula(After impact)	58.1	degree		
Angle of Spatula	60.1	degree	Index	15
Cohesion	22.2	%	Index	12
Uniformity	0		Index	25
			Total Index	66

Table B.3 The powder floodability measured by the Powder Tester

Angle of Fall	37.8	degree	Index	16
Angle of Difference	15.4	degree	Index	15
Dispersibility	18.7	%	Index	14.5
Flowability			Index	25
			Total Index	70.5

The result shows that the level of flowability is normal. The floodability result is fairly high and indicates that the powder tends to flush, and has good capability to spread.

4. Relationship between the pressure regulator setting and the inlet air flow

The calibration curve was obtained by adjusting the pressure setting of the regulator, reading the flow rate on the rotameter and plotting the relationship between the air flow rate and the pressure setting of the system. The data were shown in Table B.4.

สถาบันวิทยบริการ
จุฬาลงกรณ์มหาวิทยาลัย

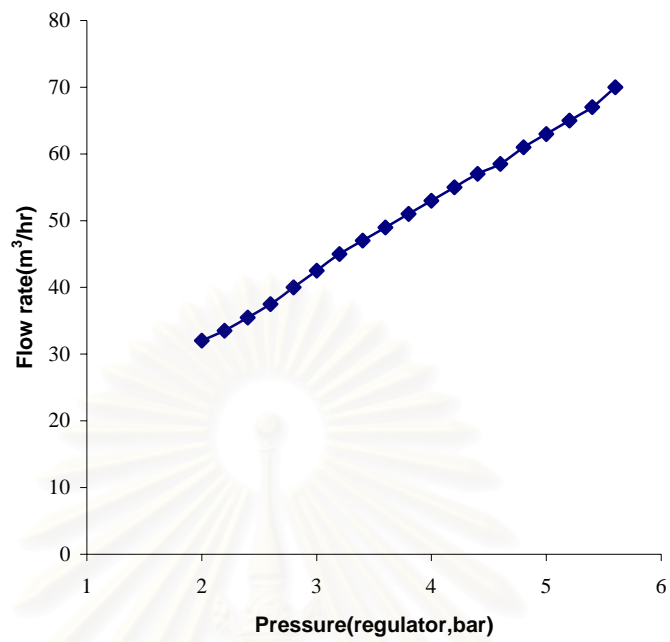


Figure B.3 Calibration curve of flow rate versus pressure setting

Table B.4 Value of flow rate versus pressure setting

Regulator Setting(bar)	Flow rate(m ³ /hr)
2.00	32.00
2.20	33.50
2.40	35.50
2.60	37.50
2.80	40.00
3.00	42.50
3.20	45.00
3.40	47.00
3.60	49.00
3.80	51.00
4.00	53.00
4.20	55.00
4.40	57.00
4.60	58.50
4.80	61.00
5.00	63.00
5.20	65.00
5.40	67.00
5.60	70.00



สถาบันวิจัยบริการ
จุฬาลงกรณ์มหาวิทยาลัย

APPENDIX C
Experimental data

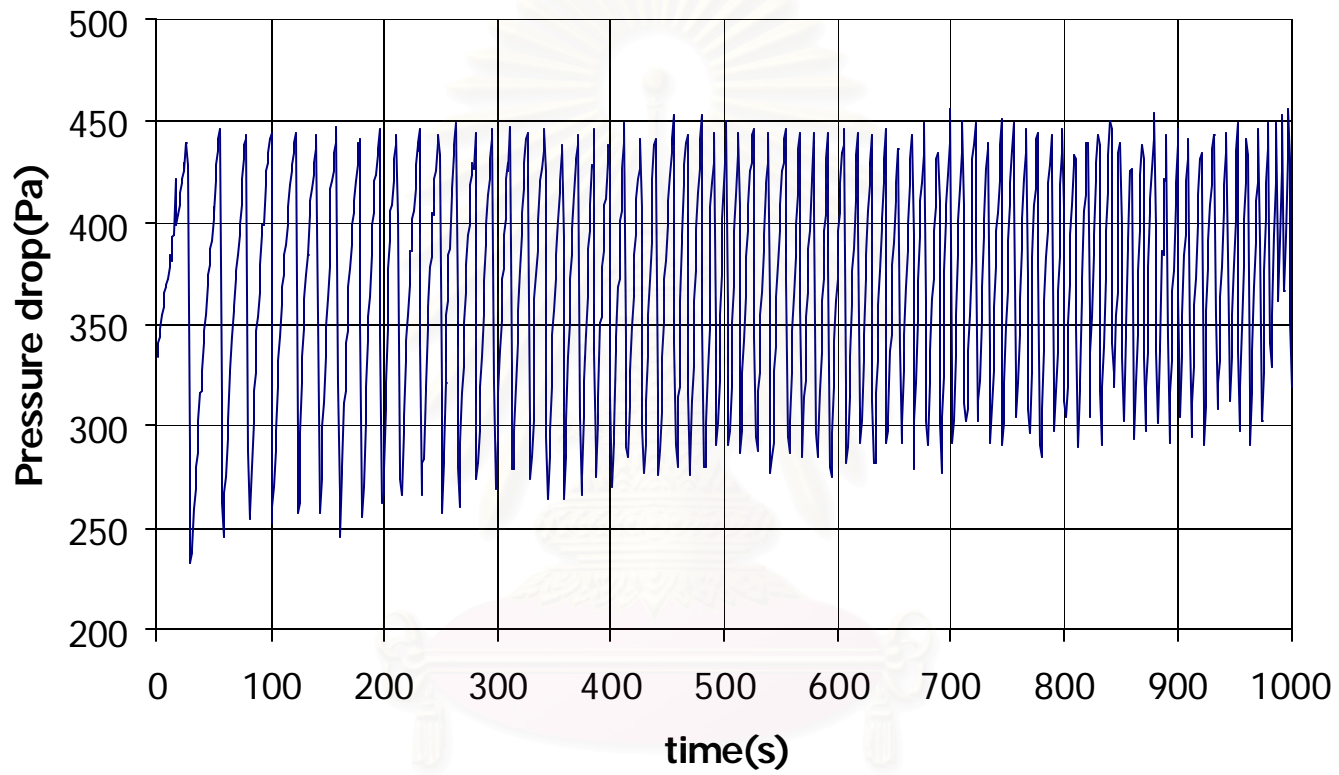


Figure C1 Run A100 (1)

สถาบันวิจัยบริการ
จุฬาลงกรณ์มหาวิทยาลัย

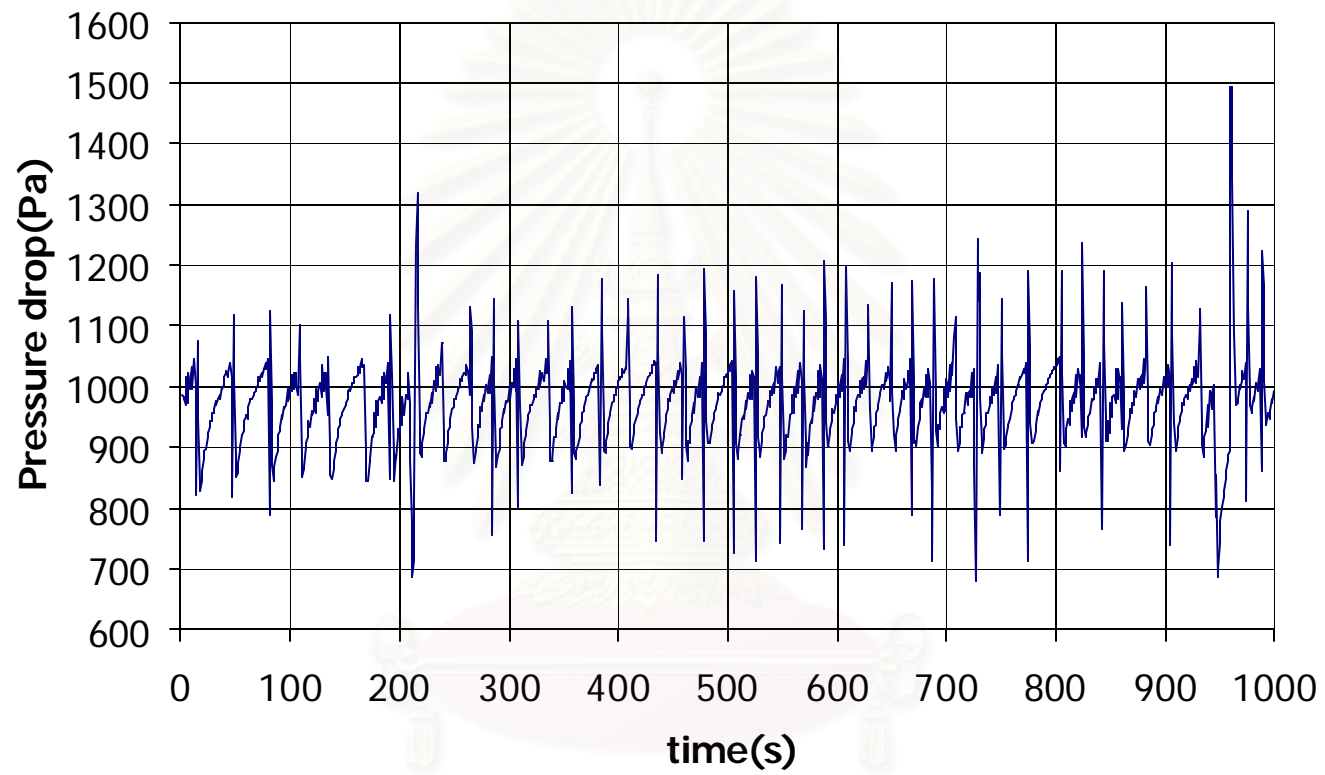


Figure C2 Run A200 (2)

สถาบันวิทยบริการ
จุฬาลงกรณ์มหาวิทยาลัย

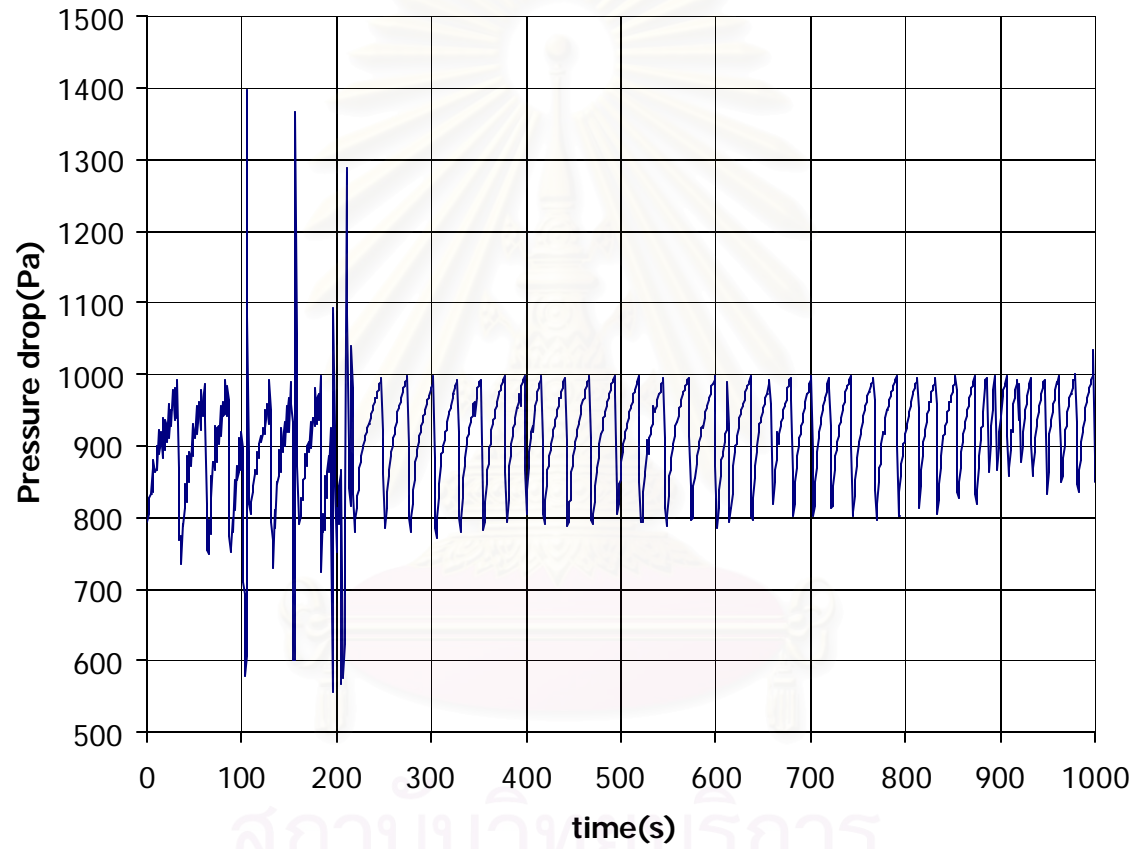


Figure C3 Run B15 (3)

สถาบันวิทยบริการ
จุฬาลงกรณ์มหาวิทยาลัย

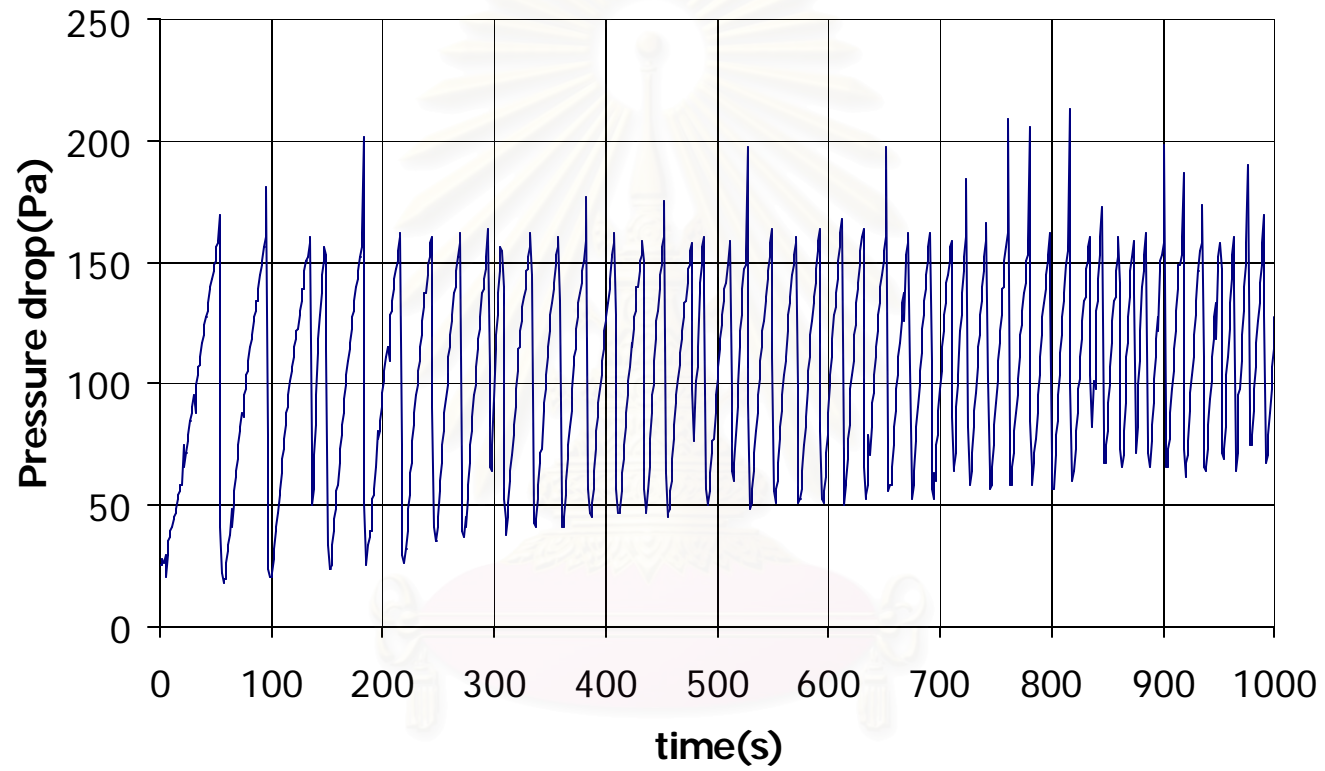


Figure C4 Run B15 (4)

สถาบันวิทยบริการ
จุฬาลงกรณ์มหาวิทยาลัย

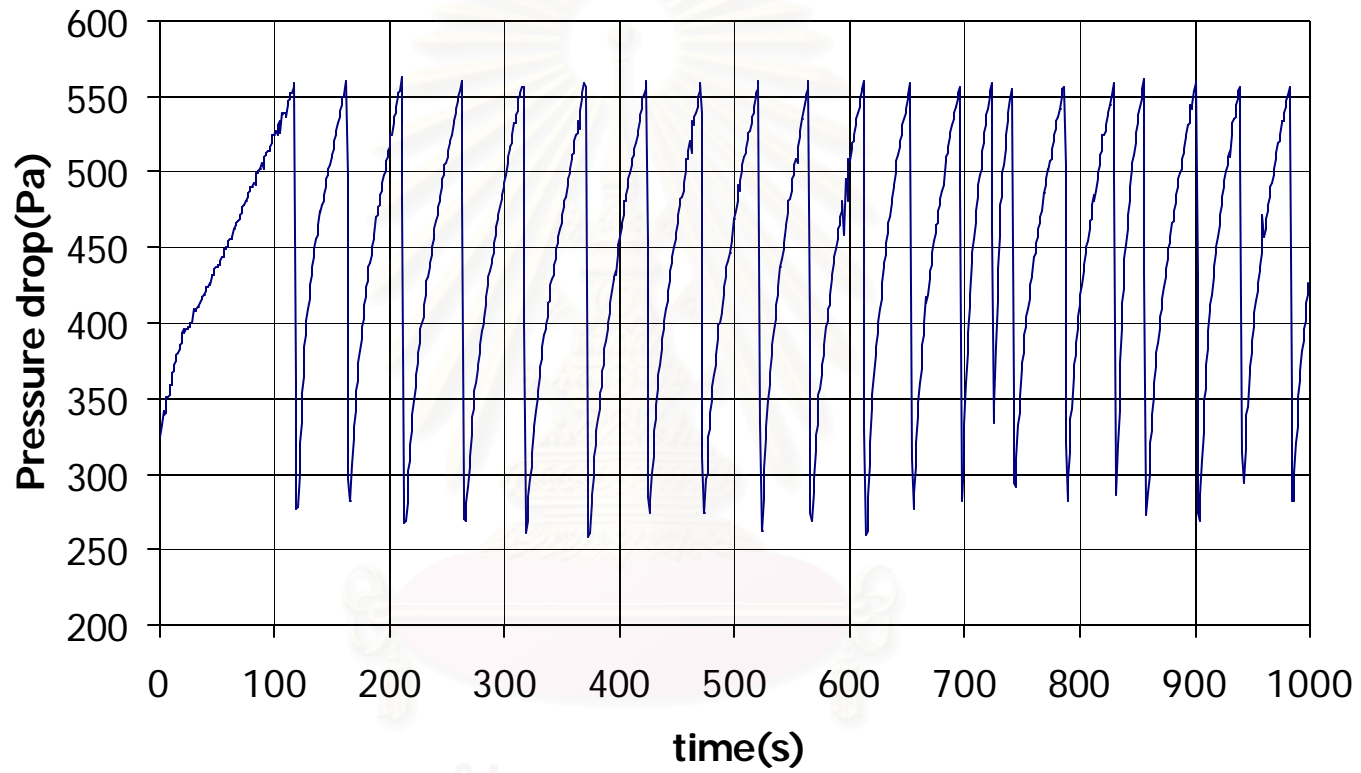


Figure C5 Run B35 (5)

สถาบันวิจัยปฏิบัติการ
จุฬาลงกรณ์มหาวิทยาลัย

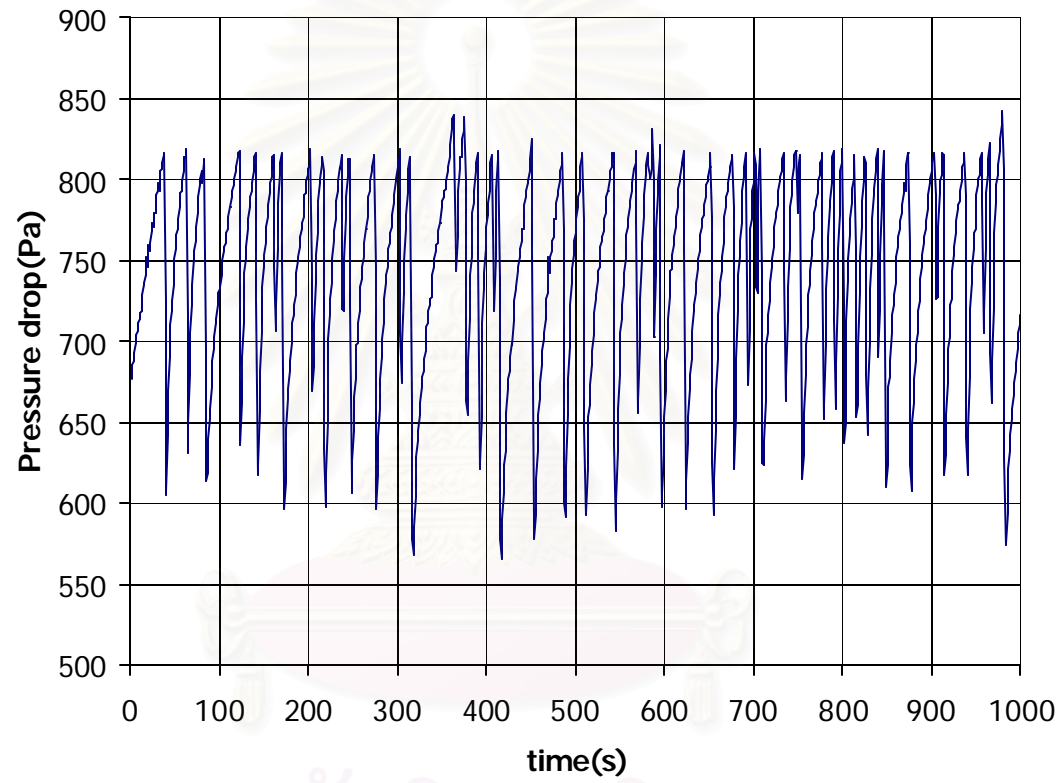


Figure C6 Run C1.724 (6)

สถาบันวิทยบริการ
จุฬาลงกรณ์มหาวิทยาลัย

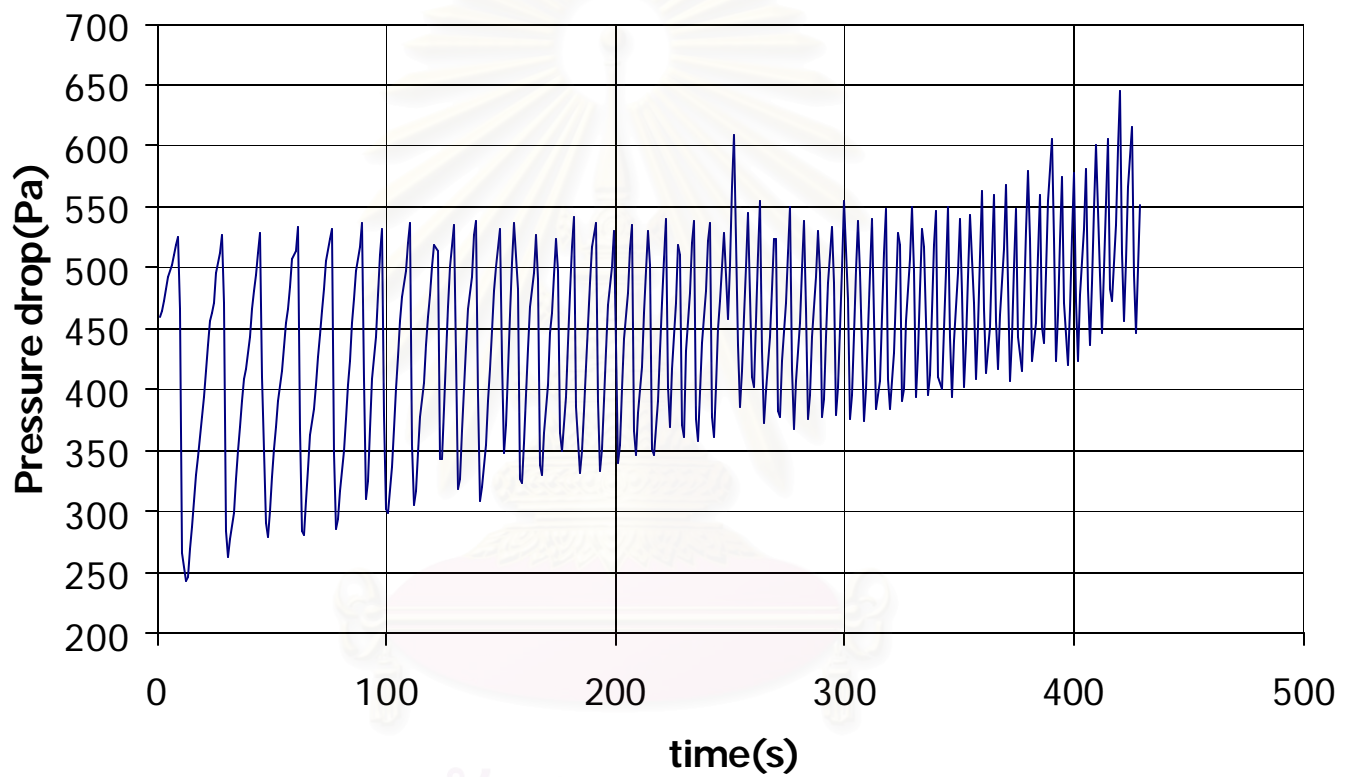


Figure C7Run C1.989 (7)

สถาบันวิจัยบริการ
จุฬาลงกรณ์มหาวิทยาลัย

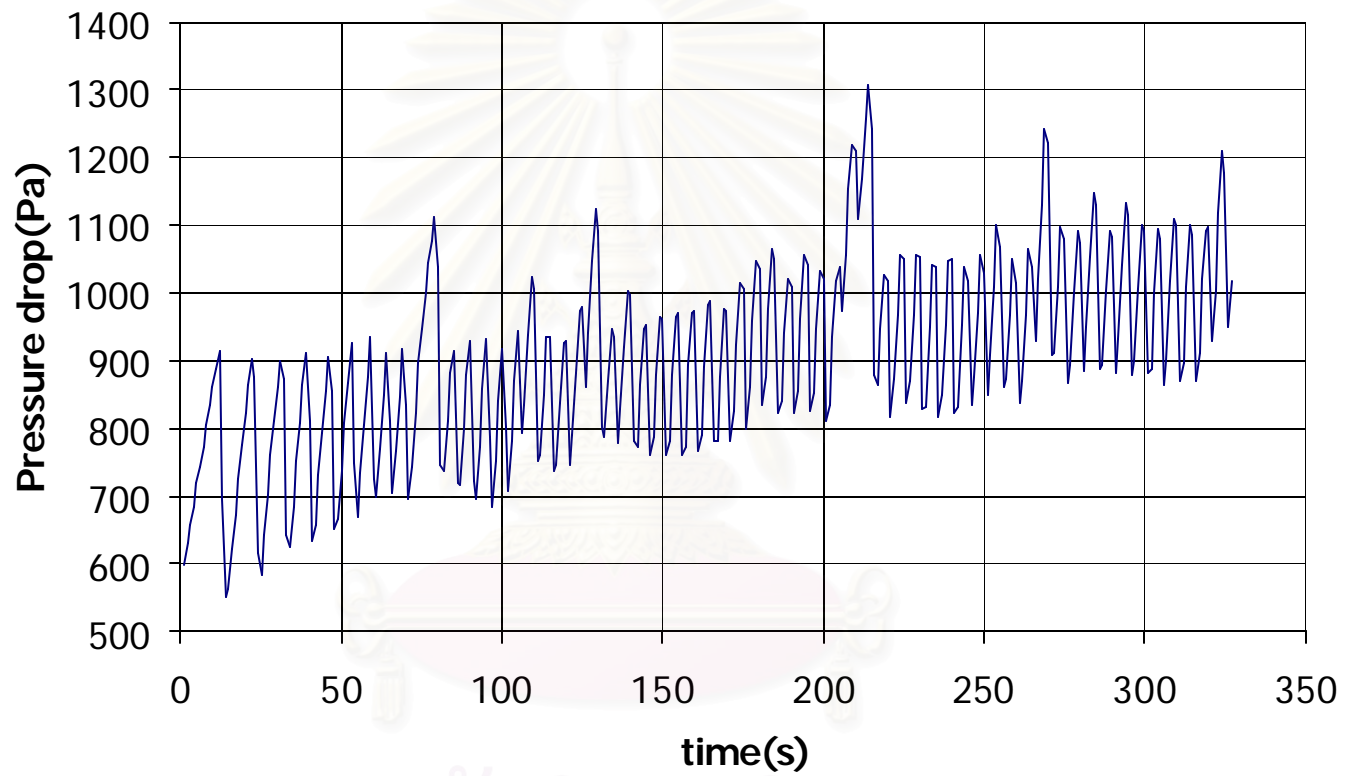


Figure C8 Run C1.724 (8)

สถาบันวิจัยบริการ
จุฬาลงกรณ์มหาวิทยาลัย

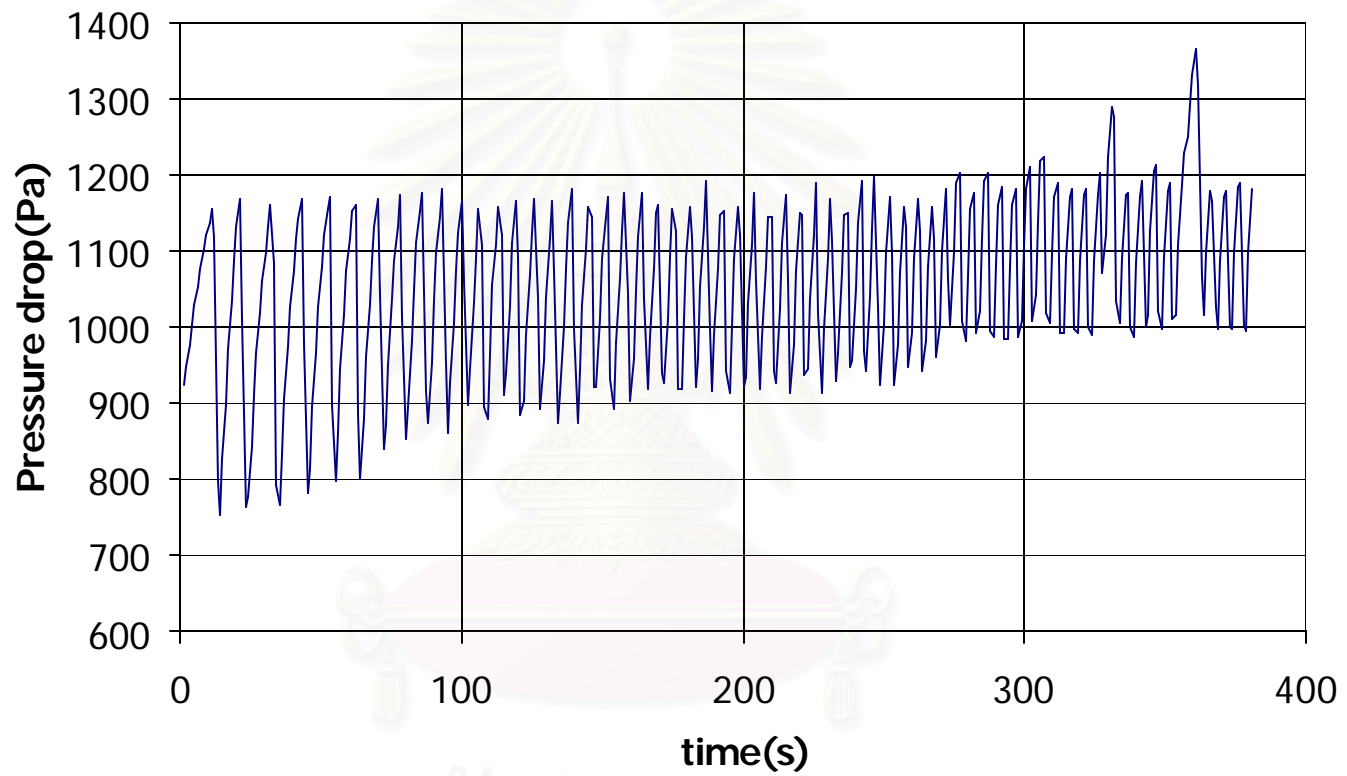


Figure C9 Run B35 (9)

สถาบันวิจัยปฏิบัติการ
จุฬาลงกรณ์มหาวิทยาลัย

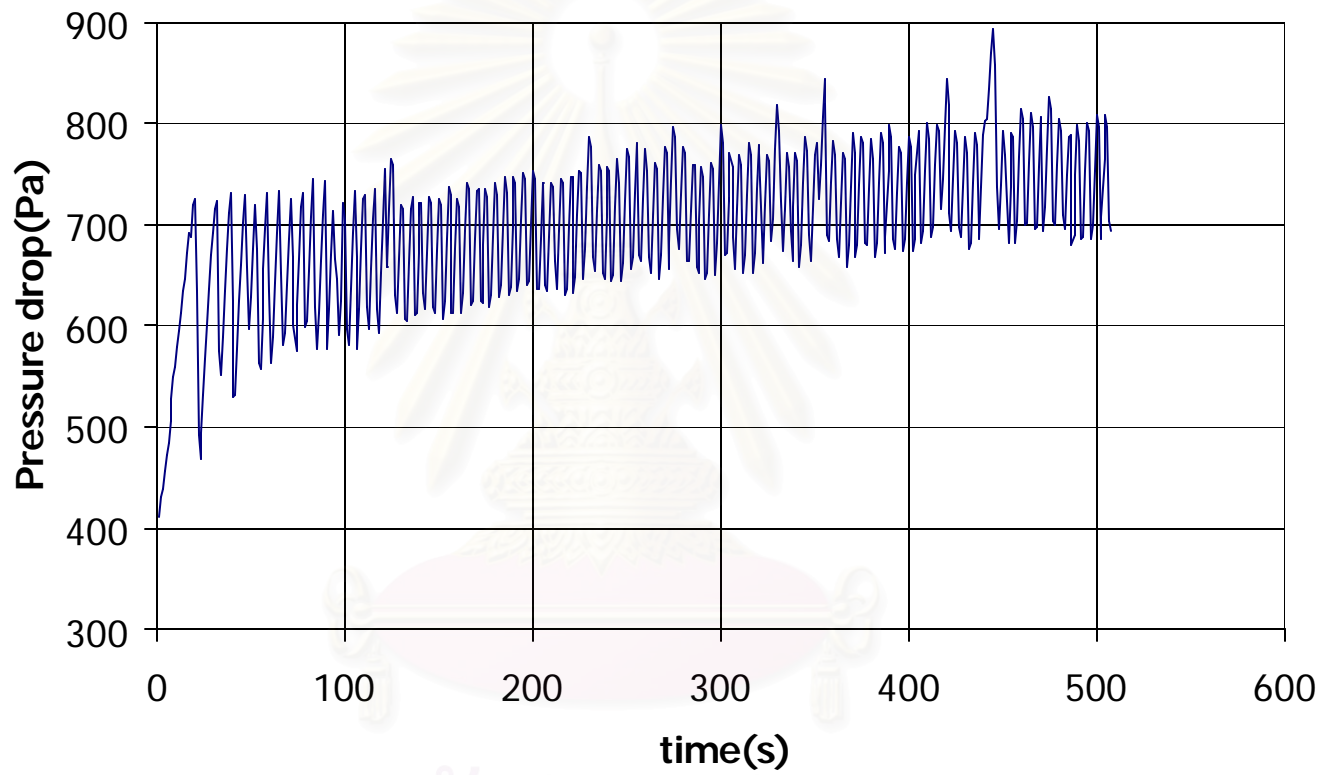


Figure C10 Run D43.64 (10)

สถาบันวิจัยดาราศาสตร์
จุฬาลงกรณ์มหาวิทยาลัย

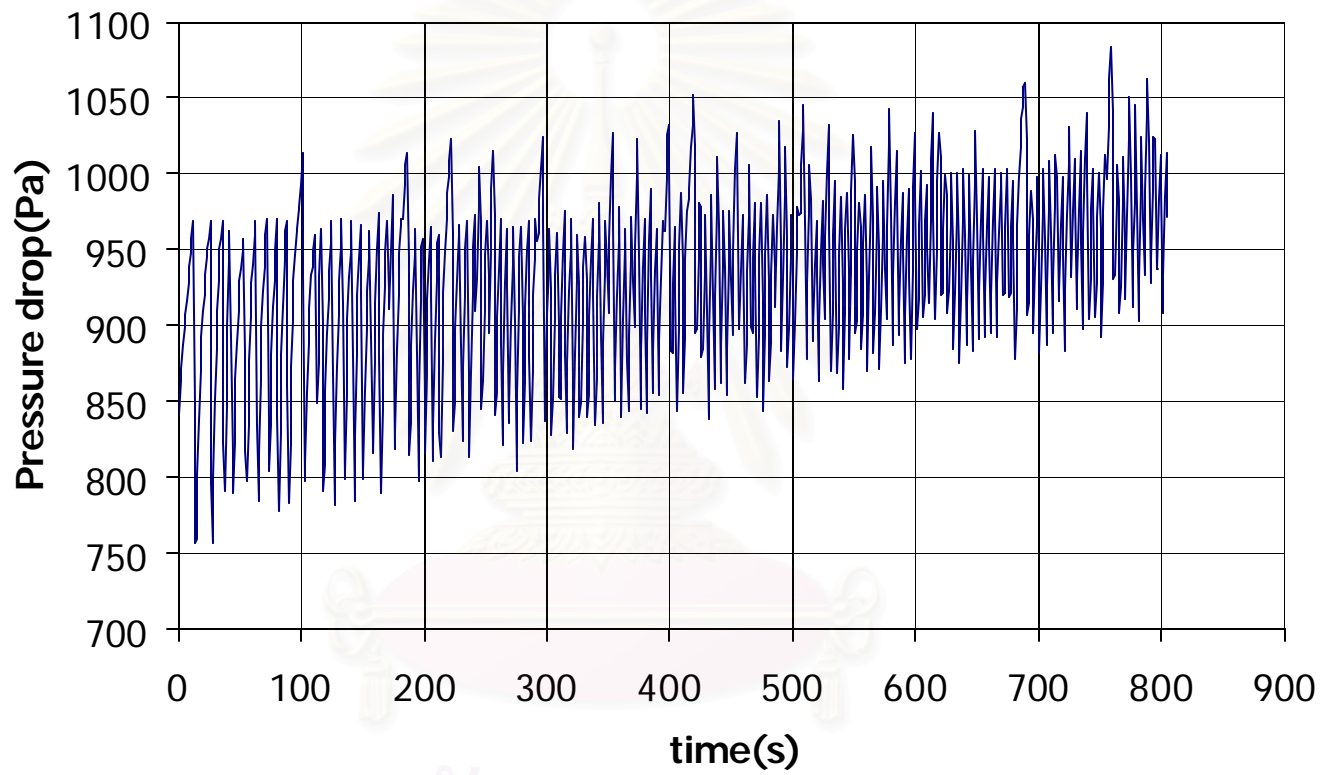


Figure C11 Run D65.45 (11)

สถาบันวิจัยสิริการ
จุฬาลงกรณ์มหาวิทยาลัย

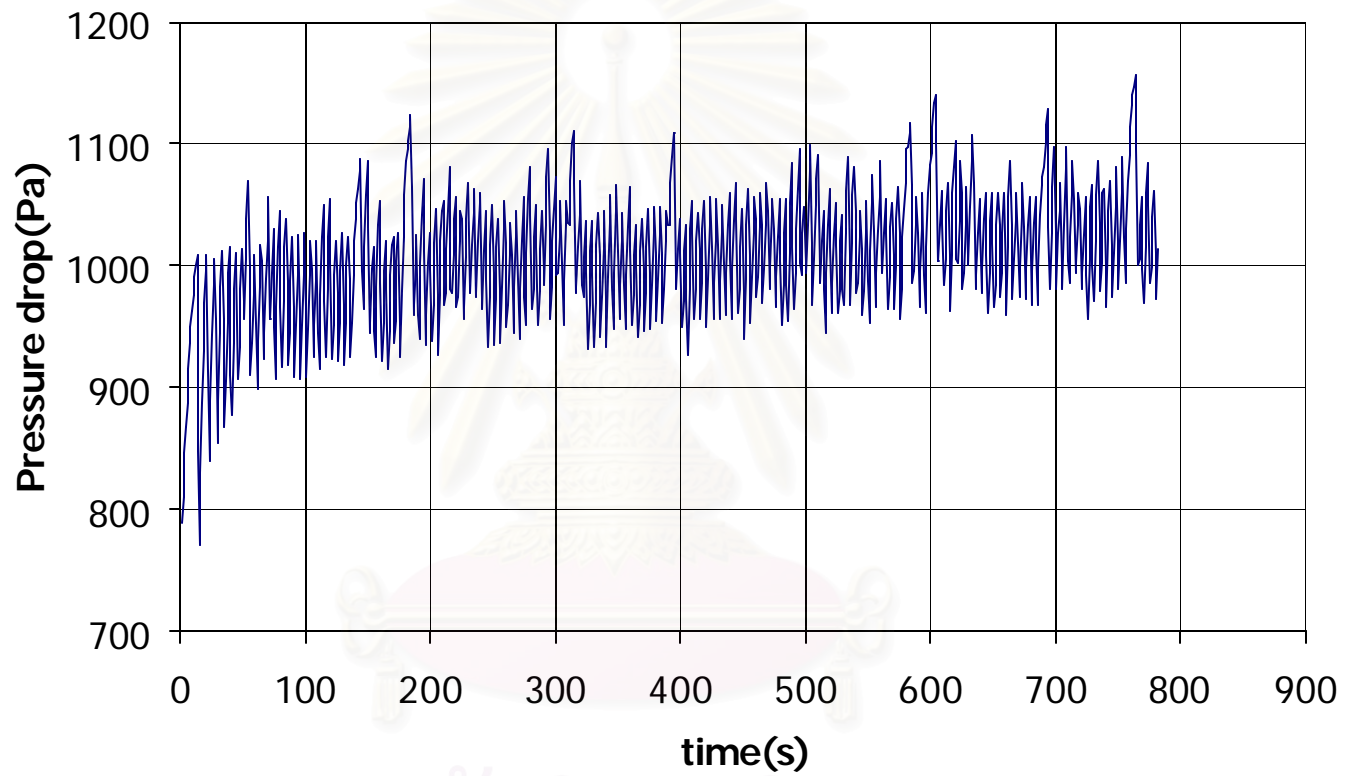


Figure C12 Run ETAN (12)

สถาบันวิจัยบริการ
จุฬาลงกรณ์มหาวิทยาลัย

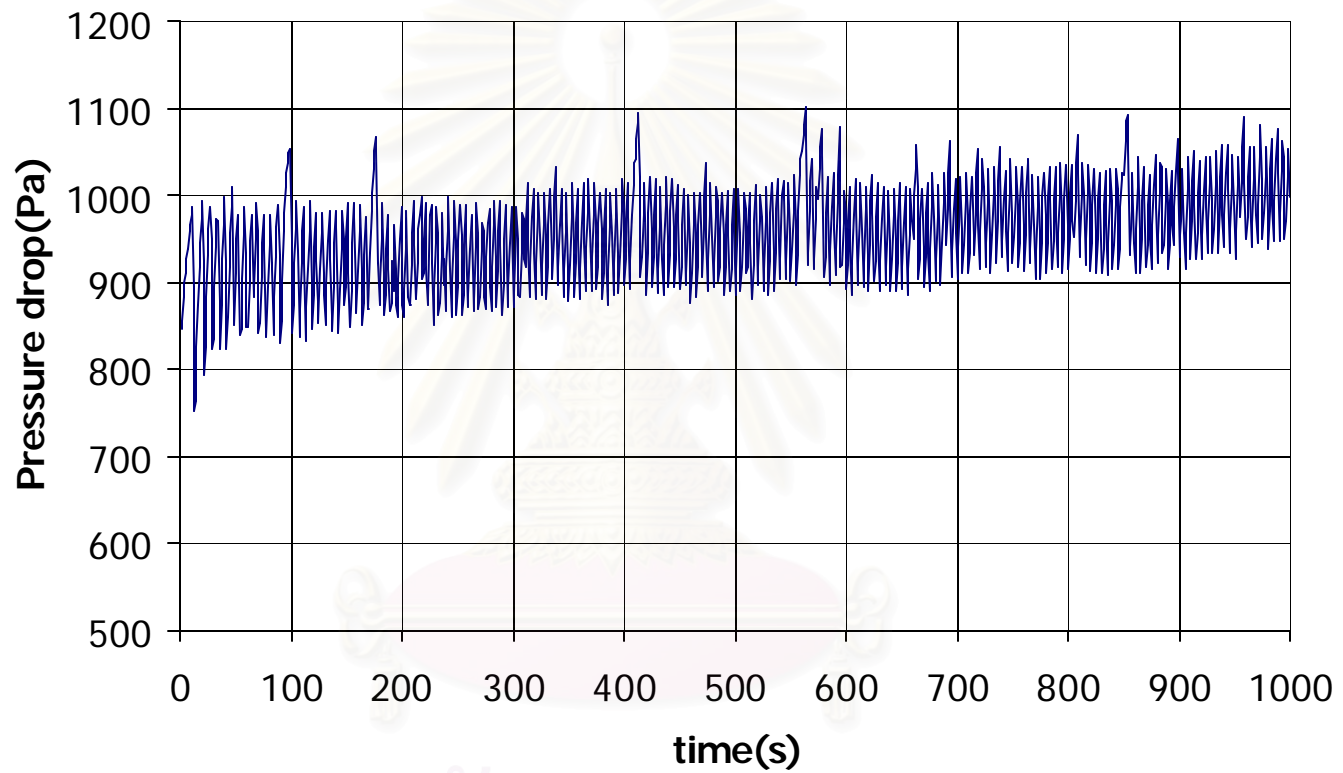


Figure C13 Run ETAN35 (13)

สถาบันวิจัยวิศวกรรม
จุฬาลงกรณ์มหาวิทยาลัย

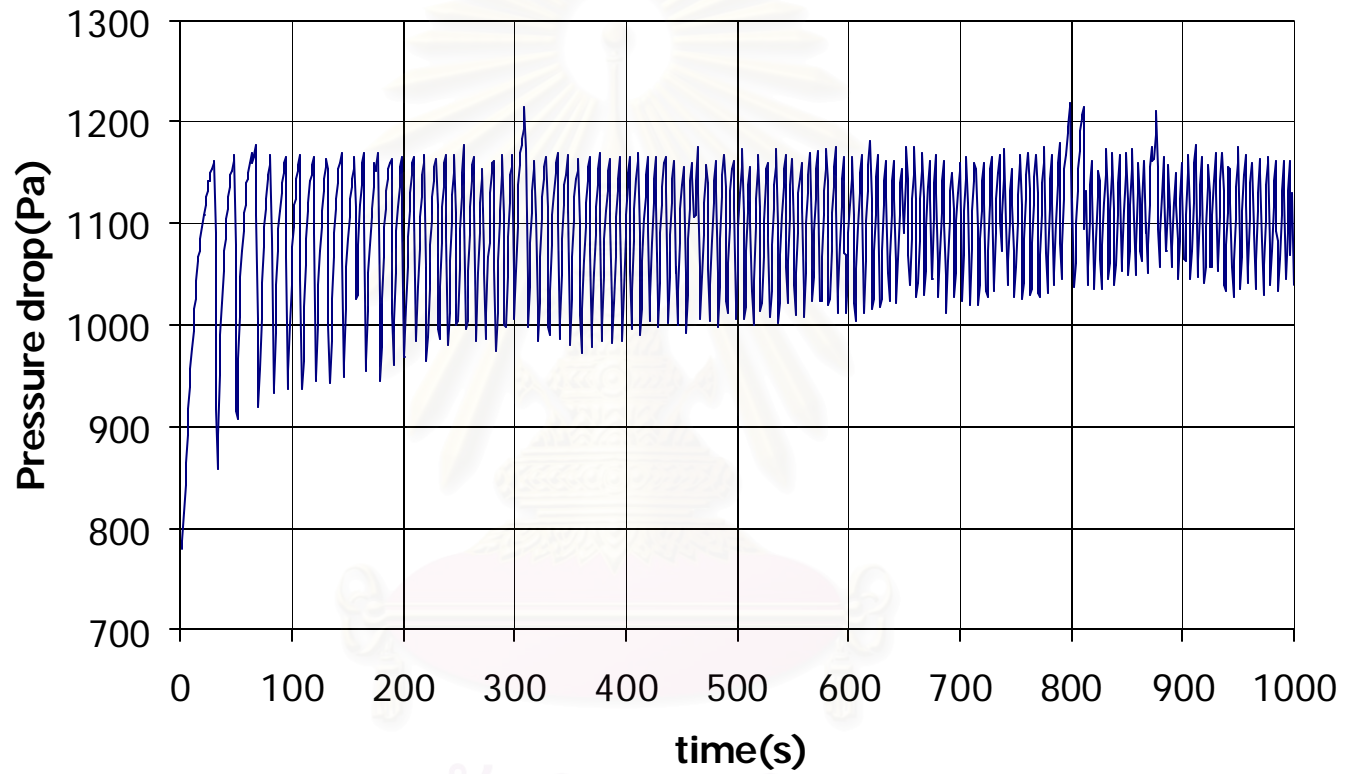


Figure C14 Run ETOP (14)

สถาบันวิจัยบริการ
จุฬาลงกรณ์มหาวิทยาลัย

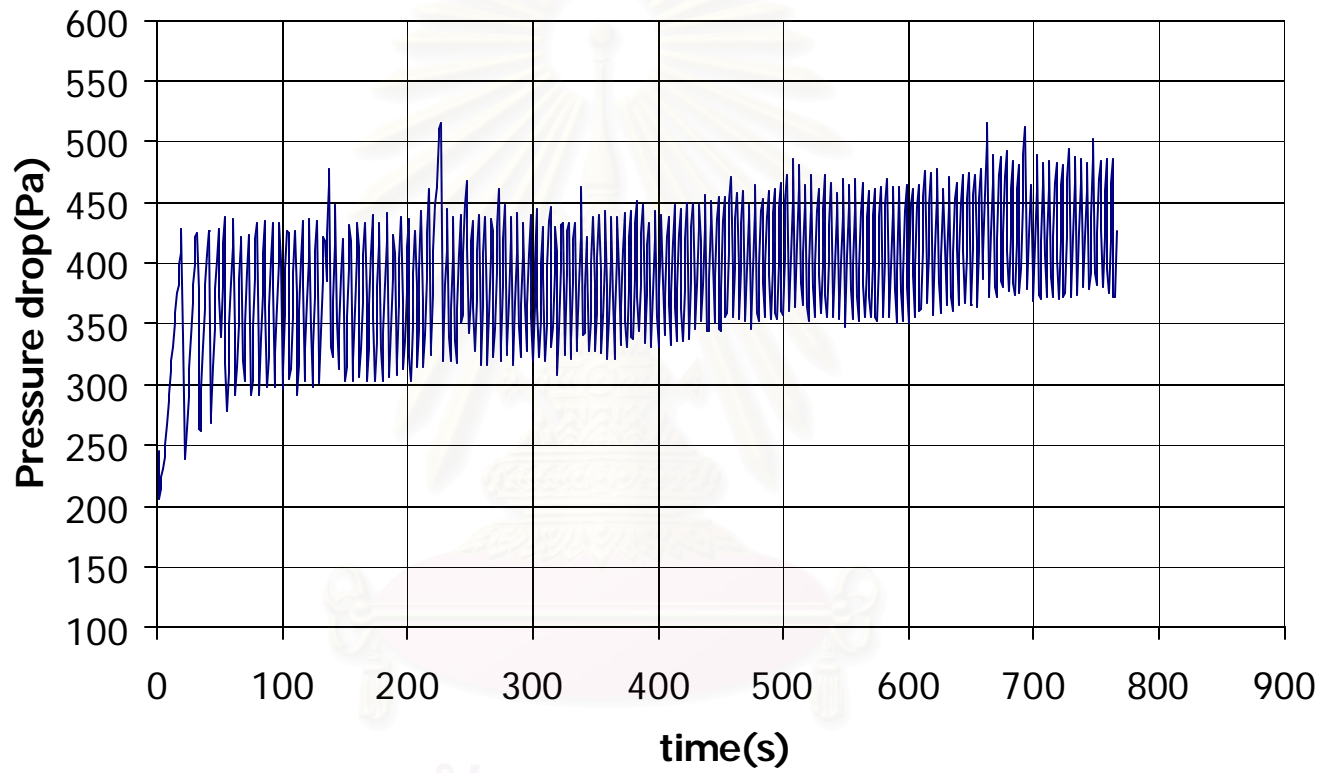


Figure C15 Run ETAN35 (15)

สถาบันวิทยบริการ
จุฬาลงกรณ์มหาวิทยาลัย

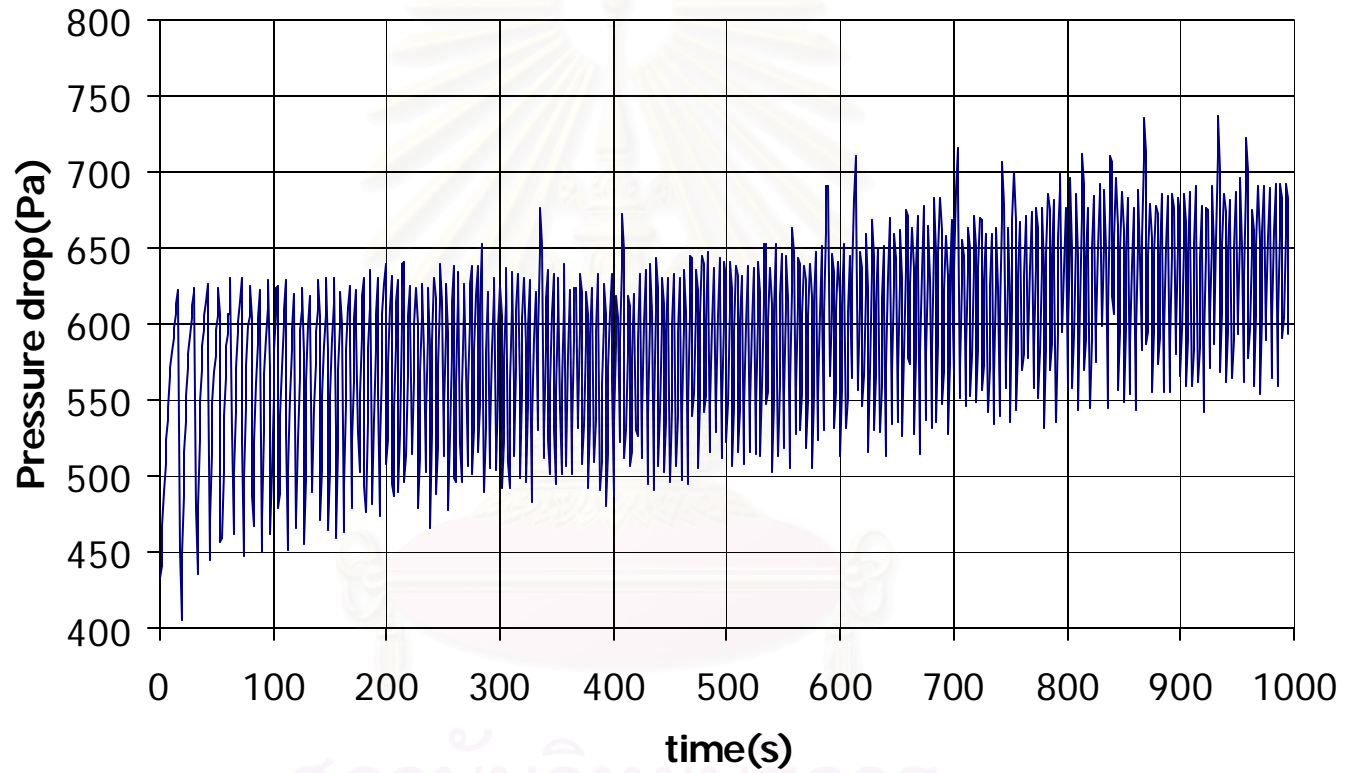


Figure C16 Run ETAN (16)

สถาบันวิทยบริการ
จุฬาลงกรณ์มหาวิทยาลัย

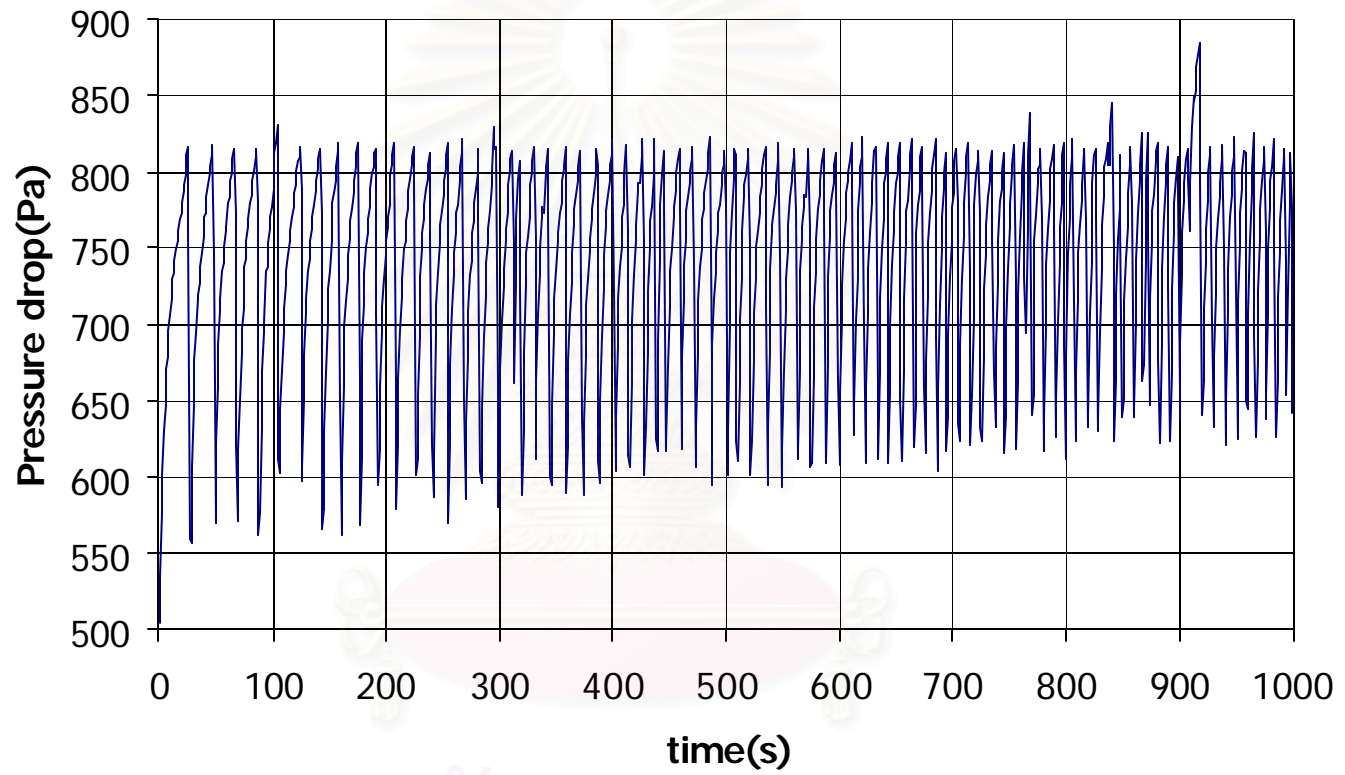


Figure C17 Run D65.45 (17)

สถาบันวิทยบริการ
จุฬาลงกรณ์มหาวิทยาลัย

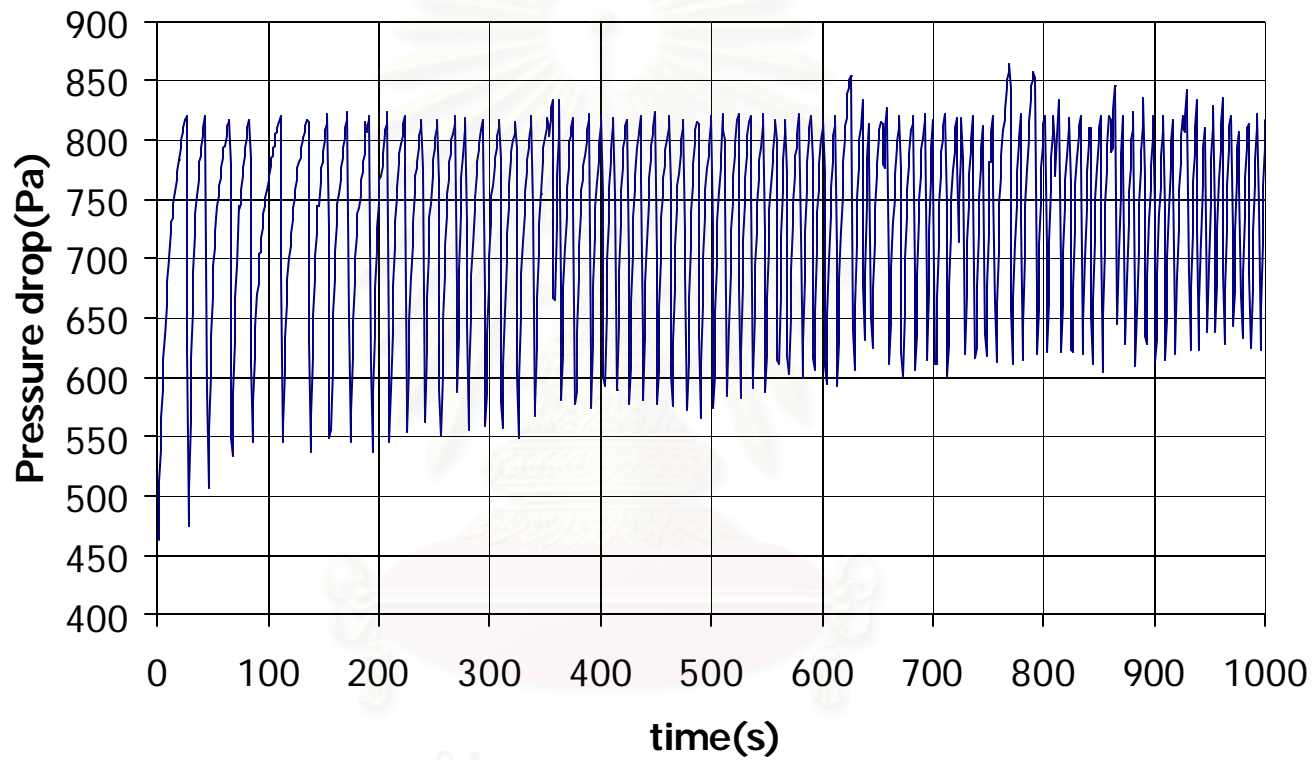


Figure C18 Run D43.64 (18)

สถาบันวิจัยสิริการ
จุฬาลงกรณ์มหาวิทยาลัย

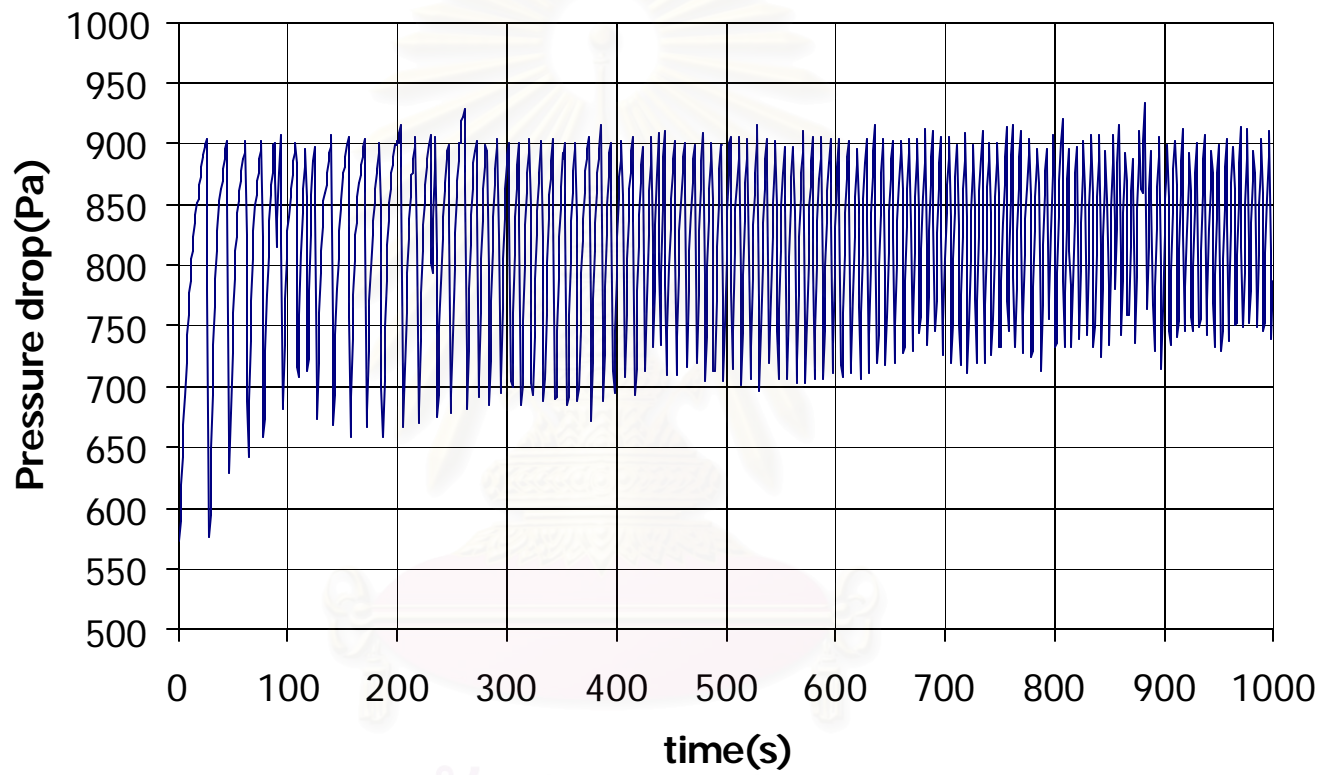


Figure C19 Run D21.82 (19)

สถาบันวิจัยดาราศาสตร์
จุฬาลงกรณ์มหาวิทยาลัย

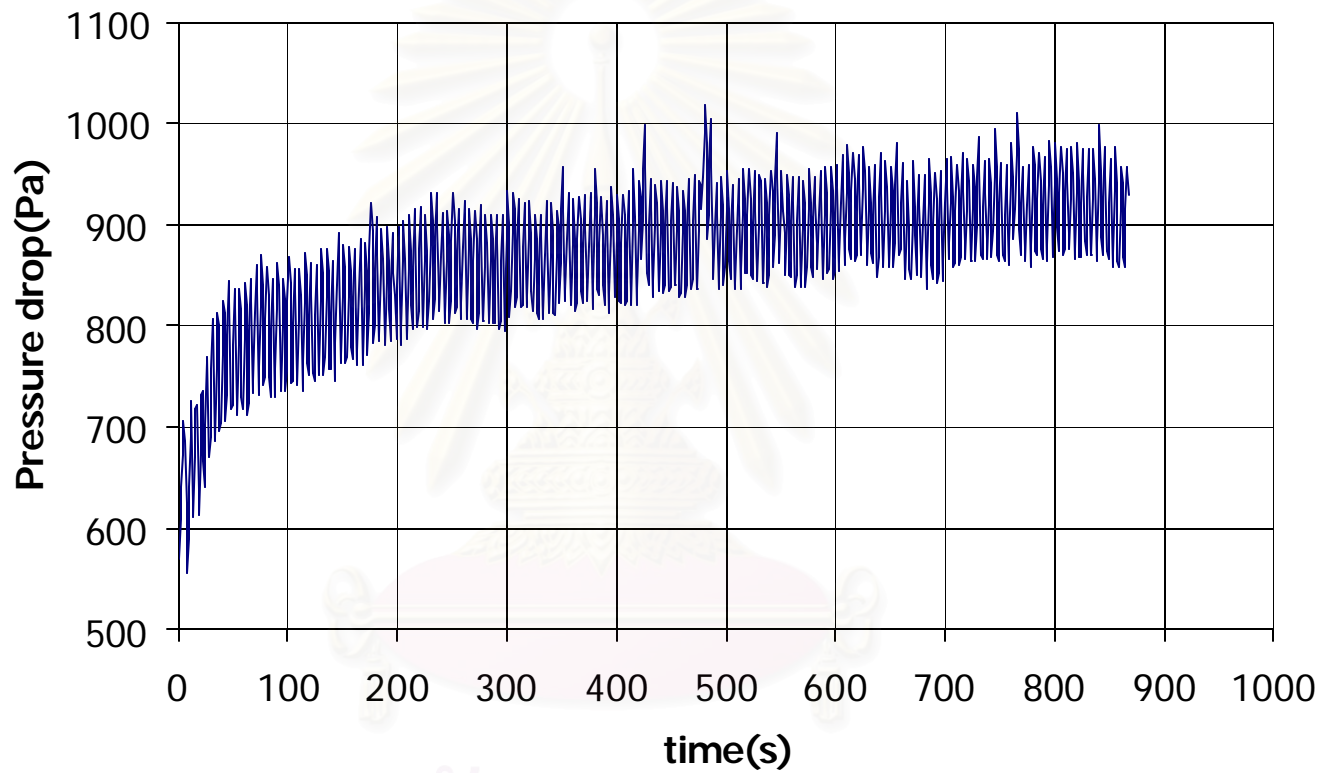


Figure C20 Run B35 (20)

สถาบันวิจัยปฏิบัติการ
จุฬาลงกรณ์มหาวิทยาลัย

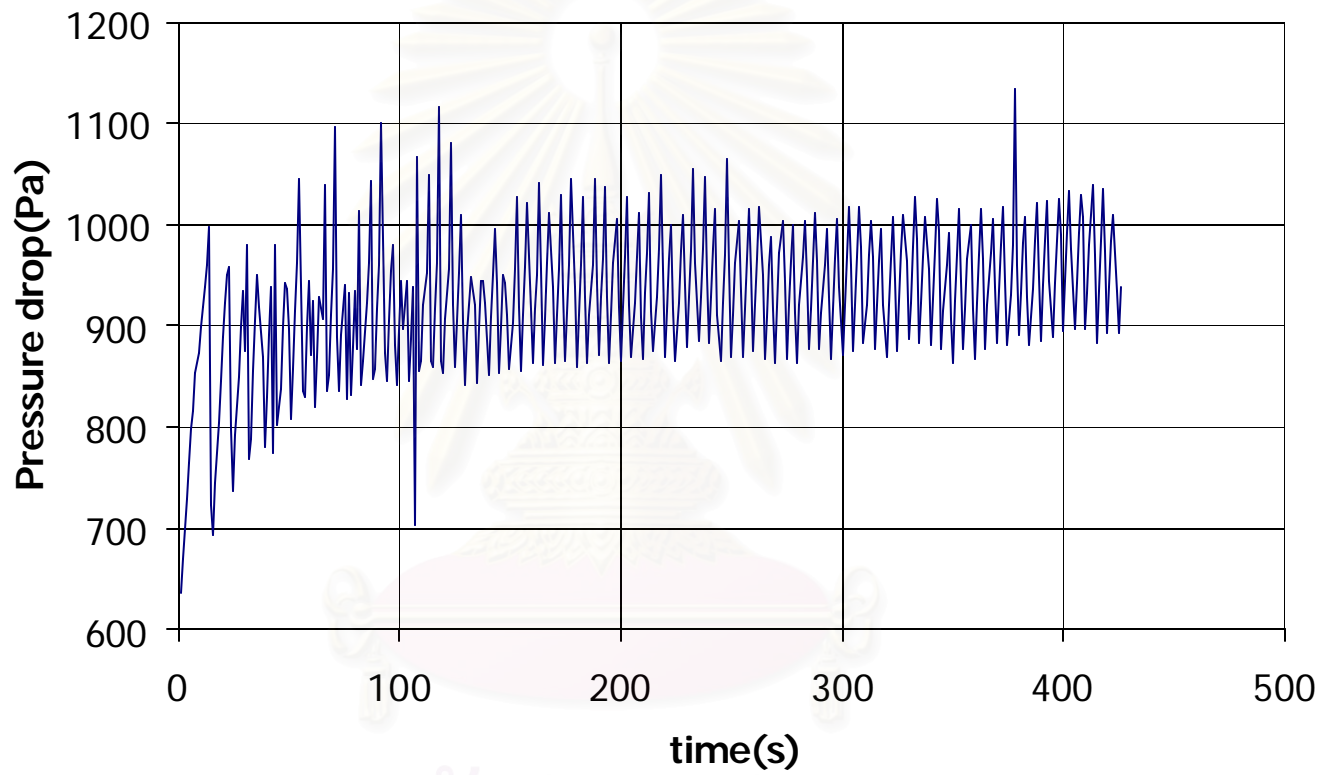


Figure C21 Run B15 (21)

สถาบันวิจัยปฏิบัติการ
จุฬาลงกรณ์มหาวิทยาลัย

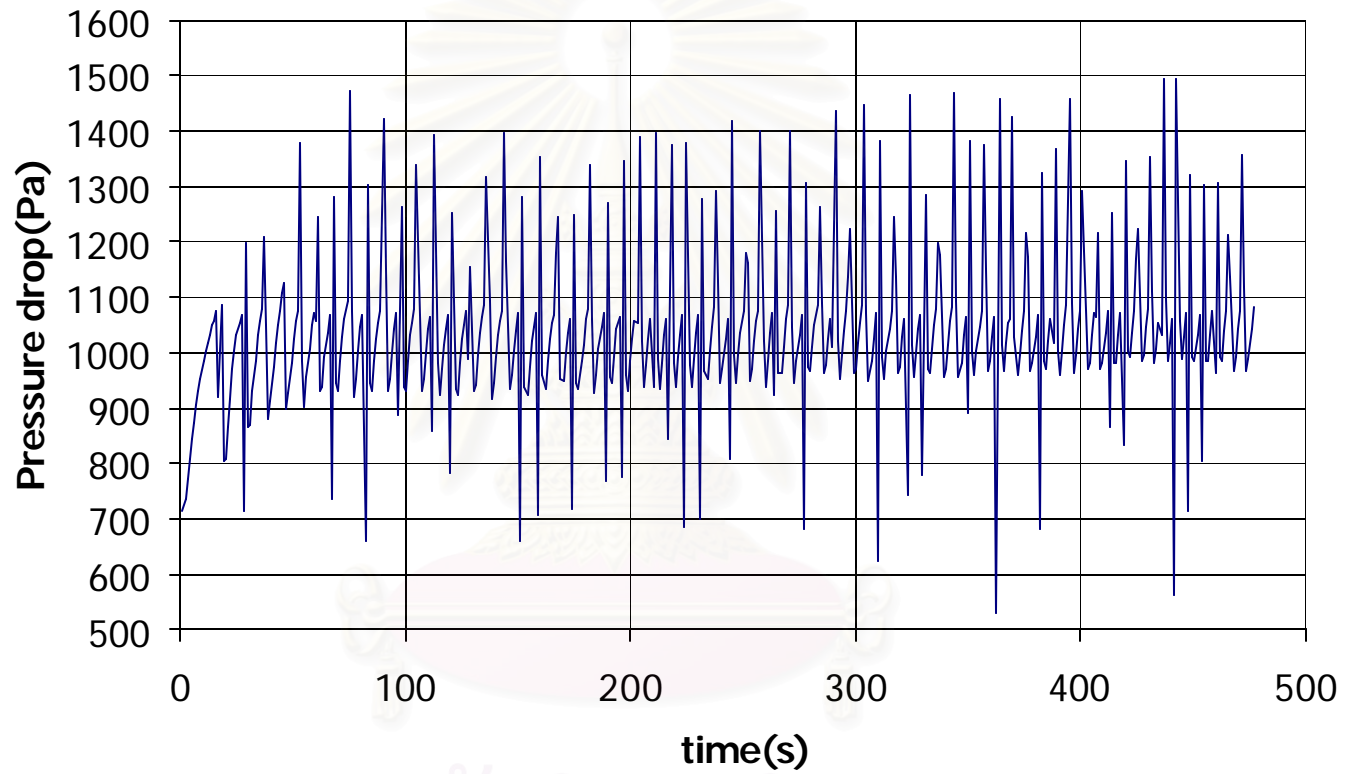


Figure C22 Run A150 (22)

สถาบันวิจัยบริการ
จุฬาลงกรณ์มหาวิทยาลัย

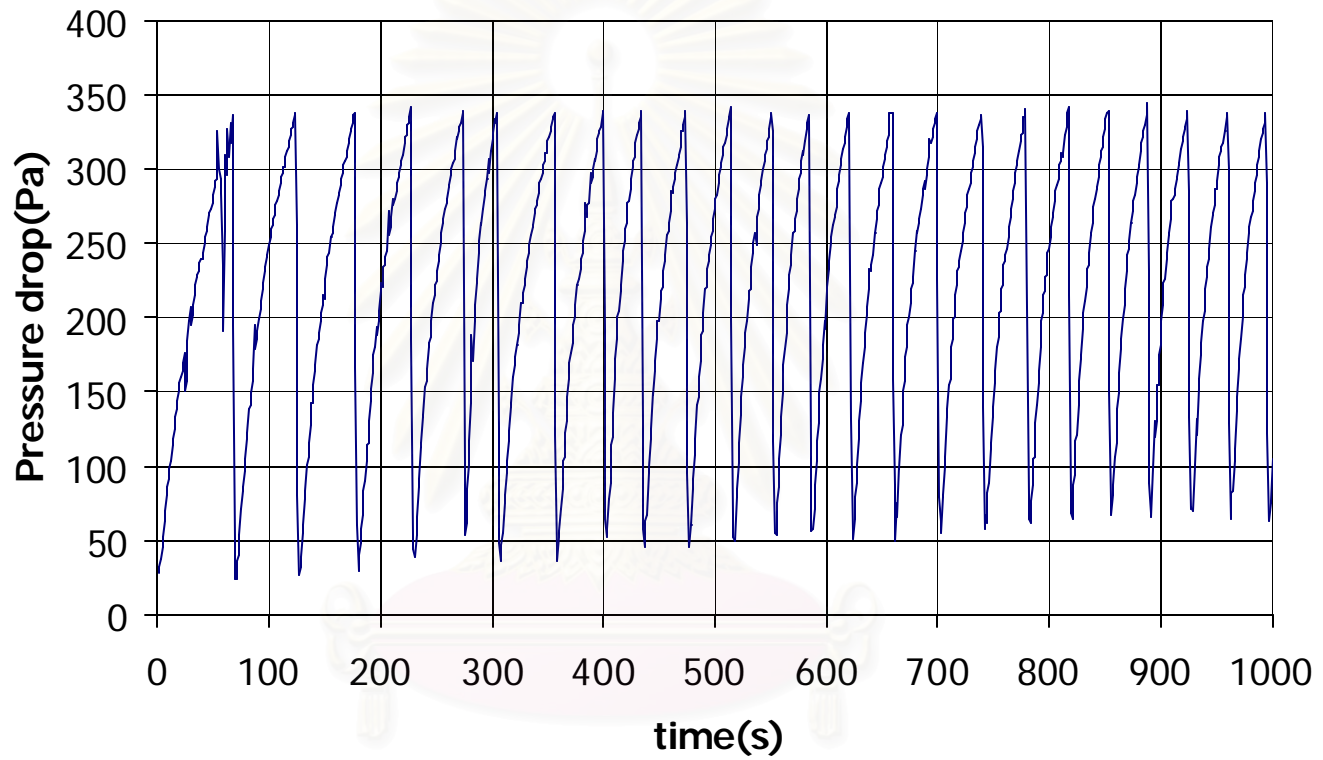


Figure C23 Run A200 (23)

สถาบันวิจัยดาราศาสตร์
จุฬาลงกรณ์มหาวิทยาลัย

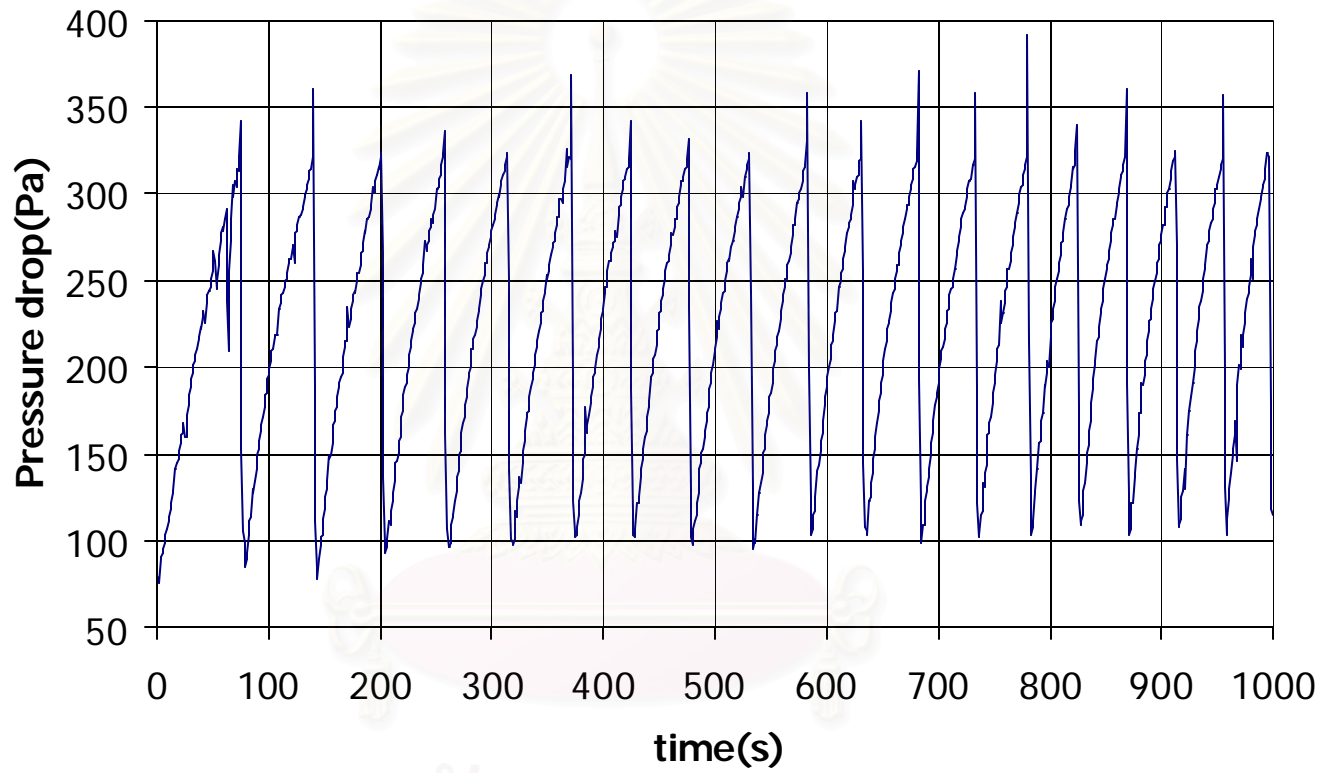


Figure C24 Run A100 (24)

สถาบันวิจัยปริมาตร
จุฬาลงกรณ์มหาวิทยาลัย

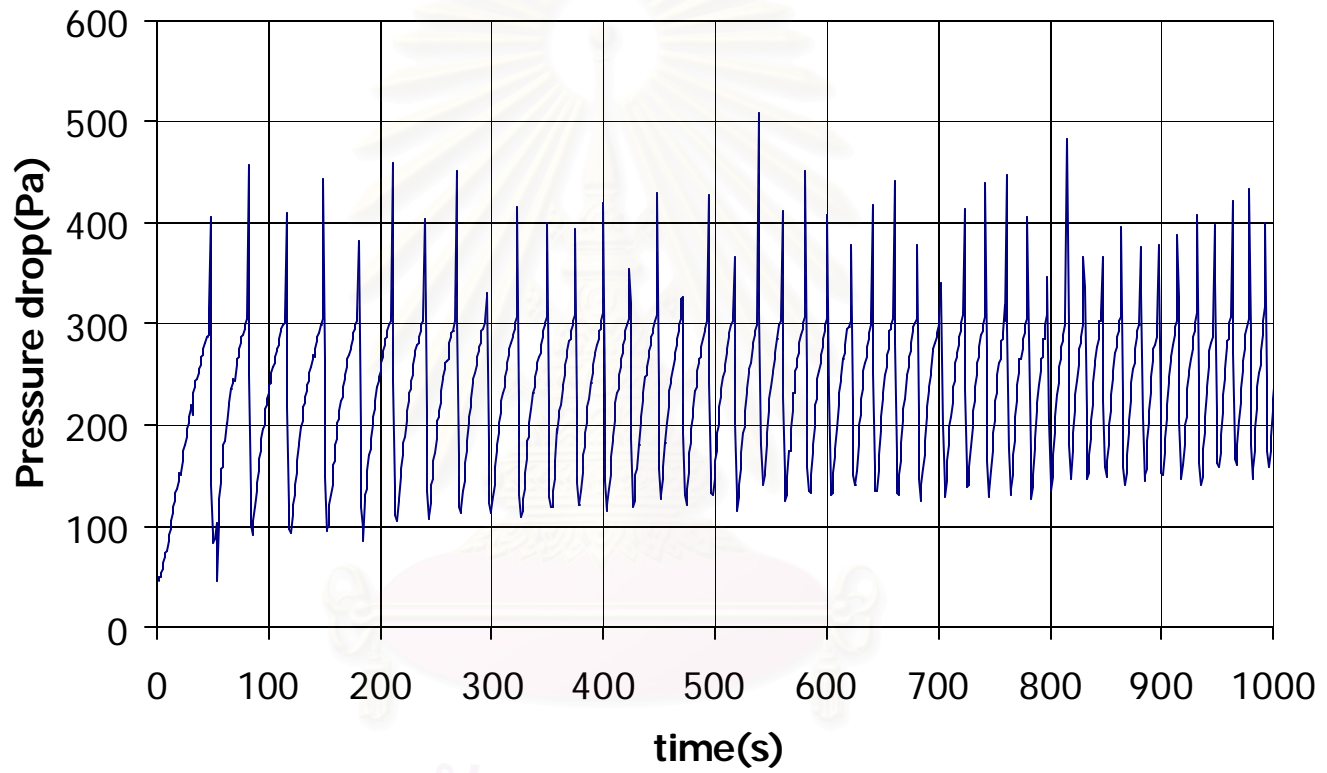


Figure C25 Run A150 (25)

สถาบันวิจัยปฏิบัติการ
จุฬาลงกรณ์มหาวิทยาลัย

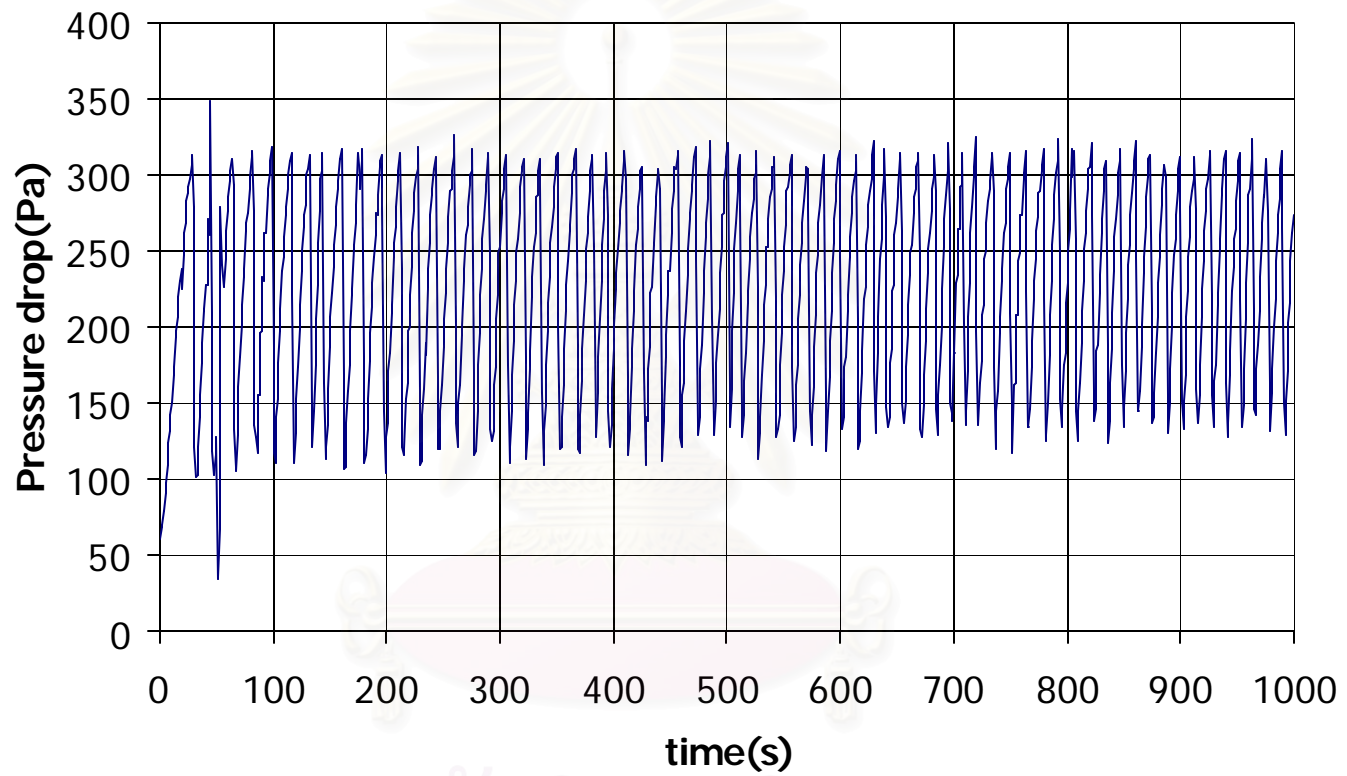


Figure C26 Run A200 (26)

สถาบันวิจัยวิชาการ
จุฬาลงกรณ์มหาวิทยาลัย



APPENDIX D

Profile velocity vector

สถาบันวิทยบริการ
จุฬาลงกรณ์มหาวิทยาลัย

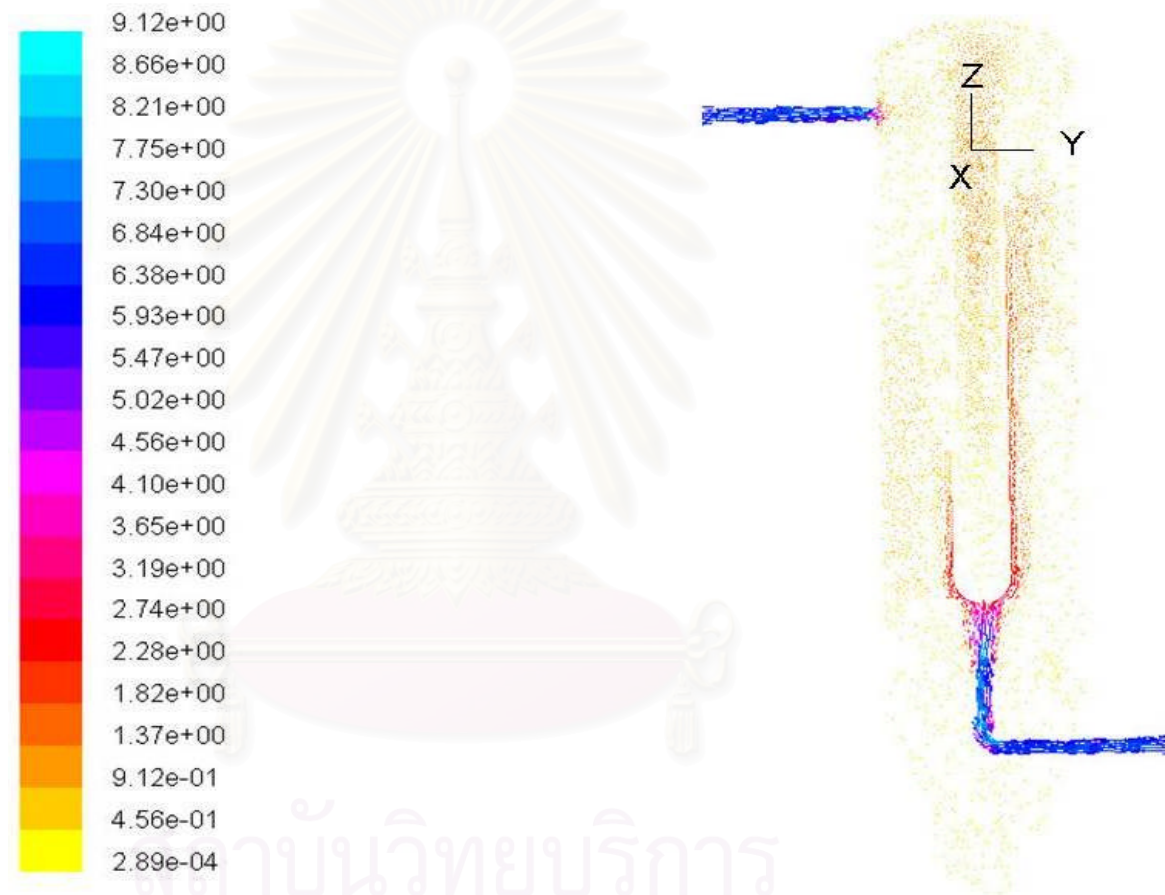


Figure D.1 Profile of velocity vector at $x = 0$ as a function of y and z for the bottom feeding port of the single ceramic candle filter (m/s)



Figure D.2 Profile of velocity vector at $y = 0$ as a function of x and z for the bottom feeding port the single ceramic candle filter (m/s)

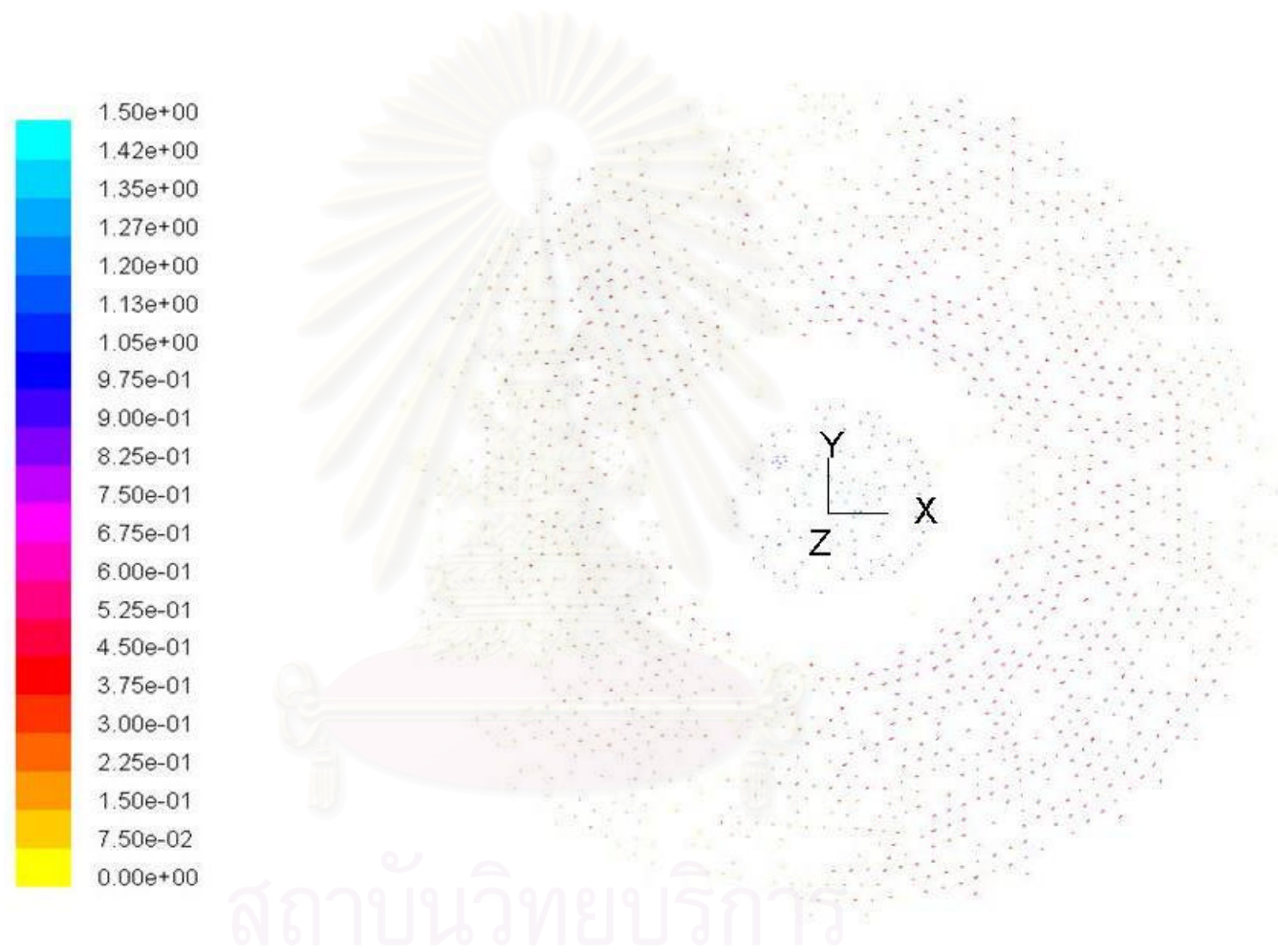


Figure D.3 Profile of velocity vector at $z = -100$ as a function of x and y for the bottom feeding port the single ceramic candle filter (m/s)

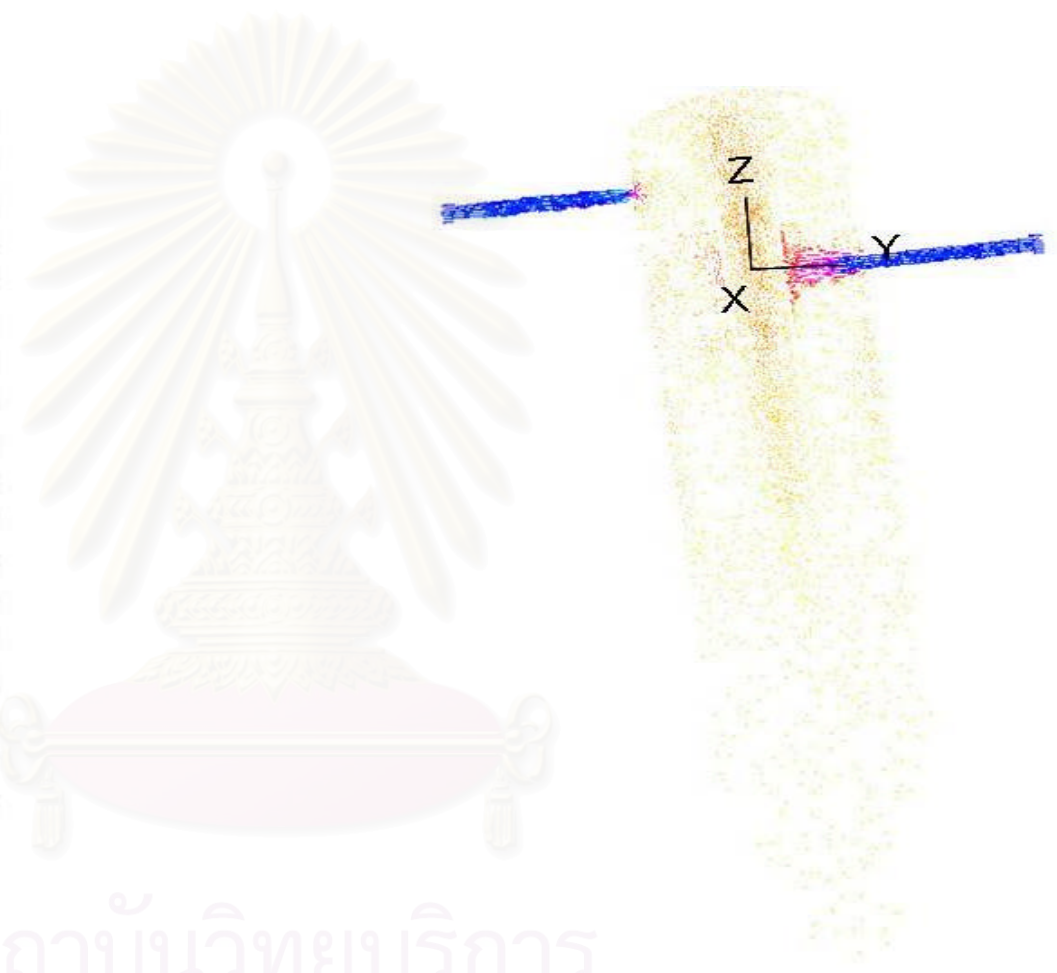
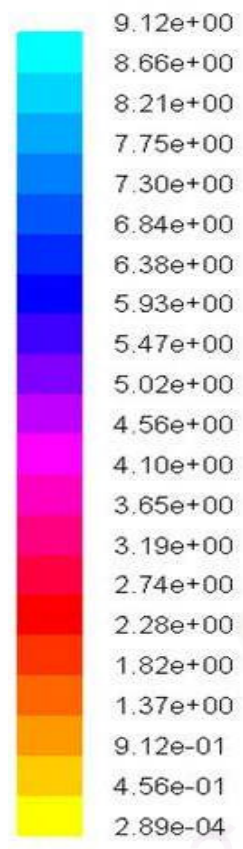


Figure D.4 Profile of velocity vector at $x = 0$ as a function of y and z for the top feeding port the single ceramic candle filter (m/s)

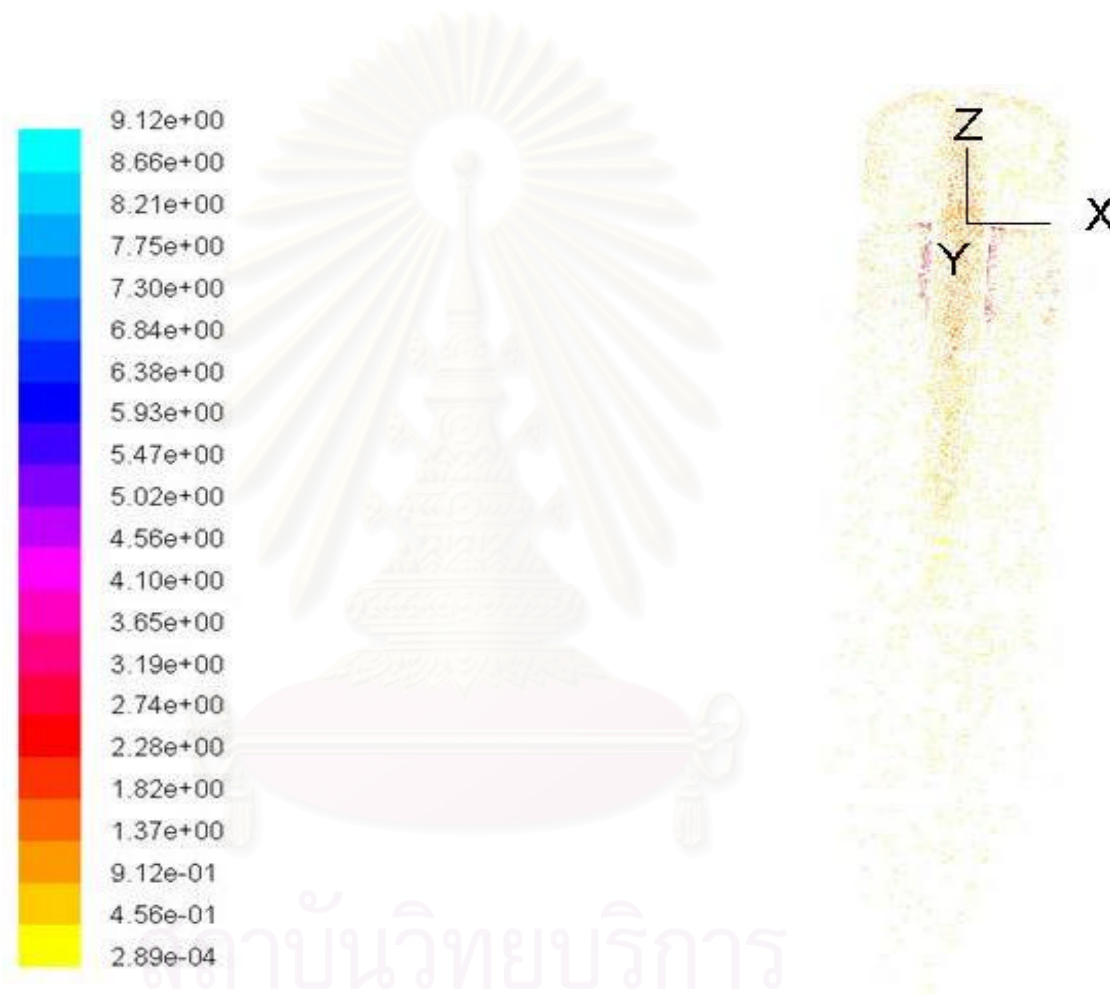


Figure D.5 Profile of velocity vector at $y = 0$ as a function of x and z for the top feeding port the single ceramic candle filter (m/s)



Figure D.6 Profile of velocity vector at $z = -100$ as a function of x and y for the top feeding port the single ceramic candle filter (m/s)

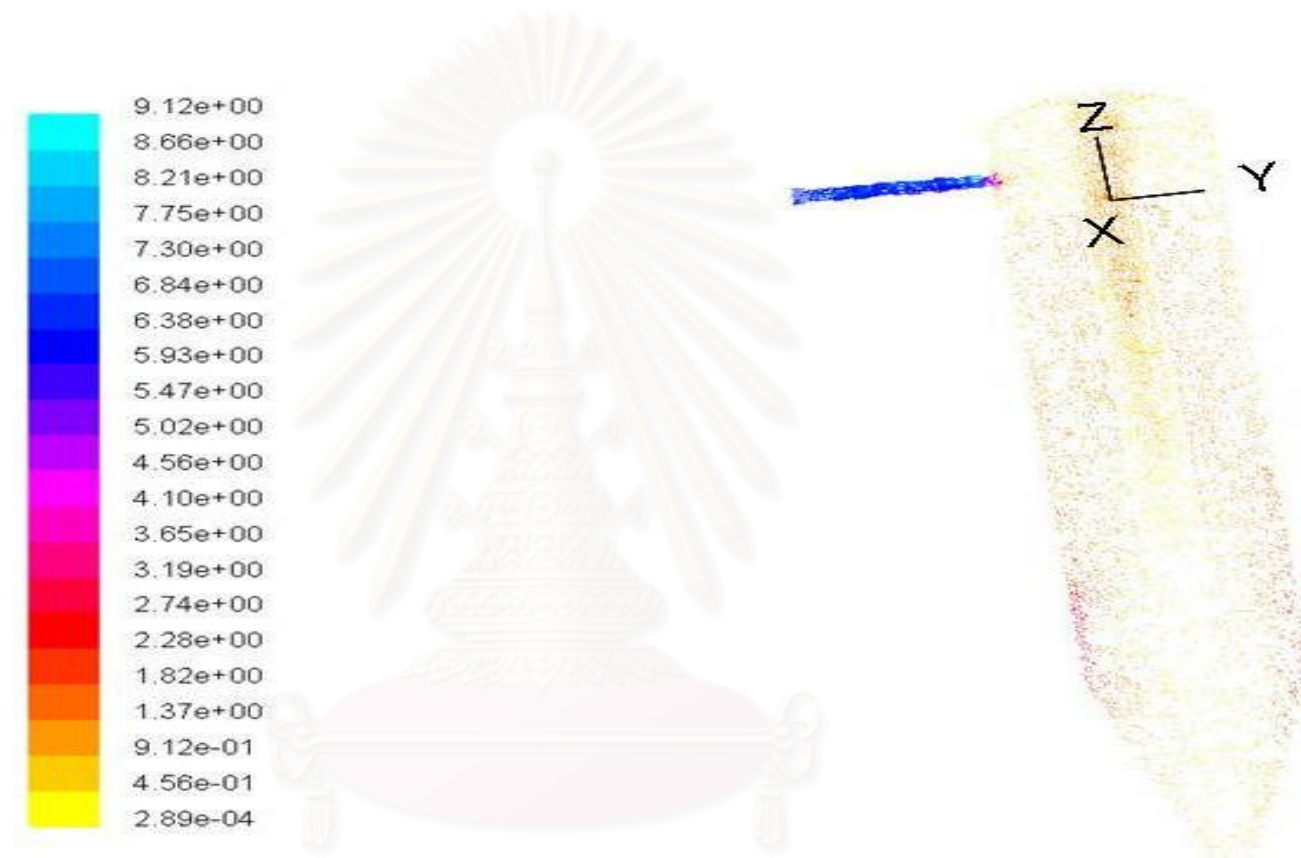


Figure D.7 Profile of velocity vector at $x = 0$ as a function of y and z for the tangential feeding port the single ceramic candle filter (m/s)

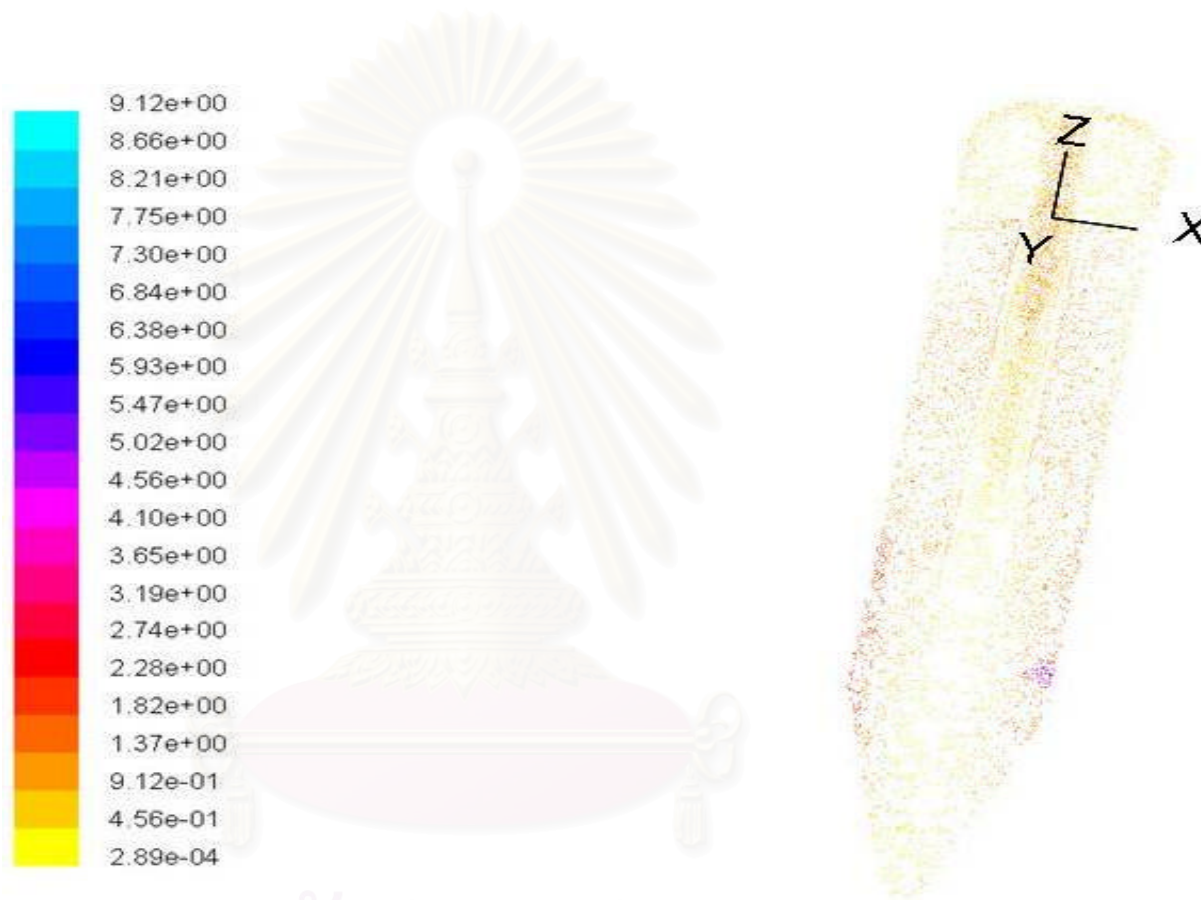


Figure D.8 Profile of velocity vector at $y = 0$ as a function of x and z for the tangential feeding port the single ceramic candle filter (m/s)

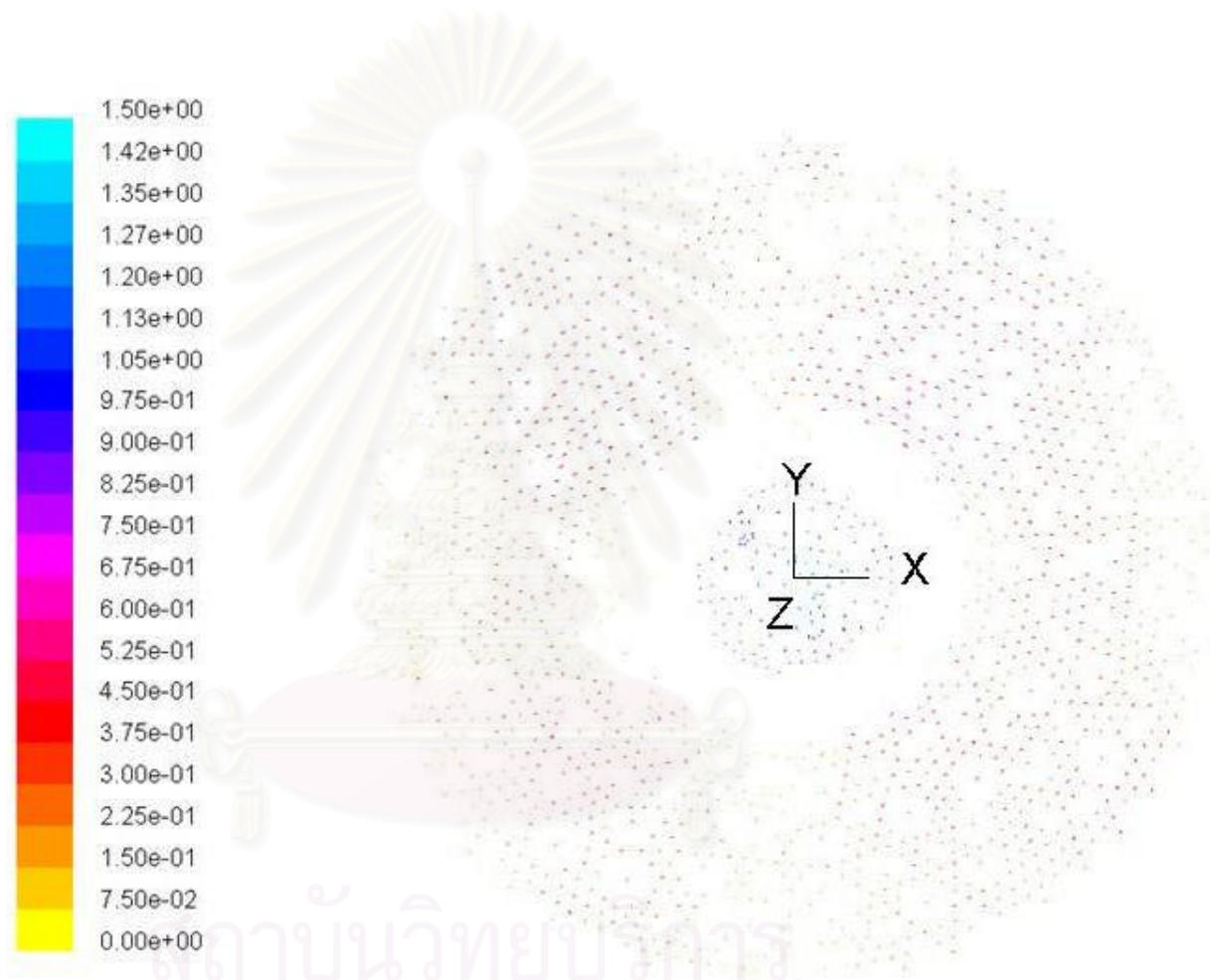


Figure D.9 Profile of velocity vector at $z = -100$ as a function of x and y for the tangential feeding port the single ceramic candle filter (m/s)

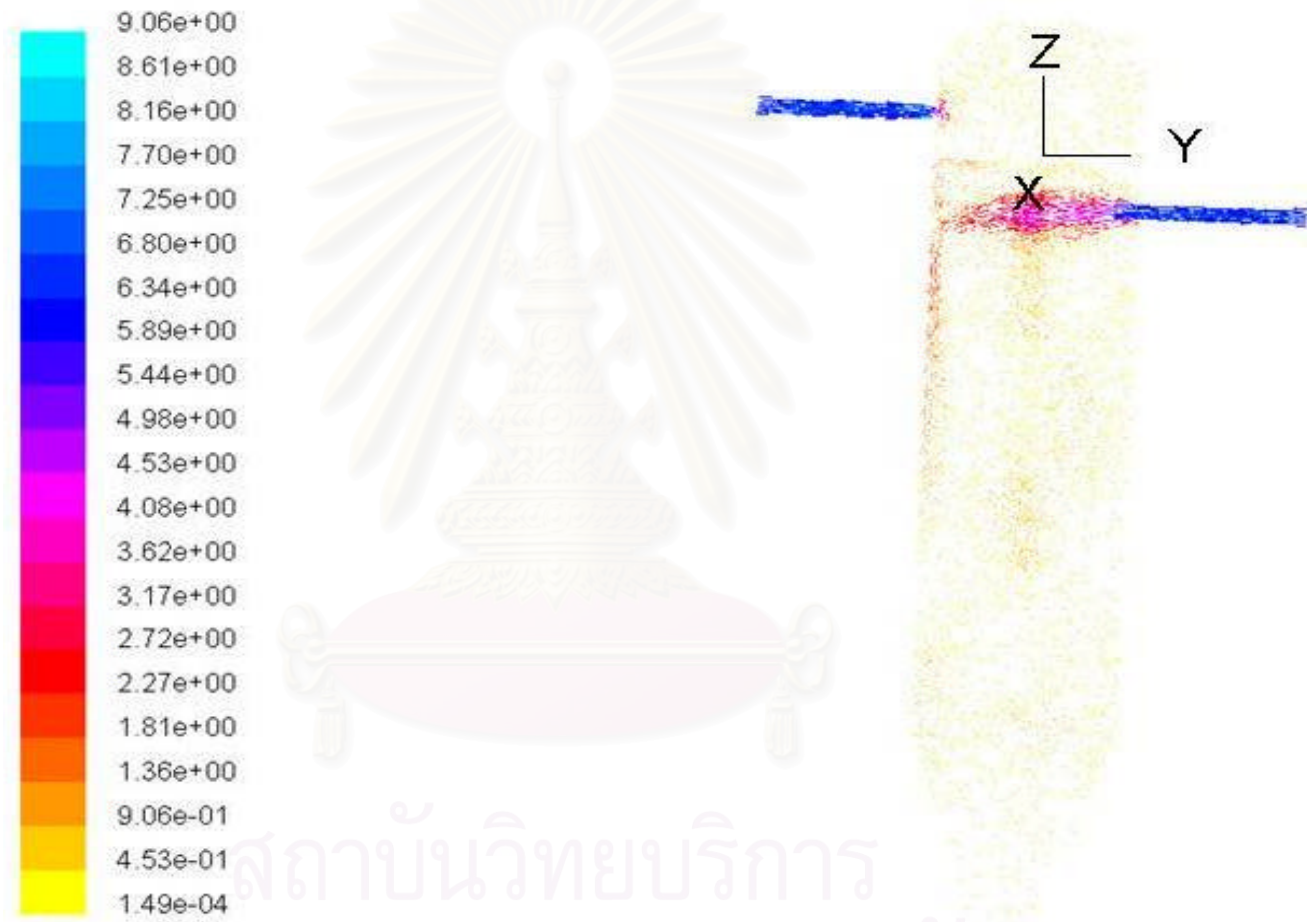


Figure D.10 Profile of velocity vector at $x = 0$ as a function of y and z for the top feeding port of the twin ceramic candles filter (m/s)

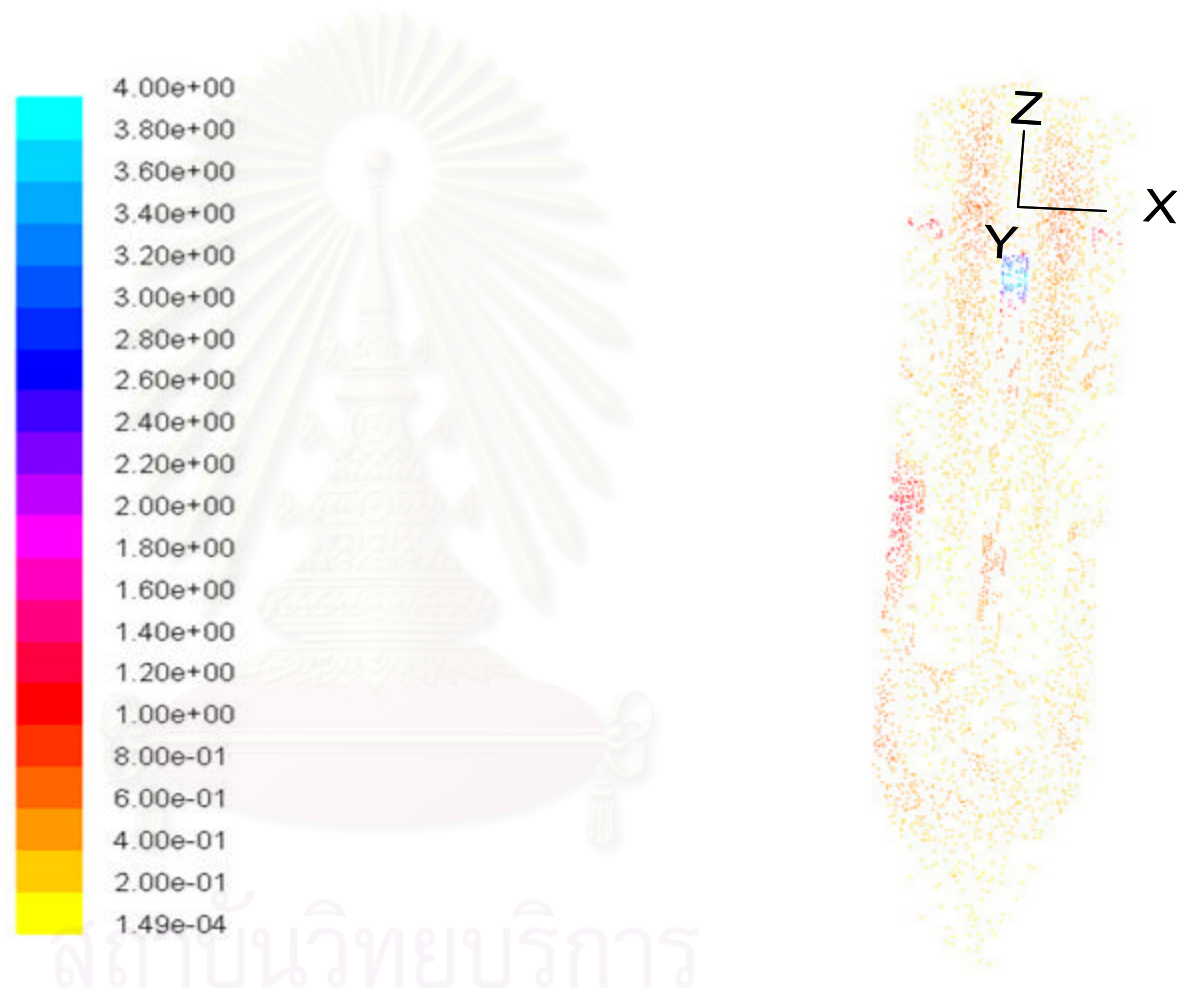


Figure D.11 Profile of velocity vector at $y = 0$ as a function of x and z for the top feeding port of the twin ceramic candles filter (m/s)

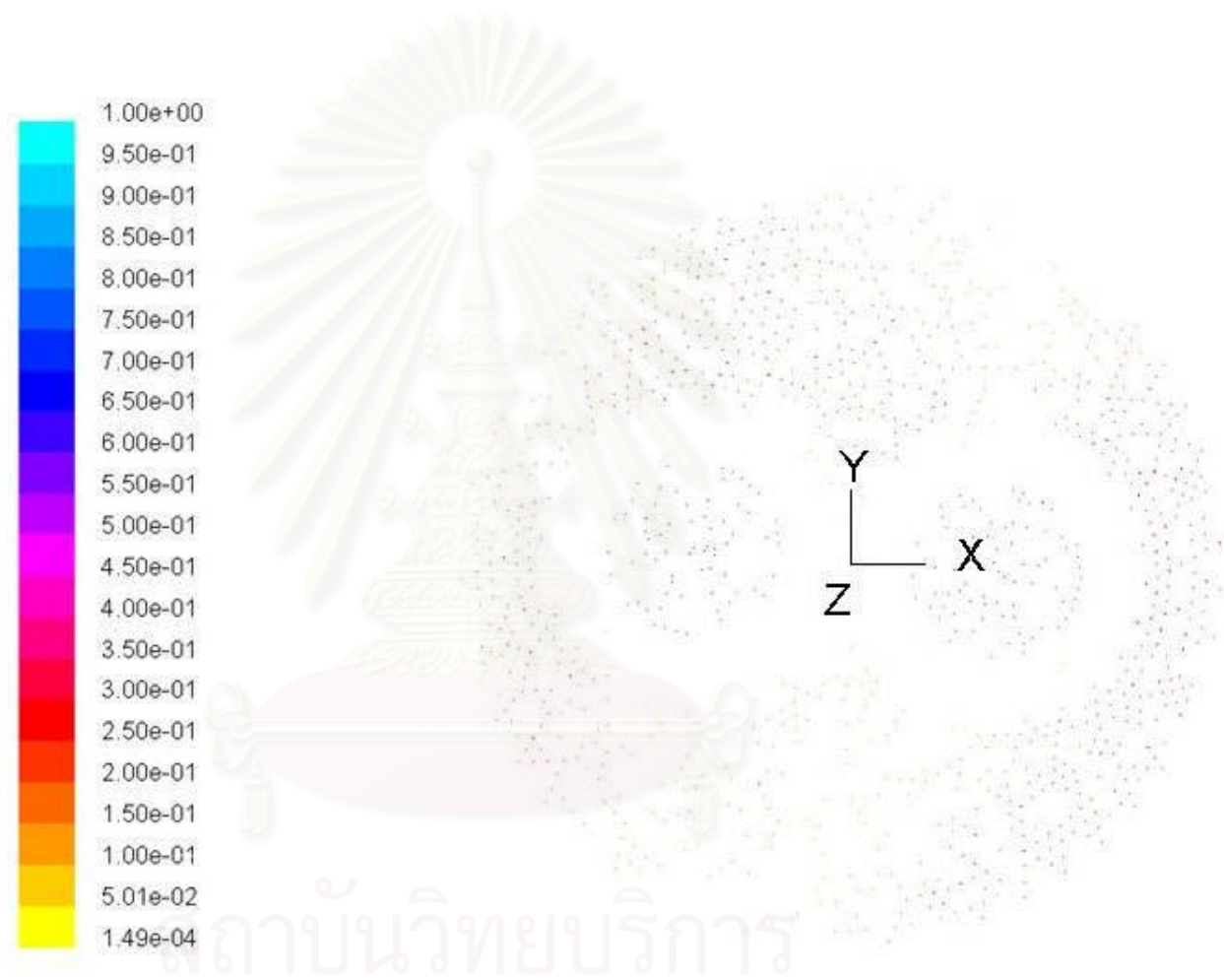


Figure D.12 Profile of velocity vector at $z = -100$ as a function of x and y for the top feeding port of the twin ceramic candles filter (m/s)

VITA

Miss Jerapan Laksameearunotai, the first daughter of Mr.Thongchai and Mrs. Benjawan Laksameearunotai, was born on August 27, 1982 in Bangkok, Thailand. She spent 6 years studying in primary school education at Saint Joseph Thippawan School, Samutprakarn. She attended Sainampeung School in Bangkok and graduated in secondary school and high school educations in 1999. In April 2003, she received her Bachelor Degree of Engineering, majoring in Chemical Engineering, Mahidol University, Nakornpratom, Thailand. She enrolled her Master Degree Program at Chulalongkorn University in 2003. She was awarded a Master degree in Chemical Engineering in March, 2006.



สถาบันวิทยบริการ
จุฬาลงกรณ์มหาวิทยาลัย